Regime dependence of Aerosol Effects on the Formation and Evolution of Pyro-convective clouds

Dissertation

zur Erlangung des Grades

"Doktor der Naturwissenschaften"

am Fachbereich Chemie

der Johannes Gutenberg-Universität

in Mainz

Di Chang

geb. in Shandong, China

Max Planck Graduate Center

mit der Johannes Gutenberg-Universität Mainz

angefertigt am Max-Planck-Institut für Chemie

I hereby declare that I wrote the dissertation submitted without any unauthorized external assistance and used only sources acknowledged in the work. All textual passages which are appropriated verbatim or paraphrased from published and unpublished texts as well as all information obtained from oral sources are duly indicated and listed in accordance with bibliographical rules. In carrying out this research, I complied with the rules of standard scientific practice as formulated in the statutes of Johannes Gutenberg University Mainz to insure standard scientific practice.

Abstract

Biomass burning is a significant source of atmospheric aerosol particles, which could serve as effective cloud condensation nuclei (CCN) and ice nuclei (IN), thereby affecting the formation of clouds and precipitation. As an extreme consequence of biomass burning, pyro-convective clouds develop directly above the fire, which transports massive amounts of water vapor, aerosol particles and other trace gases to the upper troposphere and lower stratosphere (UT/LS). The pyro-cloud provides a good example with which to study aerosol–cloud interactions, as it involves rainfall, hail, lightning, extreme winds at the surface, and in some cases even tornadoes.

A recent parcel model study showed three deterministic regimes of initial cloud droplet formation, characterized by different ratios of CCN to updraft velocities. This analysis, however, left an open question how these regimes evolve during the subsequent cloud development. To address this issue, we employed the Active Tracer High Resolution Atmospheric Model (ATHAM) with full microphysics and extended the model simulation from the cloud base to the entire column of a single pyro-convective mixed-phase cloud. A series of two-dimensional simulations (over 1000) were performed over a wide range of CCN and dynamic conditions. Fire forcing which induced updraft velocities was used to represent the dynamic parameter. The integrated concentration of hydrometeors over the full spatial and temporal scales was used to evaluate the aerosol and dynamic effects. The results show that the three regimes for cloud condensation nuclei (CCN) activation in the parcel model (namely aerosol-limited, updraft-limited, and transitional regimes) still exist within the pyro-convection simulations for cloud number concentration, but the net production of raindrops and frozen particles occurs mostly within the updraft-limited regime.

To evaluate the IN effect on the properties of pyro-convective clouds, a classical-theory-based ice nucleation parameterization (including immersion and deposition freezing) was implemented in the cloud-resolving ATHAM model to replace the original aerosol-independent ice nucleation scheme. A comparison between the results derived from original model and newly-developed model has been performed, which shows good agreement under standard configuration. Thousands of simulations with different initial

IN densities and fire forcing were conducted, which is helpful to study whether the responses of the hydrometeors to IN and dynamic forcing have continuity. It is found that for the simulated pyro-convective clouds more IN leads to more efficient heterogeneous freezing nucleation; however, the total frozen water content is insensitive to the variation in IN. IN plays a negative role in the cloud water content, which is due to the enhanced growth of ice embryos by vapor deposition that is at the expense of cloud droplet. The IN effect on raindrops and surface precipitation is very small, which can slightly increase rain water and precipitation under strong fire forcing condition. In addition, we have also examined the cloud development through the simultaneous enhancement in CCN and IN. In general, the CCN effect is dominant in cloud microphysics relative to IN.

Furthermore, the process analysis (PA) method has been included in the model configuration, with the aim to assess the contribution of the relevant microphysical processes involving individual hydrometeor. It is found that even the dependence of each hydrometeor on aerosols under different dynamic conditions seems similar, but the underlying mechanisms could be completely different. For instance, independently enhancing CCN could cause a decrease in rain water whether updrafts are weak or strong. However, the main source of rain water content under weak updraft condition is from autoconversion and accretion of cloud droplets; while most of rain water for the latter case with strong updrafts is through melting process from frozen particles. In addition, the investigation of the joint effects of CCN and IN demonstrates that the CCN influence on the cloud properties could be weakened or even counteracted by the opposite impact of IN. This is especially obvious for the total frozen particles: CCN plays a positive role in the number concentration of frozen particles, which would decrease as IN increases. As a result, simultaneous enhancement in both CCN and IN leads to the insensitivity of frozen particles to the variation in initial aerosol concentrations. The enormous simulations in combination with PA method will in-depth unravel how the underlying processes inside a cloud system influence the cloud development and properties.

The nonlinear properties of aerosol-cloud interactions challenge the conclusions drawn from limited case studies in terms of their representativeness, and ensemble stud-

ies over a wide range of aerosol concentrations and other influencing factors are strongly recommended for a more robust assessment of the aerosol effects.

In summary, this thesis investigates in detail the sensitivities of pyro-convective clouds to the variations in CCN and IN under a wide range of dynamic conditions by using a cloud-resolving model. The existing model is modified to include a PA module to evaluate the contribution of microphysical processes, and an aerosol-dependent heterogeneous ice nucleation parameterization. It is clearly shown that atmospheric aerosols, by acting as CCN and IN, could influence the microphysics of pyro-convective clouds, and hence the cloud properties. However, the similar change trends under different dynamic conditions may result from distinct chain of microphysical processes. Further modeling studies of this kind are required to determine whether this conclusion applies to other cloud types and over longer time scales.

Zusammenfassung

Verbrennung von Biomasse ist wichtige Quellen von atmosphärischen Aerosolpartikeln, die als wirksame Wolkenkondensationskeime (CCN) und Eiskerne (IN) dienen könnte, wodurch die Wolkenbildung und Niederschlagsbildung beeinflussen. Als eine extreme Auswirkung der Verbrennung von Biomasse bilden sich die Feuerwolken direkt über dem Feuer, was große Mengen an Wasserdampf, Aerosolpartikel und andere Spurengase in die obere Troposphäre und untere Stratosphäre (UT/LS) transportiert. Die Feuerwolken bieten ein gutes Beispiel mit denen man Wechselwirkungen zwischen Aerosol und Wolken untersuchen kann, da sie Regen, Hagel, Blitze, extreme Windgeschwindigkeiten in niedrigen Atmosphärenschichten und manchmal sogar Tornados hervorrufen.

Eine jüngste Paketmodel-Studie zeigte drei deterministische Regmie der anfänglichen Wolkentropfenbildung, die durch verschiedene Verhältnisse von CCN zu Aufwindgeschwindigkeit charakterisiert sind. Diese Studie lässt jedoch offen wie sich diese Regime während der Wolkenbildung entwickeln. Um diese Frage zu untersuchen haben wir das Active Tracer High Resolution Atmospheric Model (ATHAM) mit kompletter Mikrophysik benutzt und die Modelsimulation von der Wolkenbasis zur ganzen Säule einer einzigen Feuer-Mischphasen-Wolke ausgeweitet. Eine Serie von 2-D-Simulationen (über 1000) wurde über einen großen Bereich von CCN und dynamischen Bedingungen durchgeführt. Die integrierte Konzentration von Hydrometeoren über den gesamten räumlichen und zeitlichen Maßstab wurde für die Beurteilung der Aerosol- und dynamischen Effekte benutzt. Die Ergebnisse zeigen, dass die drei Regime der Aktivierung der Wolkenkondensationskeime (CNN) im Paketmodel (namentlich Aerosol begrenztes, Aufwind begrenztes und Übergangs-Regime) weiterhin in unserer Feuerwolkensimulation für die Wolken-anzahlkonzentration existieren aber die Nettoproduktion von Regentropfen und gefrorenen Partikeln findet hauptsächlich im Aufwind begrenzten Regime statt.

Um den IN-effekt auf die Eigenschaften der Feuerwolken zu prüfen, wurde eine auf der klassischen Theorie basierenden Eisnukletionparameterisierung (mit Immersions- und Depositionsgefrieren) in unser Wolkenmodel eingebaut um den ursprünglichen

aerosolunabhängigen Eisnukleationsprozess zu ersetzen. Die Ergebnisse vom Originalmodel und des neu entwickelten Models stimmen unter der Standardkonfiguration gut überein. Tausende Simulationen mit unterschiedlichen IN-Ausgangsdichten und Aufwinden wurden durchgeführt, was bei der Untersuchung, ob das Ansprechen der Hydrometeoren auf IN und dynamisches Vorantreiben kontinuierlich ist, hilfreich ist. Für die simulierten Feuerwolken gilt, dass mehr IN zu wirksamerer heterogener Gefrierungsnukleation führt; jedoch ist der Anteil des gefrorenen Wassers negativ mit der IN-variation korreliert, da weniger homogene Keimbildung auftritt. Daneben spielen IN auch eine negative Rolle, da sie durch Wasserdampfdeposition zu einem verstärkten Wachstum der Eiskristalle auf Kosten von Wolkentropfen führen. Im Gegensatz zu CCN, führt eine erhöhte Anzahl von IN zu einem leichten Anstieg von Regentropfen und des Niederschlages. Des Weiteren wurde die Wolkenentwicklung bei gleichzeitiger Erhöhung von IN und CCN untersucht. Generell gilt, dass der CCN Effekt in der Wolkenmikrophysik dominierend ist.

Die Methode der Prozessanalyse (PA) wurde, mit dem Ziel den Beitrag relevanter mikrophysikalischer Prozesse einzelner Hydrometeore zu untersuchen, in die ATHAM-Modellkonfiguration integriert. Mit dieser Methode kann gezeigt werden, dass sogar die Abhängigkeit der Hydrometeore von Aerosolpartikeln bei unterschiedlichen dynamischen Bedingungen sehr einheitlich erscheint, jedoch die zugrundeliegenden Mechanismen komplett unterschiedlich sein können. Zum Beispiel kann eine Erhöhung der CCN, sowohl für einen starken als auch einen schwachen Auftrieb, eine Verringerung von Regentropfen zur Folge haben. Für einen schwachen Auftrieb sind Akkretion und Autokonversion von Wolkentropfen die wichtigsten Quellen von Regenwasser. Im Gegensatz dazu stellt für starke Aufwinde das schmelzen von gefrorenen Partikeln die dominante Quelle von Regenwasser dar. Die Untersuchung des kombinierten Effektes von CCN und IN zeigt, dass der Einfluss der CCN auf die Wolkeneigenschaften durch den gegensätzlichen Einfluss der IN geschwächt oder sogar umgekehrt wird. Dies wird speziell für gefrorene Partikel offensichtlich, deren Anzahlkonzentration durch CCN positiv beeinflusst wird. Im Gegensatz dazu würde die Anzahlkonzentration im Fall einer Erhöhung der IN geringer. Daraus resultiert, dass eine gleichzeitige Erhöhung von IN und CCN zu einer Unabhängigkeit der gefrorenen Partikel von der anfänglichen

Aerosolkonzentration führt. Die große Anzahl an Simulation in Kombination mit PA hat das Potenzial die zugrundeliegenden Wolkenprozesse in Bezug auf Entwicklung und Eigenschaften detailliert zu untersuchen.

Die nichtlinearen Eigenschaften des Aerosol-Wolken-Wechselwirkungen Herausforderung die Schlussfolgerungen aus begrenzten Fallstudien im Hinblick auf ihre Repräsentativität und Ensemble Studien über einen weiten Bereich der Aerosolkonzentration und anderen Einflussfaktoren gezogen werden dringend für eine robustere Beurteilung der Aerosoleffekte empfohlen.

In der vorliegenden Arbeit wurden detailliert die Sensitivitäten von pyro-konvektiven Wolken auf Änderungen von CCN und IN für ein breites Spektrum dynamischer Bedingungen unter Verwendung eines wolkenauflösenden Modells untersucht. In das bereits vorhandene Modell ATHAM wurde ein PA Modul zur Untersuchung des Beitrags unterschiedlicher mikrophysikalischer Prozesse und eine Aerosol-abhängige Parametrisierung der heterogenen Eisnukleation integriert. Es konnte klar gezeigt werden, dass das atmosphärische Aerosol als CCN oder IN eine mediume Rolle in der Mikrophysik pyro-konvektiver Wolken spielt. Ähnliche Änderungsraten für unterschiedliche dynamische Bedingungen können aus unterschiedlichen mikrophysikalischen Prozessketten resultieren. Weitere Modellstudien dieser Art werden benötigt um zu untersuchen, ob die Rückschlüsse auch auf andere Wolkenarten und längere Zeitskalen übertragen werden können.

Contents

Chapter 1 Introduction

1.1 Biomass burning and pyro-convective clouds

Biomass burning is identified as a significant source of trace gases, greenhouse gases, and aerosol particles, such as carbon dioxide, carbon monoxide, volatile and semivolatile organic compounds, black carbon, and organic carbon, all of which play a remarkable role in atmospheric chemistry and climate change (Andreae, 1991; Reid et al., 2005; Luderer et al., 2006; Trentmann et al., 2006; Rosenfeld et al., 2007; Fromm et al., 2008). Mostly because of human activities, the risk of wild fires (e.g., forest, grassland, and agricultural fires) has increased significantly, especially during the last two decades. Andreae (1991) indicated that biomass burning has a contribution of 25% to greenhouse forcing on global average. Morris et al. (2006) found enhanced ozone precursor species emitted from vegetation fires, which led to significant increases in ozone concentrations by as much as 50–110% in local regions. At global scale, van der Werf et al. (2006) suggested that annually approximate 4% of the total carbon (i.e., 2.5 Pg C) fixed by plants was released to the atmosphere due to biomass burning. Hodzie et al. (2007) suggested that the amount of primary aerosols emitted from large biomass burning was comparable to the amount generated from anthropogenic sources and that long-range transport of pollutants lead to remarkable and large-scale change in atmospheric radiative properties. Chang and Song (2009) reported annually an area of ~3.5 million km^2 was subject to biomass burning worldwide based on remote-sensing data, which accounted for ~3.2% of the global continental area.

Biomass burning generates significant amounts of smoke aerosols, and the fires loft soil particles that contain minerals (Pruppacher and Klett, 1997), which could alter the Earth's energy budget, and are the drivers of climate change (IPCC, 2013). Furthermore, both of smoke particles and mineral dust particles could serve as effective cloud condensation nuclei (CCN) and ice nuclei (IN) (Hobbs and Locatelli, 1969; Hobbs and Radke, 1969; Kaufman and Fraser, 1997; Sassen and Khvorostyanov, 2008), thereby affecting the formation of clouds and precipitation. As an extreme consequence of biomass burning, pyro-convective clouds feed directly from the smoke and heat released from

fires with considerable vertical development (Andreae et al., 2004; Luderer, 2007). The photograph in Figure 1.1 schematically illustrated the structure of pyro-convective clouds. The fire-caused cumuliform cloud forms directly above the fire, which transports enormous amount of water vapor, aerosol particles and other trace gases to the upper troposphere and lower stratosphere (UT/LS). The pyro-convective clouds may involve precipitation, hail, lightning, extreme low-level winds, and in some cases even tornadoes (Fromm et al., 2006).

Figure 1.1: *Photograph of a pyro-convective cloud.*

Pyro-convective clouds provide a good example with which to study aerosol-cloud interactions (Reutter et al., 2009). Based on the in situ measurements of pyro-convection, Andreae et al. (2004) reported that the smoke particles could significantly reduce cloud droplet size, inhibit precipitation and hence weaken the aerosol scavenging process, and enhance the production of large frozen particles. Trentmann et al. (2006) described the injection of biomass burning emissions into the lower stratosphere by pyro-

convection through three-dimensional model simulations, which shows extraordinary dynamical and microphysical properties of deep pyro-convection. They found the fire-released sensible heat dominates the convection initiation, and the release of latent heat from condensation and freezing processes governs the overall energy budget. Luderer (2007) systematically simulated the evolution of pyro-cumulonimbus clouds (pyroCb) caused by a forest fire and performed sensitivity studies on the response of convective dynamics to the release of sensible heat by the fire, meteorological conditions, and ambient aerosols. Their results were consistent with observations, and illustrated that fire heating and large-scale meteorological conditions played an important role in the formation and transport of pyroCb. Rosenfeld et al. (2007) has investigated the cloud top morphology and microstructure, precipitation and cloud electrification of a pyro-convection. They concluded that the combination of heat and smoke created a cloud with extremely small and short-lived highly supercooled drops, which is incapable to produce precipitation, and has enormous climatic consequences. Tao et al. (2012) summarized the aerosol effects on the CCN activation, warm-rain process, mixed-phase clouds, and precipitation in terms of microphysical scale, cloud-resolving scale, and regional scale, which are retrieved from the theoretical analysis, observations, and numerical modeling. The underlying mechanisms and the comparison between the results from different convective cloud studies was also presented and analyzed. Fan et al. (2013) carried out monthly 3-D simulations over three different regions and found the microphysical effect controlled by aerosols is the major factor that determines the properties of deep convective clouds, rather than the updraft-related dynamics.

1.2 Aerosol-cloud interactions

Aerosol-cloud interaction and climate change:

The atmospheric aerosols alter cloud properties mainly in terms of these two aspects: radiative and microphysical processes (Graf, 2004; Koren et al., 2008; Joos et al., 2014). The radiative forcing due to aerosol-cloud interactions is formerly known as the first indirect aerosol forcing or cloud albedo effect, which is through the modification of the cloud

droplet size and surface precipitation (Ramanathan et al., 2001). Enhanced aerosol particles reduce liquid drop size, increase the number of cloud droplets and ice crystals, and suppress the precipitation at the surface. These in turn would prevent more solar radiation reaching Earth's surface, and thereby increase solar heating in the atmosphere. Radiative forcing shown in Figure 1.2 quantifies the change in energy fluxes caused by this driver, and there is large uncertainty in estimating the net change of radiative forcing (IPCC, 2013). Due to the limitation of the model used here, the radiative properties of pyroclouds are not assessed in this work.

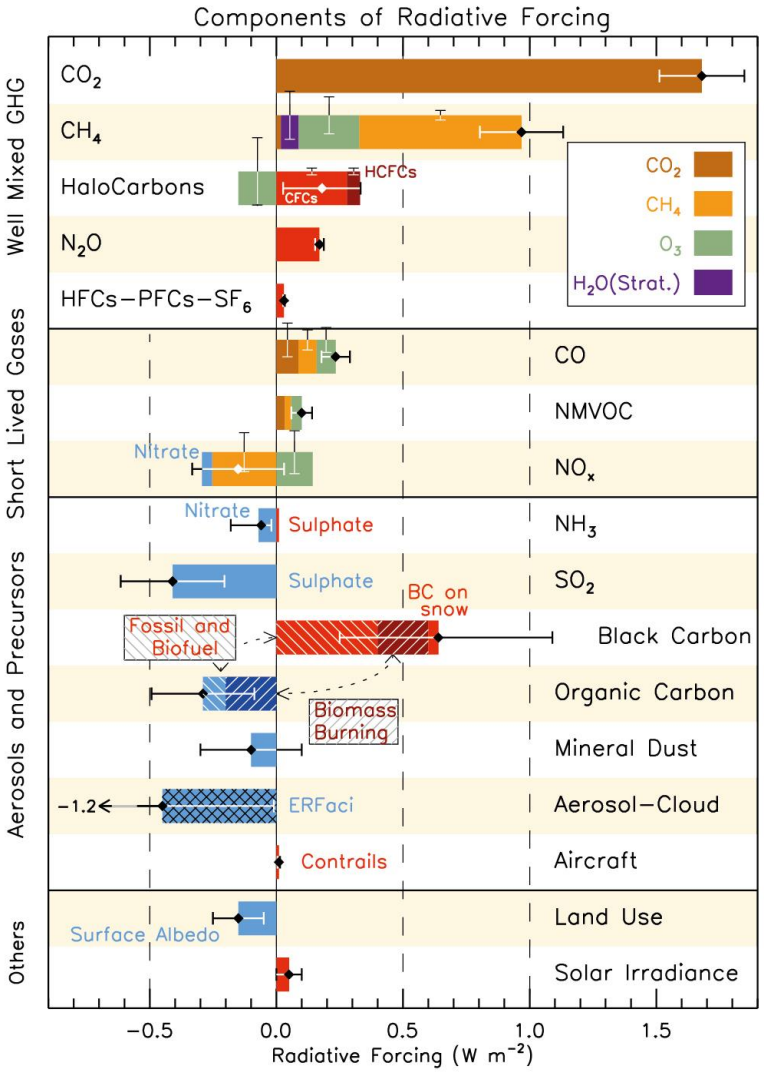

Figure 1.2: *Radiative forcing bar chart for the period 1750–2011 on the basis of released compounds (gases, aerosols or aerosol precursors) or other changes. Red colors*

denote positive forcing (warming effect), and blue denotes negative (cooling). The diamond symbols indicate the net impact of individual contributor and the horizontal error bars show its uncertainty (5–95% confidence range).

At present, numerous field measurements and modeling simulations focused on investigating the ways that the aerosol particles impact cloud microphysics by acting as CCN and IN (van den Heever et al., 2006; Fan et al., 2010; Morrison, 2012). Basically, the variation in aerosol concentrations could affect the properties of clouds (e.g., droplet size distributions, cloud depth, cloud life time, cloud fraction), warm rain process, cold rain process, and ultimately precipitation (Tao et al., 2012; Fan et al., 2013). It is well known that an increase in aerosol concentrations results in larger liquid water path and smaller droplet size. It is surprising that enhanced aerosols could lower cloud fraction, cloud size, cloud-top height and depth, which results from the competing effects of precipitation and droplet evaporation process (Xue and Feingold, 2006). It is suggested that aerosols may play a positive role in cloud fraction for larger clouds which are less sensitive to entrainment and evaporation. Increased aerosols by providing large amounts of CCN could suppress warm rain processes (e.g., autoconversion, accretion) due to the reduction in cloud droplet size and a narrow droplet spectrum that prevents collision and coalescence processes (Ramanathan et al., 2001; Rosenfeld et al., 2008). The delay of precipitation invigorates cloud dynamics, leads to rapidly ascending of cloud water to upper troposphere and lower stratosphere and enhances the consequent cold rain processes (Andreae et al., 2004; Tao et al., 2012). The regulation of precipitation due to aerosols can significantly affect the hydrologic circulation and surface energy budget of the climate system.

On the other hand, due to growing knowledge on ice nucleation, great efforts have been spent to investigate the aerosol effect on clouds by serving as IN based on field campaigns (DeMott et al., 2003a; DeMott et al., 2003b; Prenni et al., 2007; Richardson et al., 2007), laboratory research (Roberts and Hallett, 1968; Zuberi et al., 2002) and modeling simulations (Eidhammer et al., 2009; Spichtinger and Cziczo, 2010; Yun and Penner, 2012). For instance, Eidhammer et al. (2009) studied the IN impact on ice formation us-

ing a warm cloud parcel model on the basis of three types of heterogeneous ice nucleation representation, which implied different regimes for cloud ice, as well as for different ice nucleation processes. The research based cloud resolving model simulations suggest more IN leads to more efficient freezing process, deeper anvils and enhanced precipitation (van den Heever et al., 2006; Fan et al., 2010; Seifert et al., 2012).

Challenges in studying aerosol-cloud interactions:

Aerosol effects are associated with significant uncertainty in light of the seemingly contradictory resulting from different studies. For instance, several studies have indicated that increasing aerosol concentrations could reduce cloud fraction and inhibit cloud formation (Albrecht, 1989; Ackerman et al., 2000; Kaufman et al., 2002; Koren et al., 2004), whereas it is suggested that more aerosols can increase the cloud fraction in other studies (Norris, 2001; Kaufman and Koren, 2006; Grandey et al., 2013). Precipitation from stratiform clouds can be inhibited by elevated aerosol concentration (Zhang et al., 2006), while precipitation from convective clouds can be either suppressed or enhanced (Ackerman et al., 2003; Andreae et al., 2004; Altaratz et al., 2008; Lee et al., 2008; Teller and Levin, 2008; Fan et al., 2013; Camponogara et al., 2014). In addition, changing aerosol concentrations have also been found to exert non-monotonic influences (either positive or negative) on a wide range of cloud properties, such as homogeneous freezing (Kay and Wood, 2008), frozen water particles (Saleeby et al., 2009; Seifert et al., 2012), and convection strength (Fan et al., 2009).

While aerosol-cloud interactions appear puzzling at regional and global scales, the interplay at the microphysical scale, i.e., cloud condensation nuclei (CCN) activation, has been well characterized. CCN activation can be well predicted by the Köhler theory (Kohler, 1936) and by a series of extended equations (Shulman et al., 1996; Kulmala et al., 1997; Laaksonen et al., 1998). Simplified treatments that reduce the effects of aerosol chemistry on CCN activation to a single parameter have also proven effective; for example, the κ-Köhler equation has been demonstrated to be a practical method in the description of CCN activation and the prediction of CCN number concentrations (Petters and

Kreidenweis, 2007; Su et al., 2010; Gunthe et al., 2011). However, the knowledge of IN nucleation is much less than CCN activation based on current research (Tao et al., 2012). The primary difficulty is due to the lack of measurements of IN properties, i.e., their source, distribution, abundance, variety, and nucleating ability (Burrows et al., 2013), and the empirical treatments of IN nucleation involve large uncertainties for different regions (Prenni et al., 2007). When we upscale the activation of a single aerosol particle to aerosol populations at the cloud base, the impact of aerosols on the number of activated CCN still appears simple and can be well described (Conant et al., 2004; Fountoukis et al., 2007; Reutter et al., 2009; Tessendorf et al., 2013). In-situ aircraft measurements of clouds over marine and continental areas have demonstrated the significant relationship between anthropogenic aerosol concentration and cloud drop number concentration (Conant et al., 2004; Fountoukis et al., 2007). Reutter et al. (2009) implemented observationally–constrained CCN activation microphysics into parcel models, and they found three generic regimes of CCN activation at the cloud base (Figure 1.3). For IN nucleation into cloud ice, a prognostic description of ice nucleation is possible and common for present studies. Eidhammer et al. (2009) showed different ice formation regimes based on different ice nucleation schemes in a parcel model, and the predicted IN concentrations are comparable with previous ice nucleation measurements (DeMott et al., 2003a; Prenni et al., 2007; Richardson et al., 2007; Eidhammer et al., 2009). The question remains, if CCN activation (microphysical scale) and initial warm cloud formation (air parcel scale) can be described accurately, why is it so difficult to describe the interaction at regional and global scales (Stevens and Feingold, 2009)?

In particular, to what extent does complexity arise from the inclusion of other hydrometeor types, such as frozen particles and relevant microphysical processes during subsequent cloud evolution? At which scale do the aerosol–cloud interactions become complex? These questions are the first motivation for this study. One explanation for these seemingly contradictory results is that aerosol effects are regime–dependent, which means that aerosol effects can vary under different meteorological conditions (updraft velocity, relative humidity, surface temperature, and wind shear), cloud types, aerosol properties (size distribution and chemical composition) and observational or analysis scales (Levin and Cotton, 2007; Tao et al., 2007; Khain et al., 2008; Rosenfeld et al., 2008; Fan

et al., 2009; Khain, 2009; Reutter et al., 2009; McComiskey and Feingold, 2012; Tao et al., 2012). It is thus important to investigate the regime-dependence of aerosol-cloud interactions and to improve the representation of cloud regimes in models (Stevens and Feingold, 2009). Being able to distinguish those conditions under which cloud formation is updraft-limited (aerosol-insensitive) as discussed in Reutter et al. (2009) would provide the advantage for future work that one could, for many purposes, neglect aerosol effects on clouds in areas that are usually updraft-limited.

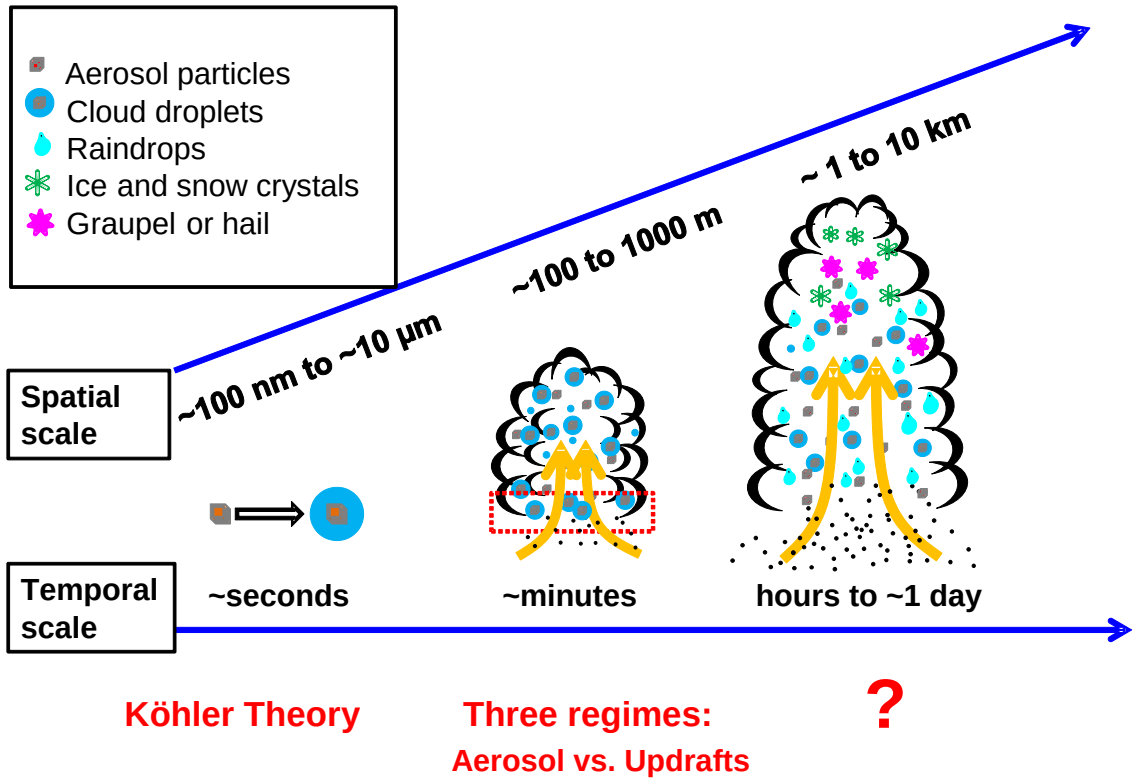

Figure 1.3: *Overview of the research approaches on multi-scale cloud initialization and development.*

Another challenge in evaluating the aerosol effects lies in the nonlinear properties of aerosol–cloud interactions. Most previous research investigated the response of clouds

and precipitation to the perturbation of aerosols based on two or several individual scenarios, by doubling or tripling the number concentration of aerosol particles. This is fine for the linear dependence. Since aerosol-cloud interaction is a nonlinear process, such method may not reflect the real aerosol effect. An exemplary case is shown in Figure 1.4, in which it is clear that the local derivatives (dY/dX) can be different from $\Delta Y/\Delta X$ determined by the difference between A and B cases.

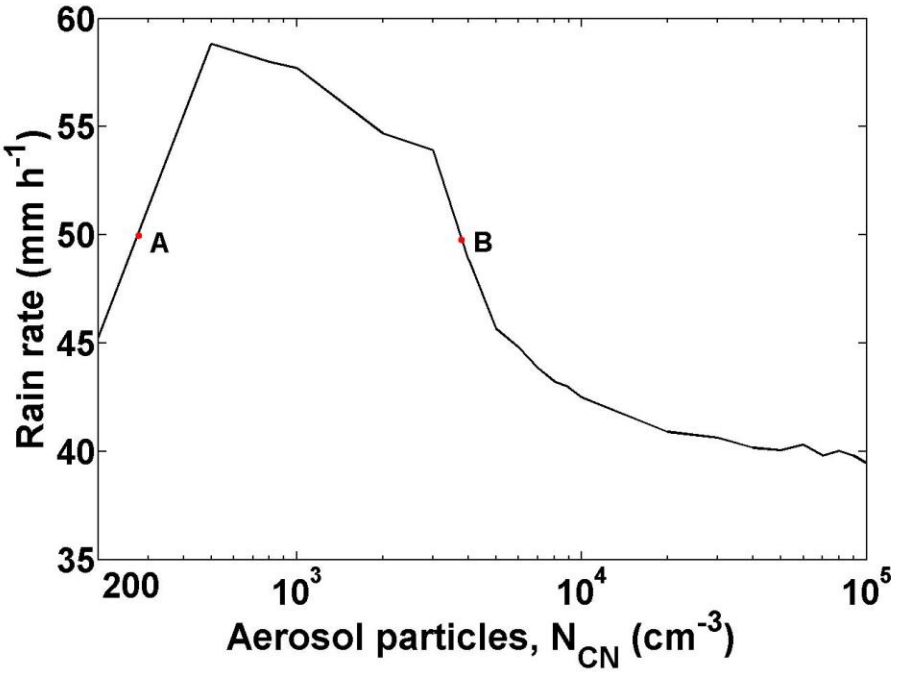

Figure 1.4: *Conceptual model of the nonlinear relationship between aerosol concentrations and rain rate (data are from 2-D simulation results of this work).*

1.3 Objectives of the thesis

The major goal of this study is to investigate and explain the regimes dependence (in comparison to the cloud parcel simulation) of cloud formation on aerosols and updrafts at a larger scale with more hydrometeors and complicated microphysical processes involved. The formation and evolution of a single pyro-convective cloud is simulated by using the Active Tracer High Resolution Atmospheric Model (ATHAM) under various aerosol and dynamic conditions. Over 1000 simulations cover a large range of aerosol concentrations

and updraft velocities, based on which the determination of regimes becomes possible. The single convective clouds represent the up-scaled cases closest to the parcel model simulation. By taking the pyro-convective clouds as an example, we demonstrate the ability of ensemble simulations to determine the regime dependence and resolve the nonlinear properties of aerosol-cloud interactions. A process scale with resolution of ca. 1 km has been suggested as the appropriate scale at which to characterize processes related to aerosol-cloud interactions (McComiskey and Feingold, 2012). In addition to cloud droplets, precipitable hydrometeors (raindrops, ice, snow, graupel, and hail) are also included in this work.

In order to quantify the complex interactions between aerosols and clouds, a process analysis (PA) module is implemented within our model. In addition to studying aerosol effect by providing CCN, the model will be expanded by implementing a classical-nucleation-theory-based parameterization of heterogeneous ice nucleation to evaluate the influence of IN number concentration on the cloud evolution and precipitation.

This thesis is organized as follows: It begins in Chapter 2, which describes the design of numerical experiments; then the model development will be presented and evaluated based on a specific case; Chapter 3 illustrates the regime dependence of individual hydrometeor (i.e., cloud droplets, raindrops, and frozen particles) on different CCN and dynamic conditions. The results for the number concentration of cloud droplets (with three different limited regimes) are in agreement with previous parcel model result. The process analysis (PA) method is applied to evaluate the dominant mechanisms in regulating the origination and evolution of cloud system. In Chapter 4, a parameterization of heterogeneous ice nucleation based on the classical nucleation theory is implemented in ATHAM model to study the IN effect on pyro-convective clouds. The joint effect of changing CCN and IN on clouds and precipitation will also be presented and discussed. Finally, a summary and a perspective are presented in Chapter 5. Much of the work presented here has been submitted to peer-reviewed international scientific journal.

Chapter 2 Numerical experiments and model development

2.1 Introduction

This work is based on a two-moment cloud-resolving model ATHAM, which could probe the sensitivity of the initiation and evolution of pyro-convective clouds to CCN number concentrations in the atmosphere. But the relevant processes cannot be evaluated on the basis of present model configuration, which is essential to analyze the underlying mechanisms of cloud evolution. On the other hand, the existing ice nucleation scheme is from the deposition-condensation nucleation formula given by Meyers et al. (1992), which ignored the impact of different aerosol types and aerosol number in atmosphere. Therefore, adjusting the present model by more detailed parameterizations is needed and will lead to a more comprehensive understanding of the microphysical processes in a cloud system.

In this chapter, the design and setup of the numerical experiments is described in Sect. 2.2; the relationship between fire forcing, the corresponding updraft velocity and temperature is discussed in Sect. 2.3; in Sect. 2.4, the modification of the ATHAM model by coupling process analysis (PA) module and detailed ice nucleation parameterization is demonstrated and evaluated. A summary will be presented in Sect. 2.5.

2.2 Design of numerical experiments

2.2.1 ATHAM: model and configuration

ATHAM is a non-hydrostatic model that is used to study both cloud formation and evolution in response to changes in updrafts and aerosol particle concentration. ATHAM was designed initially to investigate high-energy plumes in the atmosphere and applied to simulate volcanic eruptions and fire plumes (Herzog, 1998; Oberhuber et al., 1998). The model comprises eight modules: dynamics, turbulence, cloud microphysics, ash aggregation, gas scavenging, radiation, chemistry, and soil modules (Herzog et al., 1998; Oberhuber et al., 1998; Graf et al., 1999; Herzog et al., 2003). Cloud microphysical interactions are represented by an extended version of the two-moment scheme developed by

Seifert and Beheng (2006), which includes the hail modifications by Blahak (2008), and is able to predict the numbers and mass mixing ratios of six classes of hydrometeors (cloud water, ice crystals, raindrops, snow, graupel, and hail; detailed in Table 2.1) and water vapor. The microphysical scheme is presented in detail in appendix A. It has been validated successfully against a comprehensive spectral bin microphysics cloud model (Seifert et al., 2006). The cloud nucleation (CCN activation) module is based on the lookup table derived from parcel model simulations for pyro-convective clouds (Reutter et al., 2009).

Table 2.1: *Typical characterizations of the frozen hydrometeor classes.*

		Diameter (mm)	Density (g cm^{-3})	Terminal velocity (m s^{-1})
Cloud ice	Columnar crystals	0.01—1[(1)]	0.36—0.7 [(2)]	0.013—0.055[(2)]
	Plate-like	0.01—1[(1)]	~0.9[(1)]	0.02—0.06[(2)]
	Dendrites	0.1—3[(1)]	0.3—1.4[(1)]	0.25—0.7[(3)]
Snow		2—5[(1)]	0.05—0.89[(1)]	0.5—3[(1)]
Graupel		0.5—5[(1)]	~0.4[(1)]	3—14[(1)]
Hail		5—80[(1)]	0.8—0.9[(1)]	10—40[(1)]

[(1)]Pruppacher and Klett (1997).

[(2)]Jayaweer and Ryan (1972).

[(3)]Mitchell and Heymsfield (2005).

ATHAM can execute both 2-D and 3-D simulations. As our main purpose is to demonstrate a general pattern of sensitivity of clouds and precipitation to a wide range of aerosol concentrations (N_{CN}) and updrafts (represented by the intensity of fire forcing, which triggers updraft velocities), two-dimensional simulations rather than the more expensive three-dimensional runs are performed. The fire forcing and meteorological conditions are set up to simulate the Chisholm forest fire (Luderer, 2007; Rosenfeld et al., 2007), which is a well-documented case of pyro-convection. The two-dimensional simu-

lations were performed at the cross section of the fire front. The simulation domain was set at 85 × 26 km with 110 × 100 grid boxes in the x and z directions. The horizontal grid box size at the center of the x direction was equal to 500 m, and it enlarged towards the lateral boundaries due to the stretched grid (Figure 2.1). The vertical grid spacing at the surface and the tropopause was set to 50 and 150 m, respectively. The lowest vertical level in our simulation was set at 766 m above sea level, corresponding to the lowest elevation of the radiosonde data, which is close to the elevation of Chisholm at about 600 m (ASRD, 2001).

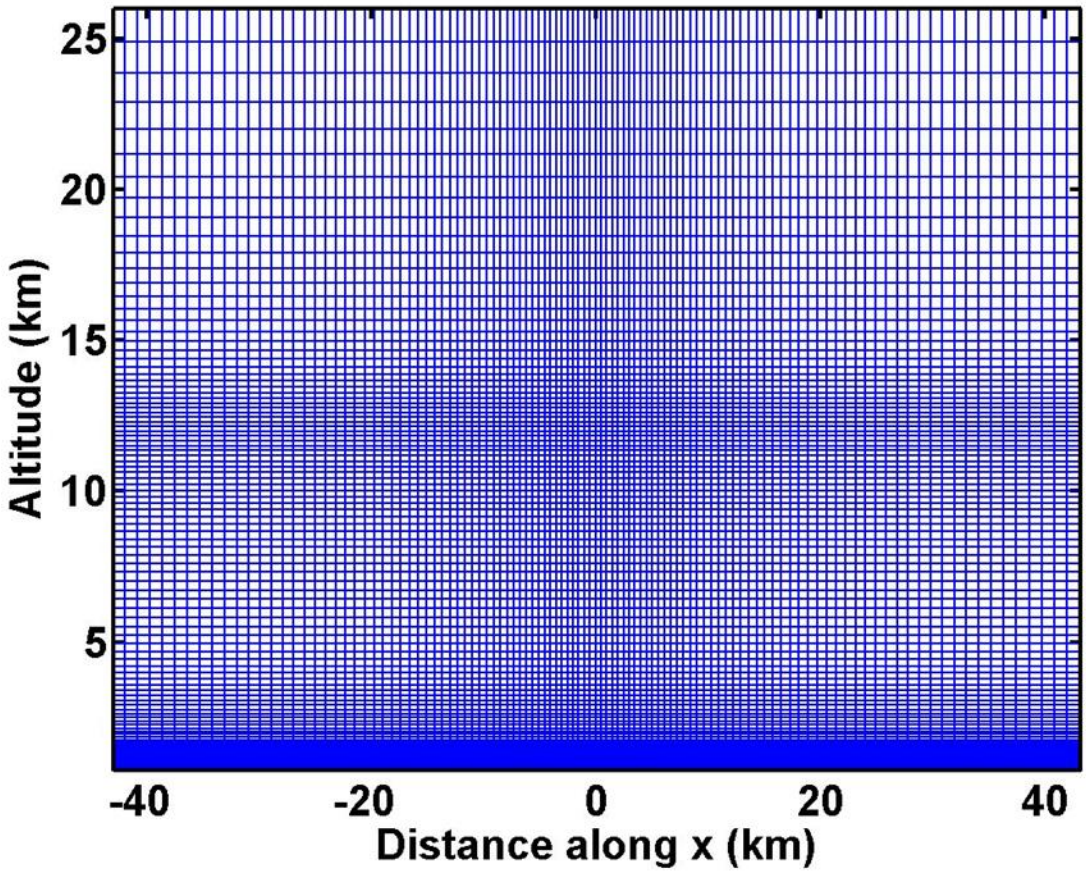

Figure 2.1: *The 110×100 grid points in the computational domain.*

The simulations were initialized horizontally homogeneously with radiosonde data from about 200 km south of the fire on 29 May 2001, which is the same as in Luderer (2007) (Figure 2.2). The vertical profiles of the temperature and dew point temperature

reveal a moderate instability in the atmosphere. Open lateral boundaries were used for the model simulations. The means of wind speed and specific humidity were nudged towards the initial profile at the lateral boundaries. The fire forcing was introduced in the middle grid in the bottom layer of the domain, and its intensity remained constant throughout the simulation of each scenario. Each case was run for three simulated hours until the clouds were fully developed and had reached steady state.

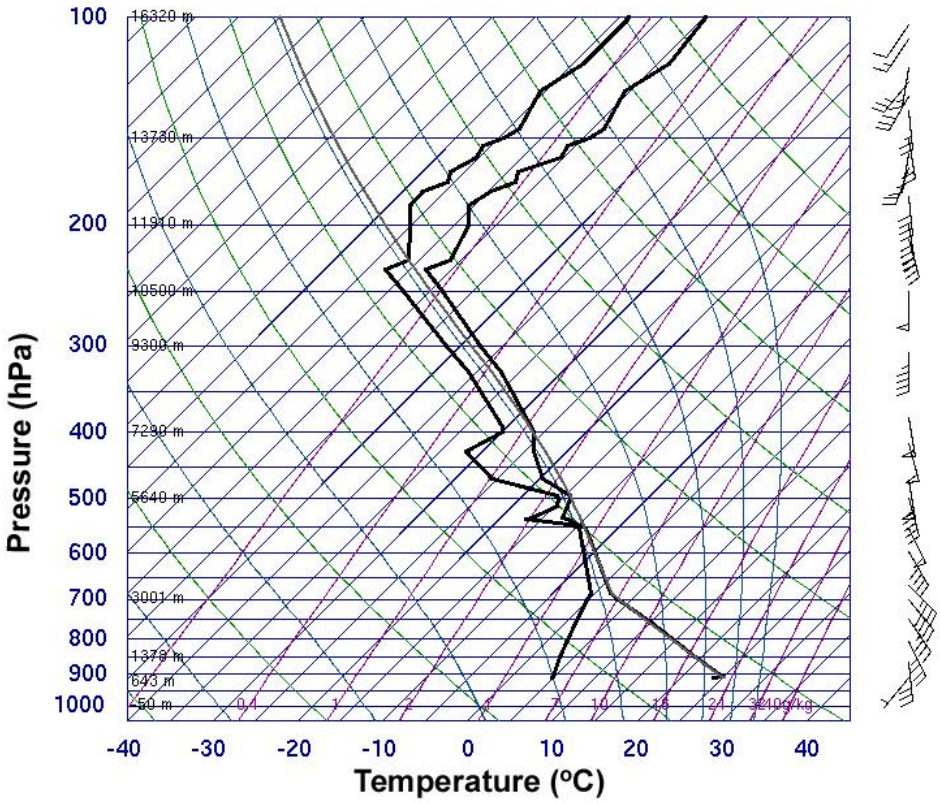

Figure 2.2: *Atmospheric sounding launched near Edmonton, Alberta on 29 May 2001. The right black line represents the temperature, and the left black line corresponds to the dew-point temperature. This weather information is from the University of Wyoming Department of Atmospheric Science (http://weather.uwyo.edu/).*

2.2.2 Aerosol particles and fire forcing

Atmospheric aerosol particles (N_{CN}) affect cloud formation through two pathways by acting as CCN and IN. In chapter 3, we limited the scope of aerosol-cloud interactions to

CCN activation only which follows the previous study of Reutter et al. (2009). Thus, in that part, changes in N_{CN} do not directly influence frozen hydrometeors by providing IN; rather, they indirectly influence them through their impact on CCN activation and subsequent processes. In chapter 4, we focus on the sensitivity of individual hydrometeor to various potential ice nuclei (IN) number concentrations and updraft velocities. Therefore, changes in N_{CN} only directly influence frozen hydrometeors by providing primary IN, without exerting effect through CCN activation (potential CCN concentration is fixed to be 10,000 cm^{-3}). The joint influence of aerosols by serving as both CCN and IN is also simulated and discussed.

In the study of CCN effect, 1302 cases (31 N_{CN} × 42 fire forcing values) were simulated to evaluate the interplay of aerosol concentration and updrafts on the formation of clouds and precipitation. The N_{CN} varied from 200 to 100,000 cm^{-3}. In each case, N_{CN} was prescribed (distributed uniformly across the modeling domain and kept identical throughout the simulation). A similar treatment and approach has been used in previous studies (Seifert et al., 2012; Reutter et al., 2014). Some previous studies have pointed out that a prescribed aerosol scheme overestimates the magnitude of CCN concentrations compared to a prognostic aerosol scheme because it lacks a representation of the efficient removal of particles by nucleation scavenging (Wang et al., 2013). As mentioned above, we used the lookup table of Reutter et al. (2009) for the CCN activation. This table is determined for fresh biomass burning aerosols with a hygroscopicity parameter κ of 0.2 and a log-normal size distribution (a geometric mean diameter of 120 nm and a geometric standard deviation of 1.5; Reutter et al. 2009). For the present study, the aerosol characteristics, such as size distribution, chemical composition, hygroscopicity and mixing state, are in fact rather unimportant compared with the order-of-magnitude changes in the aerosol number concentration (Reutter et al., 2009; Karydis et al., 2012). Therefore, the effects of variations in aerosol characteristics were not considered in our study. In all simulations, clouds were triggered by the fire forcing, which was assumed constant during the simulation. The fire forcing intensity varied from 1×10^3 to 3×10^5 W m^{-2}. The correlation between the initial fire forcing and corresponding updraft velocity and temperature at the cloud base was probed and is described in Sect. 2.3.

In the study of IN effect, over 1000 cases were also carried out to evaluate the dependency of cloud hydrometeors to IN concentrations and updrafts. The N_{CN} varied from 200 to 100,000 cm^{-3} and the fire forcing intensity varied from 1×10^3 to 3×10^5 W m^{-2}. N_{CN} was also prescribed with log-normal size distribution. Within this work, only the efficiency of soot particles acting as IN is investigated.

In reality, the composition and quantity of biomass burning emissions depend on the moisture content of fuels, combustion conditions, weather situation, and fire behavior (Bytnerowicz et al., 2009). Furthermore, the biomass burning plumes can in turn change the relative humidity as well. The aerosol particle number concentrations in biomass burning plumes usually exceed 10^4 cm^{-3}, and can be up to ~10^5 cm^{-3} (Andreae et al., 2004; Reid et al., 2005). In contrast to regular convection, the updraft velocities in pyro-convective clouds are normally larger than 20−30 m s^{-1} (Khain et al., 2005). On the basis of these facts, within our work more attention is paid to situations with higher aerosol concentration (>10^4 cm^{-3}) and strong updrafts (>20 m s^{-1}), which are more representative of pyro-convective clouds.

2.3 Relationship between updraft velocity, temperature, and fire forcing

Fire forcing does not affect the cloud activation of aerosols directly, but it can affect activation indirectly by triggering strong updraft velocities. Updrafts are of importance in the formation of clouds and precipitation for redistributing energy and moisture. To cover a wide range of conditions, the updraft velocities range from ca. 0.25 to 20 m s^{-1} (Reutter et al., 2009), which represent the range found in trade wind cumulus to thunderstorms (Pruppacher and Klett, 1997).

The probability distribution function of vertical velocities (w) at cloud base layer under different fire forcing conditions is shown in Figure 2.3a. The velocity on top of the input fire forcing is usually the largest, and decreases towards the lateral sides. These largest velocities under different fire forcing conditions are plotted against the input fire forcing (range of 1×10^3 to 3×10^5 W m^{-2}, $N_{CN} = 1 \times 10^3$ cm^{-3}) in Figure 2.3b. The shaded area indicates the variability of estimation over each simulation period. According to

the figure, *w* at cloud base varies monotonically from 1.8 to 27 m s^{-1} as fire forcing increases from 1 $\times 10^3$ to 3 $\times 10^5$ W m^{-2}. The positive relationship suggests that fire forcing could be a good indicator of vertical velocity. Because it is a variable of central interest to the cloud research community, the maximum vertical velocity is provided along with the fire forcing values as an additional axis in the following plots.

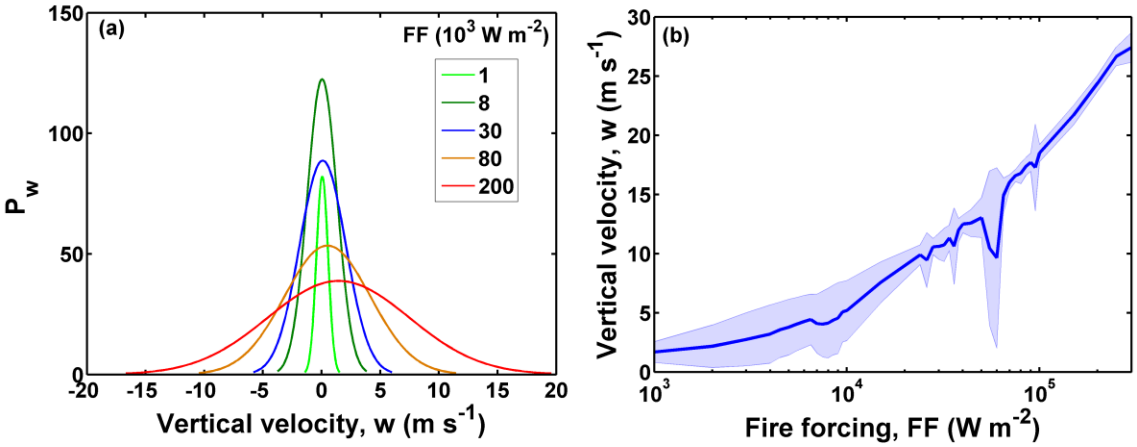

Figure 2.3: *Probability distribution function of vertical velocities (w) at cloud base under different fire forcing (FF) conditions (a). Relationship between input FF and induced vertical velocity (w) at cloud base (b). The aerosol concentration is 1,000 cm^{-3}. The shaded area represents the variability of estimation (±0.5σ).*

Another variable of key meteorological interest is the maximum temperature at cloud base. To clarify how temperature is affected by fire forcing in our simulations, the relationship between fire forcing and the corresponding maximum temperature at cloud base is shown in Figure 2.4. As variations in aerosol number concentrations have very little effect on the temperature profile, we show this relationship for only one aerosol concentration (N_{CN}=5,000 cm^{-3}) as an example. As can be seen in Figure 2.4, the cloud base temperature increases linearly from 7.6 to 16.4 ℃, as fire forcing is enhanced from 1 × 10^3 to 3 $\times 10^5$ W m^{-2}. In order to more clearly convey the effect of the heating imposed in the simulation, we have used this linear relationship to add the maximum cloud base temperature as a secondary axis in the following figures.

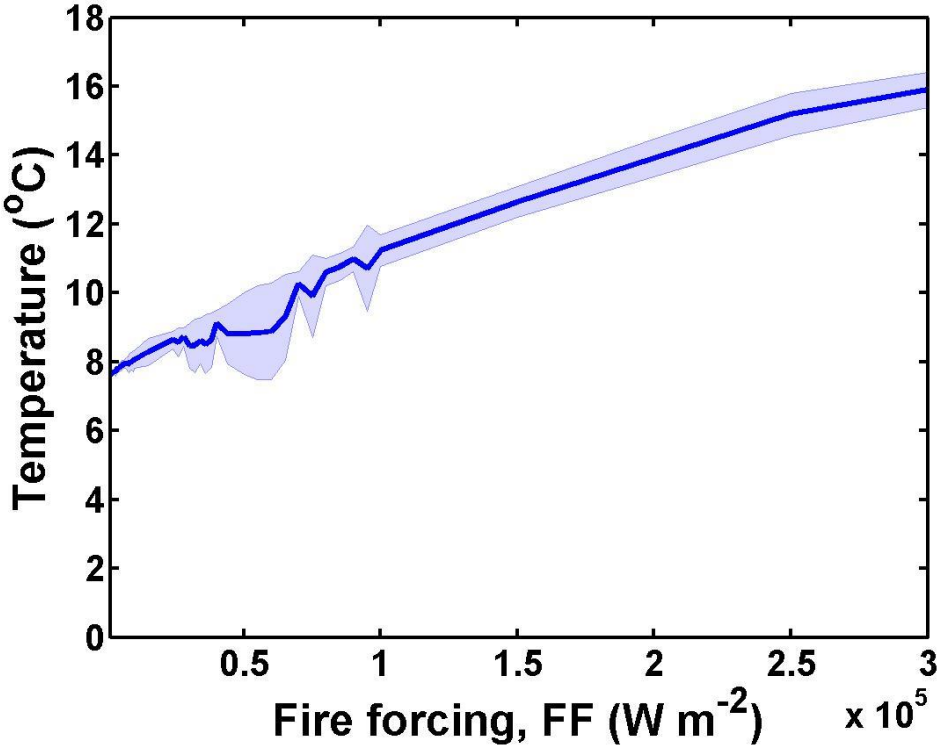

Figure 2.4: *The correlation of fire forcing and the corresponding maximum temperature at cloud base. The shaded area indicates the variability of estimation (±0.5σ) over each simulation period.*

Finally, we note that the horizontal wind shear can also affect the convection strength (Fan et al., 2009), which could be investigated in detail in future studies.

2.4 Model development

2.4.1 Process analysis

Cloud properties are subject to several tens of microphysical processes, e.g., cloud droplet nucleation, autoconversion, freezing, condensation, and evaporation (Figure 2.5, Seifert and Beheng, 2006). Elevated concentrations of hydrometeors can be caused either by an increase in their sources or by a decrease in their sinks. It is necessary to quantify and qualify those processes and feedbacks in order to unravel the underlying mechanisms,

and to make clear which cloud regimes are influenced in which manner by which path of processes. For a better understanding of the mechanisms, we employed the process analysis (PA) method to quantify the causation of changes in the concentrations of individual hydrometeor classes. The PA method has been widely utilized to investigate the formation and evolution of gaseous pollutants and particulate matter (Tonse et al., 2008; Yu et al., 2009; Liu et al., 2010), and has also been successfully implemented in cloud simulation research (Lin et al., 1983). The PA calculates the time-integrated rate of change in the mass or number concentration of each hydrometeor type caused by a particular process, thereby enabling the determination of the relative importance of relevant microphysical processes under different fire forcing and aerosol conditions.

In addition to the standard model output (e.g., time and spatial series of mass and number concentrations of hydrometeors, and meteorological output), the inclusion of PA module archives additional parameters, i.e., the time rate of change in hydrometeors due to individual microphysical processes. Appendix B summarizes all the microphysical processes and their abbreviations.

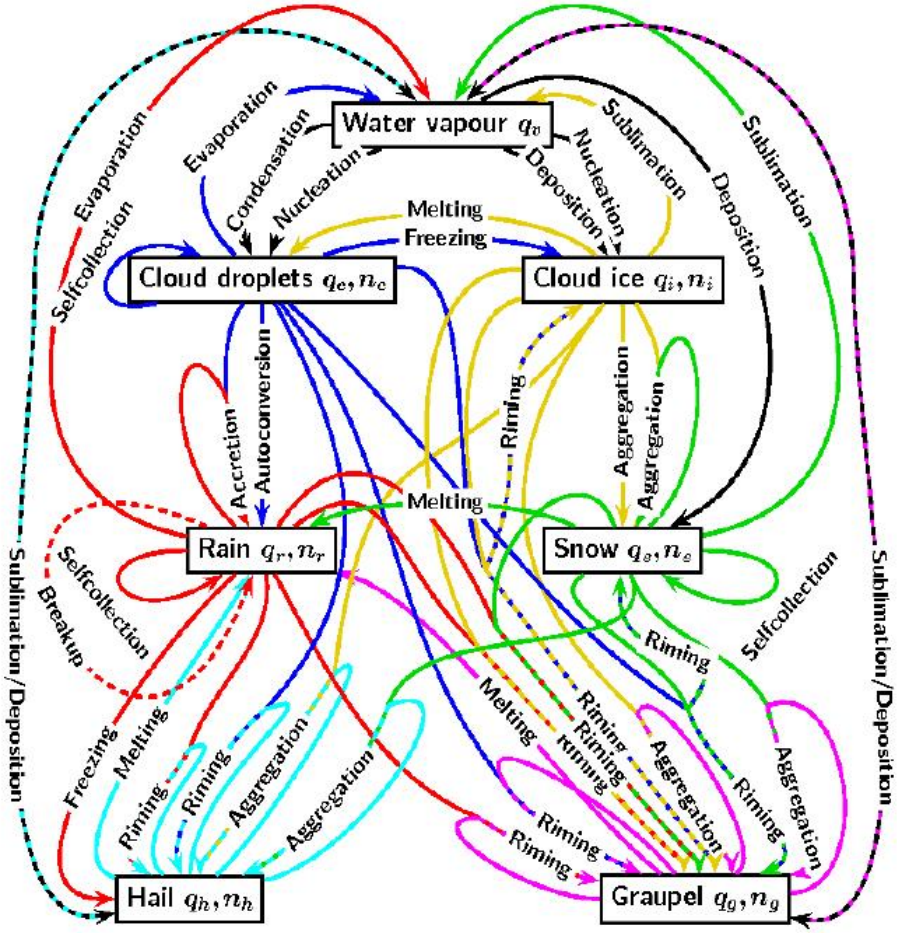

Figure 2.5: *Simplified schematic diagram of the microphysical interactions in the two-moment Seifert scheme (from U. Blahak, private communication).*

To examine the PA module, we take a case with strong fire forcing (300,000 W m^{-2}) and low aerosol number concentration (200 cm^{-3}) for example and the discussion is as follows. Figure 2.6a illustrates the spatiotemporal distribution of cloud water content, while the microphysical processes involving cloud droplet formation are displayed in Figure 2.6b. What is the percentage of the contribution of each process and how do they response to the changing updrafts and aerosols in the atmosphere? This is the fundamental questions with which the newly-developed PA module tries to deal.

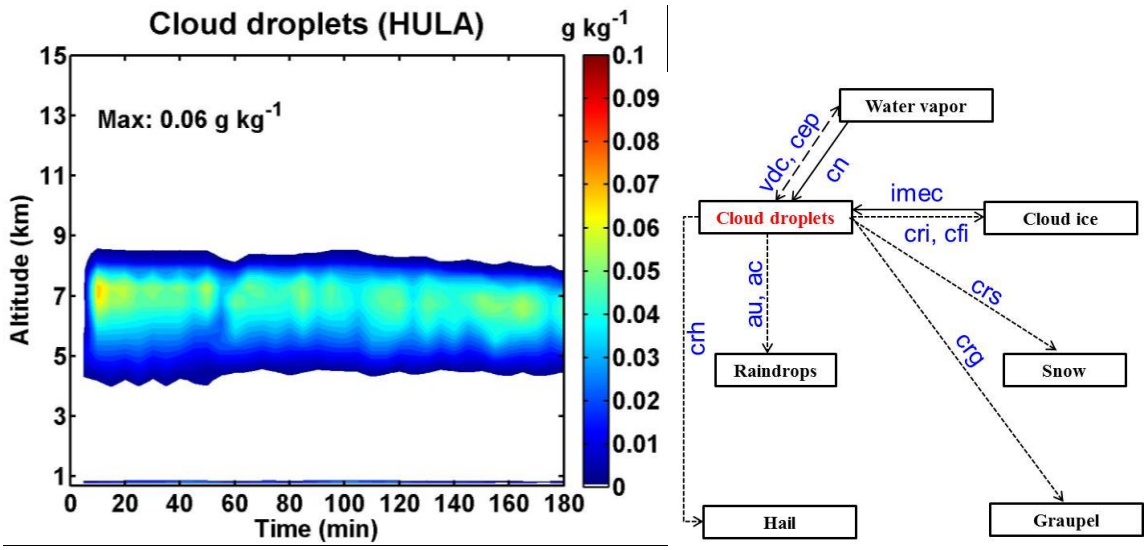

(a) **(b)**

Figure 2.6: *Temporal distribution of horizontally-averaged cloud water content (g kg^{-1}) as a function of altitude (a), and the corresponding microphysical processes involving cloud droplet formation (b). The acronyms indicate cn: cloud nucleation; crh/i/g/s: riming of cloud droplets to form hail/ ice/graupel/snow; cfi: freezing of cloud droplets to form ice crystals (including homogeneous and heterogeneous freezing); imc: melting of ice crystals to form cloud water; au: autoconversion; ac: accretion; vdc: vapor depositional growth of cloud droplets; cep: the evaporation of cloud droplets, which is the opposite process of vdc.*

It is very helpful to quantify and qualify the underlying mechanisms involving a single pyro-convective cloud by the PA module. Figure 2.7 shows the estimation of time-averaged change rate of the main processes. Besides cloud nucleation (*cn*) process which initiates the formation of cloud droplets, the comparison has also highlighted the importance of the processes of condensational growth of cloud droplets by vapor and droplet evaporation (*vdc* and *cep* respectively), and freezing of cloud droplets to form ice (*cfi*), which dominate the net change of cloud water content. Their significance is also emphasized in Figure 2.8, from which the leading process in each simulation grid of a single cloud could be clearly displayed. It is shown that *cfi* process (including homogeneous and heterogeneous freezing) usually occurs at the top of the cloud with supercooled cloud wa-

ter. At cloud base, the cloud droplets grow and dissipate through the processes of *vdc* and *cep* respectively. The center of a cloud represents the transition between hydrometeors, as several processes could happen in a same grid and at the same time. In the margin area, usually one grid is dominated by one major process.

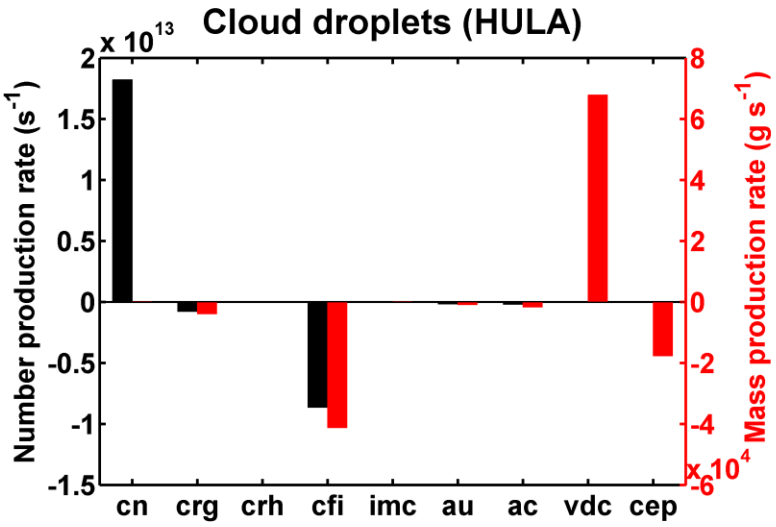

Figure 2.7: *The time-averaged rates of change for the main processes, which were obtained from the domain-integrated values. Histograms indicate contributions of processes to number concentration (black) and mass concentration (red). Sources are plotted as positive values, and sinks are negative. The meaning of the acronyms is the same as in Figure 2.6.*

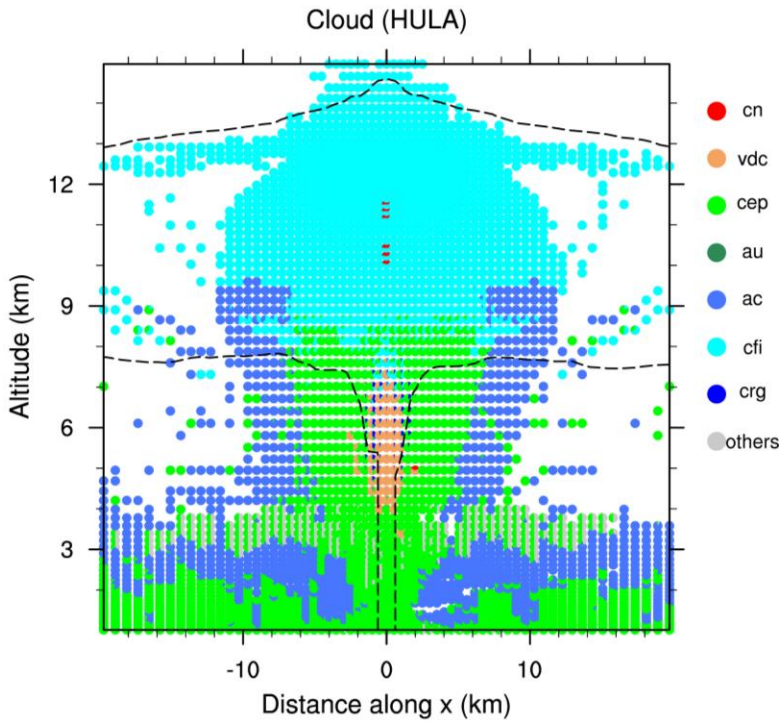

Figure 2.8: *The pie charts demonstrate the time-averaged relative contribution of individual process at each simulation grid. The black dashed line is the 0.1 μg kg^{-1} isoline of the interstitial aerosol, indicating the shape of smoke plume. The meaning of the acronyms is the same as in Figure 2.6.*

2.4.2 Ice nucleation

As shown in Figure 2.9, ice nucleation mechanisms include homogeneous and heterogeneous nucleation. Homogeneous refers to the direct conversion of supercooled cloud droplets to form ice crystals without the attendance of aerosol particles. When aerosol particles participate the formation of ice crystals, the nucleation process becomes efficient, but complicated, which is called heterogeneous nucleation. The main heterogeneous nucleation mechanisms are deposition nucleation, condensation-freezing, contact and immersion freezing nucleation. In the atmosphere, only some specific aerosol particles (e.g., mineral dust, soot, volcanic ash, and primary biological particles) have the potential to act as ice nuclei (IN), and their fraction that could serve as IN varies largely with the chemical composition, temperature, relative humidity, coating condition, and ice supersaturation (Eidhammer et al., 2009; Hoose et al., 2010; Liu et al., 2013). The heterogeneous ice nucleation used in existing ATHAM model ignored the influence of the particle

type, and the variation of ambient IN number concentration, and it did not distinguish different freezing modes which may initiate ice phase (Seifert and Beheng, 2006). The original model uses diagnostic parameterization that calculate the number of ice nuclei only as a function of temperature (Bigg, 1953) or as a function of supersaturation with respect to ice (Meyers et al., 1992), which, for example, will overestimate ice crystals number when potential IN concentration is low (Prenni et al., 2007). Expanding knowledge of ice nucleation from laboratory and field investigation, and increased capacity to parameterize more detailed aerosol treatment in models, has led to the development of heterogeneous ice nucleation parameterization that consider different IN types and different nucleation mechanisms (Diehl and Wurzler, 2004; Phillips et al., 2008; Hoose et al., 2010). Therefore, within this work, the existing ATHAM model was expanded to include more detailed heterogeneous nucleation parameterization, which links aerosol type and number concentrations to ice initiation, and also takes account of different freezing modes (i.e., immersion freezing, and deposition freezing). The freezing ability of soot particles will be evaluated within our newly-developed nucleation scheme. Mineral dust and biological aerosols acting as IN are not included in the present pyro-cloud simulations, even though it is reported that about 77% heterogeneous nucleation globally is caused by dust particles (Hoose et al., 2010).

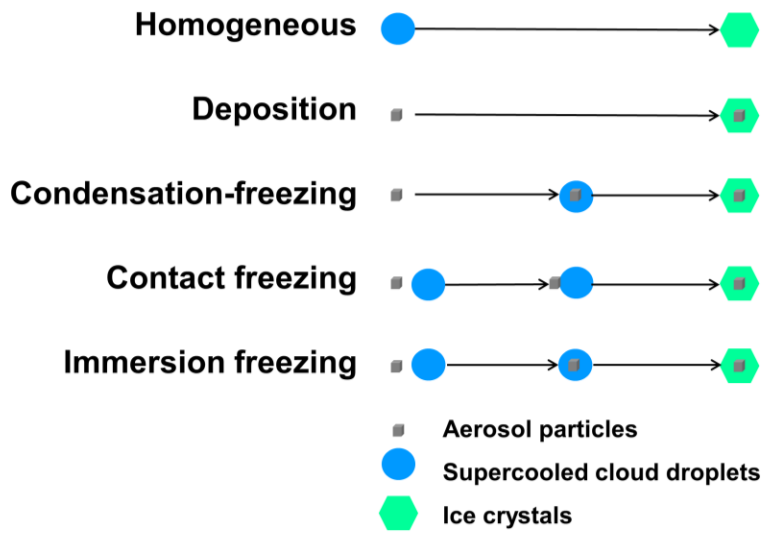

Figure 2.9: *Multiple ice nucleation modes.*

At present, there are numerous amounts of research which have made great effort to parameterize the heterogeneous nucleation process. For example, some parameterization was based on classical heterogeneous nucleation theory (Khvorostyanov and Curry, 2000; Hoose et al., 2010); some schemes rely on the laboratory studies of droplet freezing (Diehl and Wurzler, 2004), and some are from field studies constrained by laboratory cloud chamber studies (Phillips et al., 2008). The classical-nucleation-theory-based parameterization developed by Hoose et al. (2010) treats ice initiation through three main nucleation mechanisms (i.e., deposition, immersion and contact freezing nucleation), and considers three different IN types (soot, dust, and biological aerosols), each with different activation properties. This nucleation scheme has been successfully implemented in global model, and agrees well in a statistical sense with continuous-flow diffusion chamber (CFDC) measurements (Hoose et al., 2010). Within this study, the heterogeneous nucleation parameterization (deposition and immersion freezing) proposed by Hoose et al. (2010) is applied and the treatment of ice nucleation process will be described in detail. Due to the negligible contribution of the contact nucleation (Wang et al., 2014a), it is not taken into account within our work.

To validate the newly-developed ice nucleation parameterizations, the activated IN densities predicted by original and new ice nucleation schemes will be compared. The existing ice nucleation in ATHAM model is parameterized following the deposition-condensation nucleation formula given by Meyers et al. (1992), which is a function of supersaturation with respect to ice:

$$N_{IN} = N_{M92} \times \exp\,(a + b \times S_i) \qquad (1)$$

Where N_{M92} equals 1,000 m^{-3}, a is -0.639 and b is 12.96. S_i is the supersaturation with respect to ice. This formula is illustrated by the red line in Figure 2.10a under the condition of water saturation.

According to the parameterization in Hoose et al. (2010), the change rate in ice crystal concentration N_i through vapor deposition freezing can be obtained by summing up the contributions of each aerosol species x:

$$\frac{dN_i}{dt}\Big|_{dep} = \sum_x J_{dep,x,RH=0.98} \times (1-f_{\ell,x}) \times (1-f_{x,coated}) \times N_{CN} \qquad (2)$$

Where $J_{dep,x}$ stands for the deposition nucleation rate per aerosol particle and time (s^{-1}); $f_{\ell,x}$ denotes the fraction of particles that is activated to liquid droplets; $f_{x,coated}$ denotes coated fraction of particles of species x; N_{CN} is the initial aerosol number concentration. Because it was found that the relative humidity (RH) in mixed-phase clouds is close to saturation over water (Korolev and Isaac, 2006), a RH of 98% (over water) is assumed inside mixed-phase clouds (Hoose and Mohler, 2012).

Based on this formula, the condition with three different aerosol concentrations (200, 2,000, and 20,000 cm^{-3}), and updraft velocity of 1 m s^{-1} ($f_{\ell,x}$ =84%, 27%, and 4.2% for three aerosol conditions respectively, which is derived from the lookup table for cloud nucleation), leads to the IN density as a function of temperature, which is described by the blue lines in Figure 2.10a. Due to the limitation regarding the data of the fraction of aerosols that is coated ($f_{x,coated}$), we take 50% coating fraction during our simulation. As shown in Figure 2.10a, the case with aerosols of 200 cm^{-3} is comparable to the result of Meyers et al. (1992).

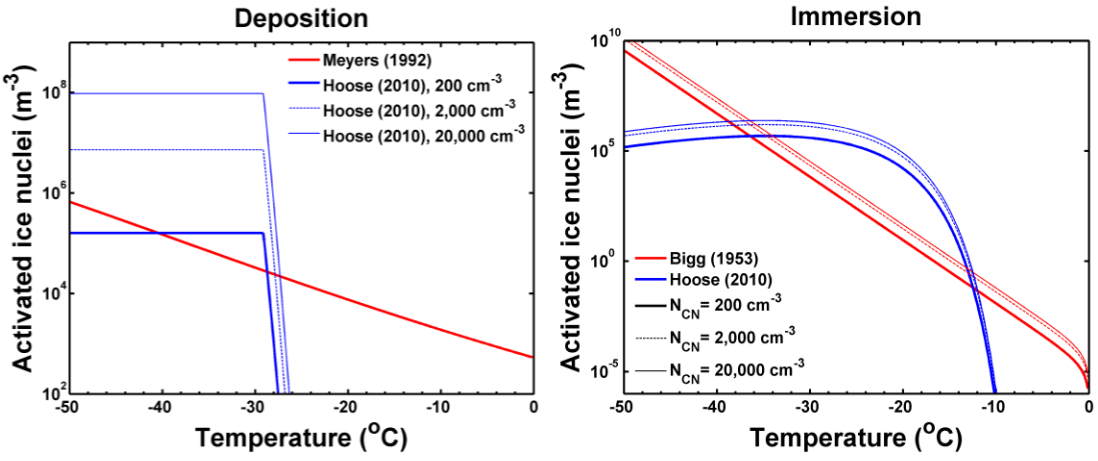

(a) **(b)**

Figure 2.10: *Number density of activated ice nuclei (IN) as a function of temperature predicted by Hoose et al. (2010) (blue lines) and the original ice nucleation parameterizations used in ATHAM model (red lines).*

Heterogeneous freezing of cloud droplets in existing ATHAM model follows the classical work of Bigg (1953), which is a function of temperature (T):

$$\frac{dN_i}{dt}|_{het}=J_{het}(T) \times M_{CD} = 100 \times(\exp(-0.66 \times T)-1.0) \times M_{CD} \quad (3)$$

Where M_{CD} is mass density of cloud droplets, which is derived from the CCN activation lookup table according to aerosol concentration and updraft velocity.

The change rate in ice crystal concentration N_i through immersion nucleation in Hoose et al. (2010) can be obtained by summing up the contributions of each aerosol species x:

$$\frac{dN_i}{dt}|_{imm}=\sum_x J_{imm,x} \times f_{\ell,x} \times N_{CN} \quad (4)$$

Where $J_{imm,x}$ stands for the rate of immersion freezing per particle and time (s^{-1}); $f_{\ell,x}$ denotes the fraction of particles that is activated to liquid droplets; N_{CN} is the aerosol number concentration. The freezing point suppression due to solute effect is not included by defining water activity (a_w) of the cloud droplet equal to 1.

Figure 2.10b shows the comparison of IN number densities predicted by Bigg (1953) and by Hoose et al. (2010) with different aerosol levels (200, 2,000, and 20,000 cm^{-3}), and updraft velocity of 1 m s^{-1}. As shown, increased N_{CN} results in an increase in IN density in both original and new ice nucleation schemes. However, the effect of N_{CN} on IN density in Bigg (1953) is not directly through affecting ice nucleation, but indirectly via cloud nucleation. According to the comparison, we found a big difference between new and old ice nucleation parameterizations is the onset temperature, and the new ice nucleation representation is constrained with very low temperature. In order to be consistent with deposition nucleation, we choose aerosol concentration of 200 cm^{-3} as the standard condition, which is used to validate the modeling results based on the ice nucleation given by Hoose et al. (2010).

The parameters (i.e., aerosol number concentration and updraft velocity) used in Figure 2.10 serve as our standard configuration. A comparison of the original and new ice

nucleation parameterizations using ATHAM model is conducted under the standard configuration and is shown in Figure 2.11, in which the domain-averaged concentrations of individual hydrometeor for every 3 minute are compared. In general, the concentrations of all hydrometeors are linearly correlated between original parameterization and new ice nucleation scheme, especially for cloud ice, snow and graupel.

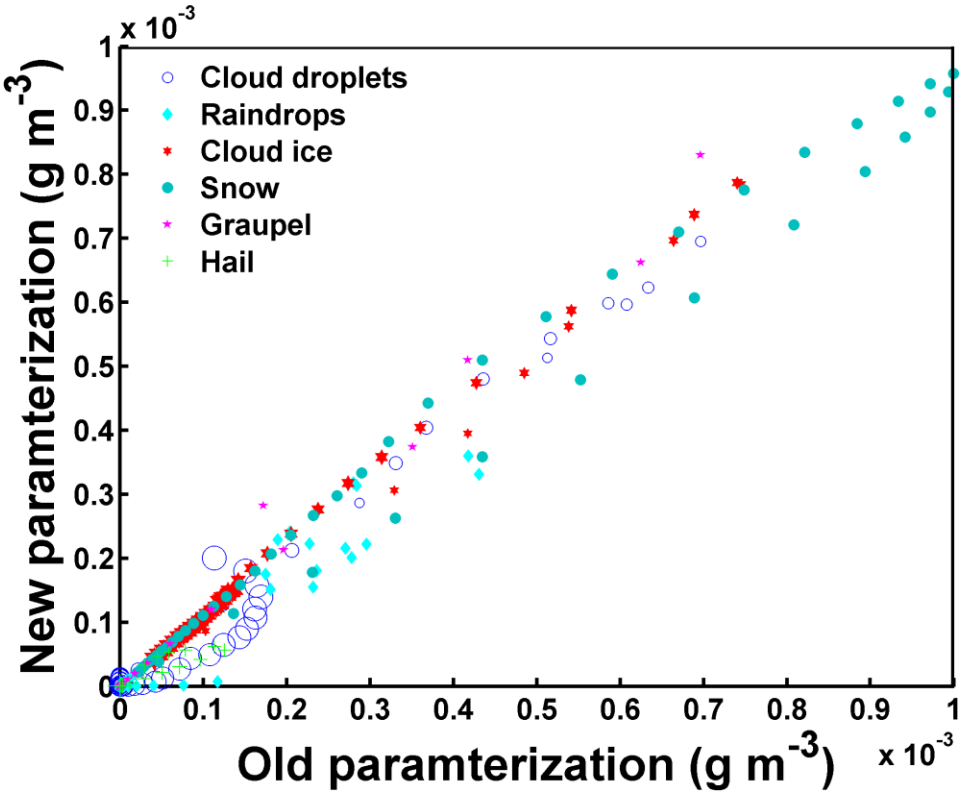

Figure 2.11: *Correlations of individual hydrometeor predicted by original and new ice nucleation parameterizations over 3 simulation hours. Each point denotes the domain-averaged mass concentration at three-minute intervals and its size is proportional to the time. The corresponding equations and R^2 values of the linear regression are $y = 1.01x-5.25\times10^{-6}$ (cloud droplets, $R^2 = 0.98$), $y = 0.87x-1.58\times10^{-6}$ (raindrops, $R^2 = 0.93$), $y = 1.05x+3.32\times10^{-6}$ (cloud ice, $R^2 = 1.00$), $y = 0.95x+1.14\times10^{-5}$ (snow, $R^2 = 0.99$), $y = 1.12x+2.04\times10^{-6}$ (graupel, $R^2 = 1.00$), and $y = 0.54x+5.19\times10^{-7}$ (hail, $R^2 = 0.89$), respectively.*

2.5 Summary

In this chapter, a newly-developed model configuration was presented where a cloud-resolving model was coupled with additional process analysis (PA) module and detailed treatment of ice nucleation parameterization.

It was shown that by adding PA module, the evolution of clouds could be decoupled to several main processes. Instead of only investigating the spatial and temporal distributions of clouds in most previous studies, focusing on the individual process or several dominant processes, will give a clearer picture how the underlying mechanisms inside a cloud system proceed. This is very helpful to cloud modeling community in improving the model in the future by revealing which process is worthy of further scrutiny, and which one does not need extra effort.

Previous studies have found that changing IN concentrations can significantly influence cloud initiation and evolution (van den Heever et al., 2006; Eidhammer et al., 2009; Fan et al., 2010). However, the original ice nucleation parameterization in ATHAM model does not connect the IN nucleation to ambient aerosol properties. Therefore, we try to implement a classical-nucleation-theory-based parameterization established by Hoose et al. (2010) in our model, which is capable to include the information of aerosol properties. The comparison of the concentrations of individual hydrometeor predicted by original and new ice nucleation parameterizations shows good agreement under the standard configuration. The newly-implemented parameterization is a helpful modification to study the development of pyro-convective clouds with different IN number concentrations.

Chapter 3 CCN effects on cloud formation and evolution

3.1 Introduction

Clouds have a considerable effect on the radiation, climate, and water cycle of the Earth (IPCC, 2013). CCN-cloud interactions are one of the most uncertain factors influencing the formation, persistence, and ultimate dissipation of clouds (Stevens and Feingold, 2009). Previous studies usually concentrate on several specific scenarios. Within this work, we have developed a more complete understanding of aerosol-cloud interactions by conducting over 1000 simulations, allowing us to study whether the responses of the hydrometeors to CCN and dynamic forcing have continuity, and the reasons behind this behavior. The ice nucleation scheme is still based on the existing ATHAM model, without considering aerosol effect by acting as IN. In addition, the existing ATHAM model is modified to include the process analysis (PA) module to computer the time-integrated rate of change in the mass or number concentration of each hydrometeor type (cloud droplets, raindrops and frozen water content) caused by a particular process.

3.2 CCN effects and its regime dependence

In this section, the spatiotemporal distribution of each hydrometeor type will be briefly presented, followed by the modeled dependency of various hydrometeors on N_{CN} (CCN) and fire forcing (*FF*). Note here that only the characteristics of dependency are presented, while the underlying mechanisms will be discussed and interpreted in more detail in Sect. 3.3. For an individual hydrometeor type, the averaged concentrations (over the entire domain and simulation period) were used as metrics in our evaluation, and the condensed water reaching the surface was used as a metric for precipitation.

3.2.1 Cloud droplets

Figure 3.1 shows the temporal evolution of horizontally averaged mass concentration of cloud droplets (M_{CD}) under the four pairs of *FF* and N_{CN} conditions. Under weak fire forcing conditions (LU), the formation of cloud droplets usually occurs after 20 min, and most of cloud droplets locate in an altitude of 4-7 km. The duration of cloud droplets is

usually short (40~60 min). Under strong fire forcing conditions (HU), the cloud droplets form earlier (around 5 min), and most cloud droplets are located at a height of 5-9 km. Moreover, the cloud droplets reach steady state because of the cycling of cloud formation.

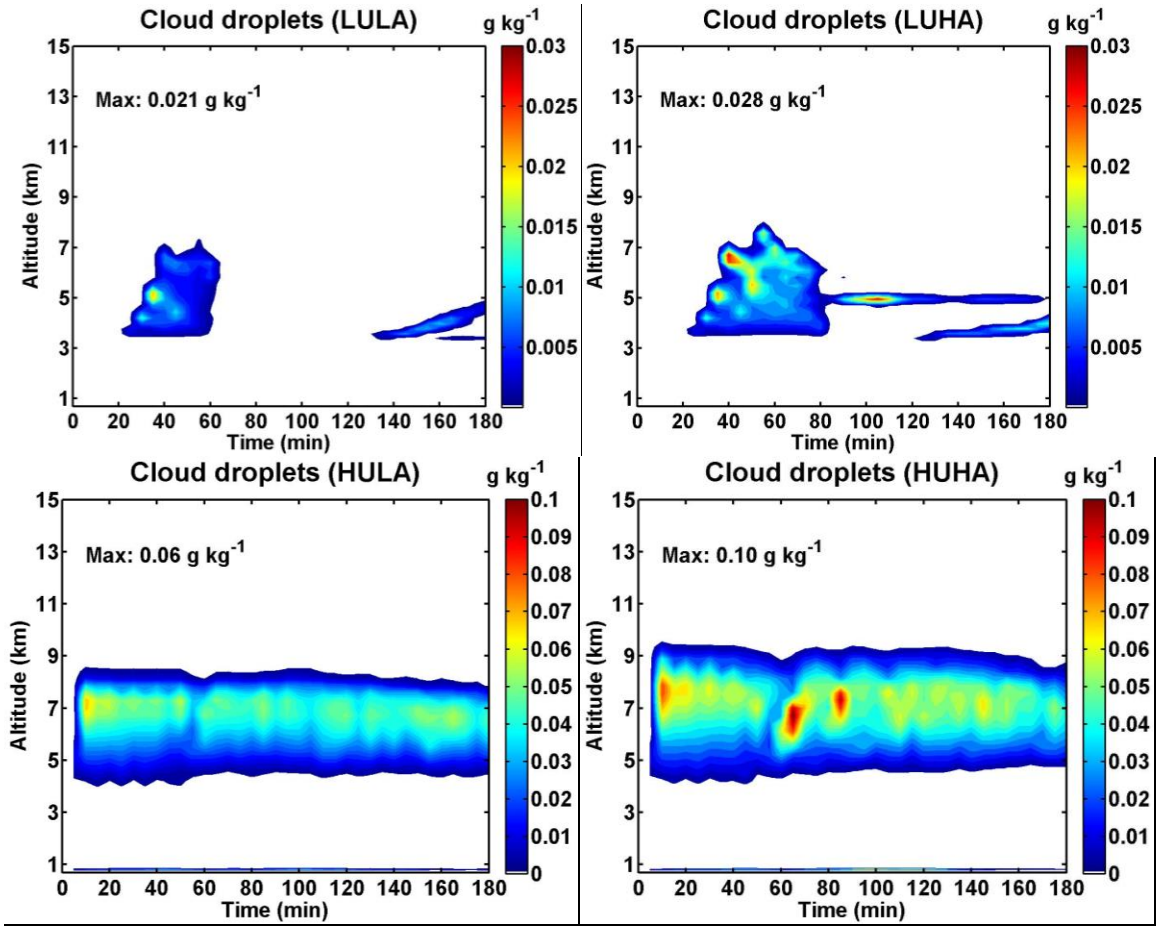

Figure 3.1: *Time evolution of horizontally averaged cloud water content (g kg^{-1}) as a function of altitude for four extreme cases, which are referred to as (1) LULA: low updrafts (2,000 W m^{-2}) and low aerosols (200 cm^{-3}); (2) LUHA: low updrafts (2,000 W m^{-2}) and high aerosols (100,000 cm^{-3}); (3) HULA: high updrafts (300,000 W m^{-2}) and low aerosols (200 cm^{-3}); and (4) HUHA: high updrafts (300,000 W m^{-2}) and high aerosols (100,000 cm^{-3}). Maximum values for each episode are also shown.*

To investigate the sensitivity of an individual hydrometeor to changes in N_{CN} and *FF*, we adopted the definition of relative sensitivity *RS*(*X*) (of one variable *Y* against the variable *X*) as:

$$RS_Y(X) = \frac{\partial Y / Y}{\partial X / X} = \frac{\partial \ln Y}{\partial \ln X} \quad (5)$$

In this study, X is the factor affecting cloud formation, i.e., N_{CN} and FF, and Y is the mass or number concentration of each hydrometeor type (cloud droplets, raindrops, and frozen particles). By using a natural logarithmic calculation of the variables (i.e., X, Y), the percentage change in an individual parameter relative to its magnitude could be reflected better. This logarithmic sensitivity evaluation has been applied commonly in the assessment of aerosol-cloud interactions (Feingold, 2003; McFiggans et al., 2006; Kay and Wood, 2008; Reutter et al., 2009; Sorooshian et al., 2009; Karydis et al., 2012).

Figure 3.2a shows the dependence of cloud water droplets (N_{CD}) on N_{CN} and FF. The shape of the isolines is generally consistent with the regime designations reported by Reutter et al. (2009). Following Reutter et al. (2009), a value of the $RS(N_{CN})$ to $RS(FF)$ ratio of 4 or 0.25 was taken as the threshold value to distinguish different regimes (the same criteria were employed for rainwater and frozen water content). Red dashed lines in Figure 3.2a indicates the borders between different regimes. This resulted in an aerosol-limited regime in the upper left sector of the panel (N_{CD} is sensitive mainly to N_{CN} and is insensitive to fire forcing), an updraft-limited regime in the lower right sector of the panel (N_{CD} displays a linear dependence on FF and a very weak dependence on N_{CN}), and the transitional regime along the ridge of the isopleth (FF and N_{CN} play comparable roles in the change in N_{CD}). The regimes of Reutter et al. (2009) are derived from simulations of the cloud parcel model of CCN activation at the cloud base. Our results demonstrate that the general regimes for CCN activation still prevail, even when considering full micro-physics and the larger temporal and spatial scales of a single pyro-convective cloud system. Figure 3.2c and d demonstrates the sensitivity of N_{CD} to variations in N_{CN} and FF, respectively. High sensitivities were found for low conditions of N_{CN} and FF. While there are some deviations (which appear to be random numerical noise), in general, as either N_{CN} or FF increases, the impact of further changes to either the variable on the cloud droplet number concentration becomes weaker (Figure 3.2c, d). The reduced sensitivity of cloud droplets to aerosols can be explained by the buffering effect of the cloud micro-

physics, so that the response of the cloud system to aerosols is much smaller than would have been expected.

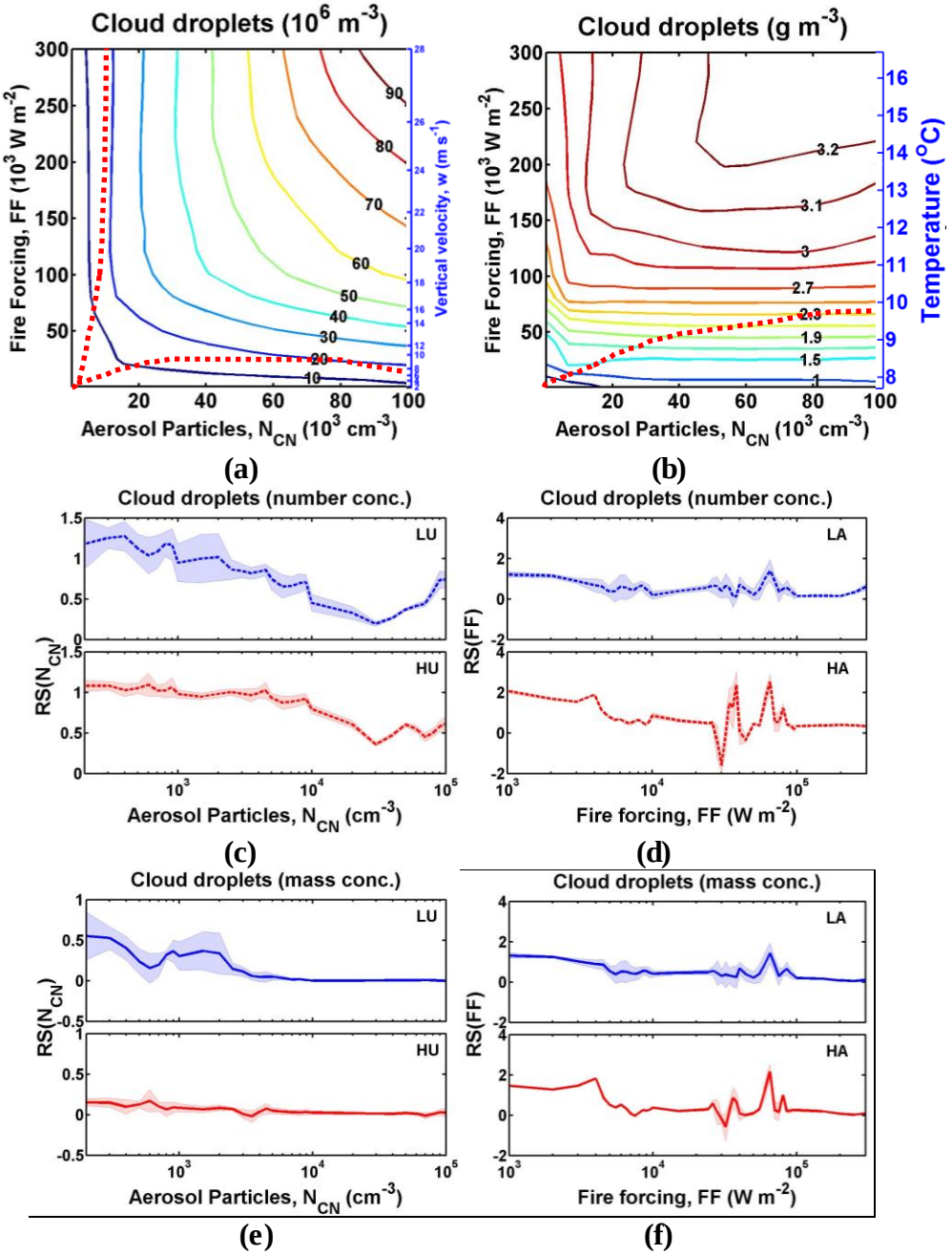

Figure 3.2: *Number (a) and mass concentration (b) of cloud droplets calculated as a function of aerosol number concentration (N_{CN}) and updraft velocity (represented by FF). Red dashed lines indicate the borders between different regimes defined by RS (N_{CN})/RS(FF)=4 or 0.25. Relative sensitivities with respect to N_{CN} (left) and FF (right) for number (panels (c) and (d)) and mass (panels (e) and (f)) concentration of cloud droplets under different conditions. The thick dashed or solid lines represent the mean values under a given condition, and the shaded areas represent the variability of estima-*

tion (±0.5σ). Abbreviations are as follows: LU, low updrafts (1,000–7,000 W m^{-2}); HU, high updrafts (75,000–300,000 W m^{-2}); LA, low aerosols (200–1,500 cm^{-3}); and HA, high aerosols (10,000–100,000 cm^{-3}).

Compared with N_{CD}, the cloud mass concentration (M_{CD}) is less sensitive to N_{CN}, and there is hardly an aerosol-limited regime in the contour plot for M_{CD} (Figure 3.2b). There are only two regimes indicated by the red dashed line in Figure 3.2b: an updraft-limited regime in the lower right sector of the panel, and the transitional regime in the upper sector (an aerosol- and updraft-sensitive regime). The $RS(N_{CN})$ of N_{CD} is on average 10 times higher than that of M_{CD}, independent of the intensity of the *FF*. As N_{CN} increases, M_{CD} becomes insensitive to the change in N_{CN}. Averaged $RS(FF)$ values over simulated *FF* ranges for N_{CD} (0.60) and M_{CD} (0.50) are commensurate (Figure 3.2d, f, respectively), which implies that both the number and mass concentrations of cloud droplets are very sensitive to updrafts. These results are derived from simulations with persistent fire forcing over the modeling period. We have also examined the case in which the fire forcing was shut down after the first half hour of simulation (not shown). The same regimes were found in these simulations, with boundaries in good agreement with the findings presented in this work.

3.2.2 Raindrops

Figure 3.3 exhibits the temporal evolution of the horizontally integrated mass concentration of raindrops under four different conditions. Compared with cloud droplets (Figure 3.1), the occurrence of raindrops is much later, especially when N_{CN} and fire forcing are at a high level. Only for LULA case can numerous raindrops be found in a high altitude (5-7 km); for other cases, most of the raindrops are located below 5 km (~0 ℃).

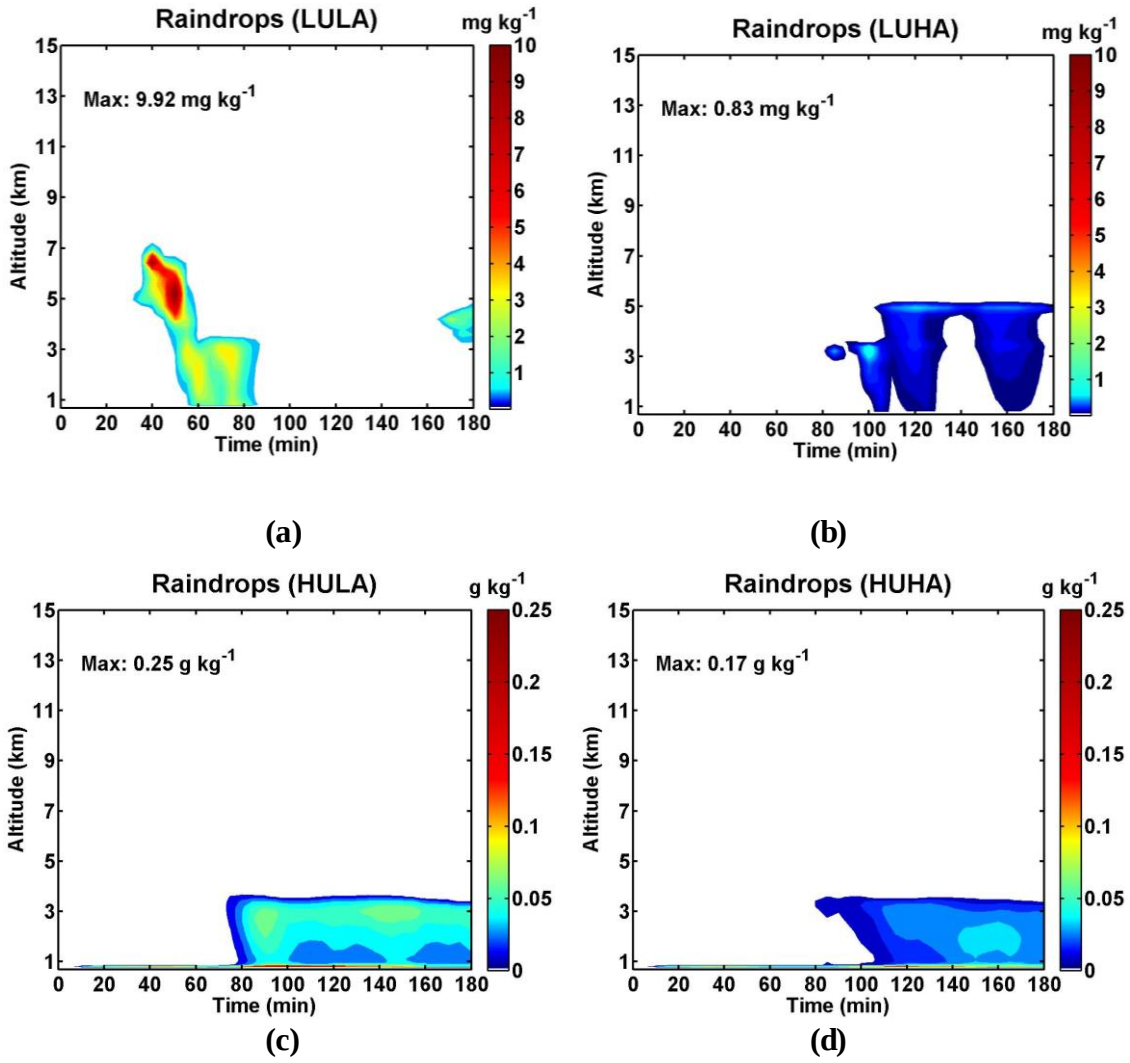

Figure 3.3: *Same as Figure 3.1 but for raindrops.*

The response of the raindrop number concentration (N_{RD}) to fire forcing and N_{CN} is more complex (Figure 3.4a). The impact of *FF* on N_{RD} is non-monotonic. In general, enhanced *FF* leads to an increase in N_{RD} under weak updraft conditions (<~4,000 W m^{-2}), while further increases in *FF* result in the reduction in N_{RD}. The aerosol influence varies in the course of N_{CN} change. Under low-aerosol condition (<~1,500 cm^{-3}), increased N_{CN} can enhance the production of N_{RD}. Under high-aerosol condition (>~2,000 cm^{-3}), the influence of N_{CN} on N_{RD} is very small.

As *FF* increases in magnitude, the amount of rain produced (M_{RD}) increases (Figure 3.4b), but the size of raindrops varies because of the complex behavior of the re-

sponse of the raindrop number (N_{RD}) to *FF* (Figure 3.4a). The aerosol effect is non-monotonic: M_{RD} increases with aerosols in the lower range of N_{CN} values (<~1000 cm^{-3}), but further increases in N_{CN} result in a decrease in M_{RD}. Combined with the relative sensitivities (Figure 3.4e, f), the influence of *FF* is much more significant than that of N_{CN} in most cases. For example, the upper left corner (an aerosol-limited regime for N_{CD}) becomes a transitional regime for M_{RD}, with *RS* (*FF*) of 0.1 and *RS* (N_{CN}) of -0.06. High *RS*(N_{CN}) values of M_{RD} were found at low-N_{CN} conditions, and this decreases as N_{CN} increases (Figure 3.4e). The N_{CN} plays the most negative role in M_{RD} under intermediate N_{CN} conditions (N_{CN} of several 1000 cm^{-3}). In contrast to cloud droplet number concentration, an aerosol-limited regime for M_{RD} scarcely exists in our simulations (Figure 3.4b). The response of the raindrops to aerosols is much weaker than the response of cloud droplets to aerosols. This finding is consistent with the idea of clouds acting as a buffered system formulated by Stevens and Feingold (2009). Detailed analysis of the microphysical buffering processes will be presented in Sect. 3.3.2.

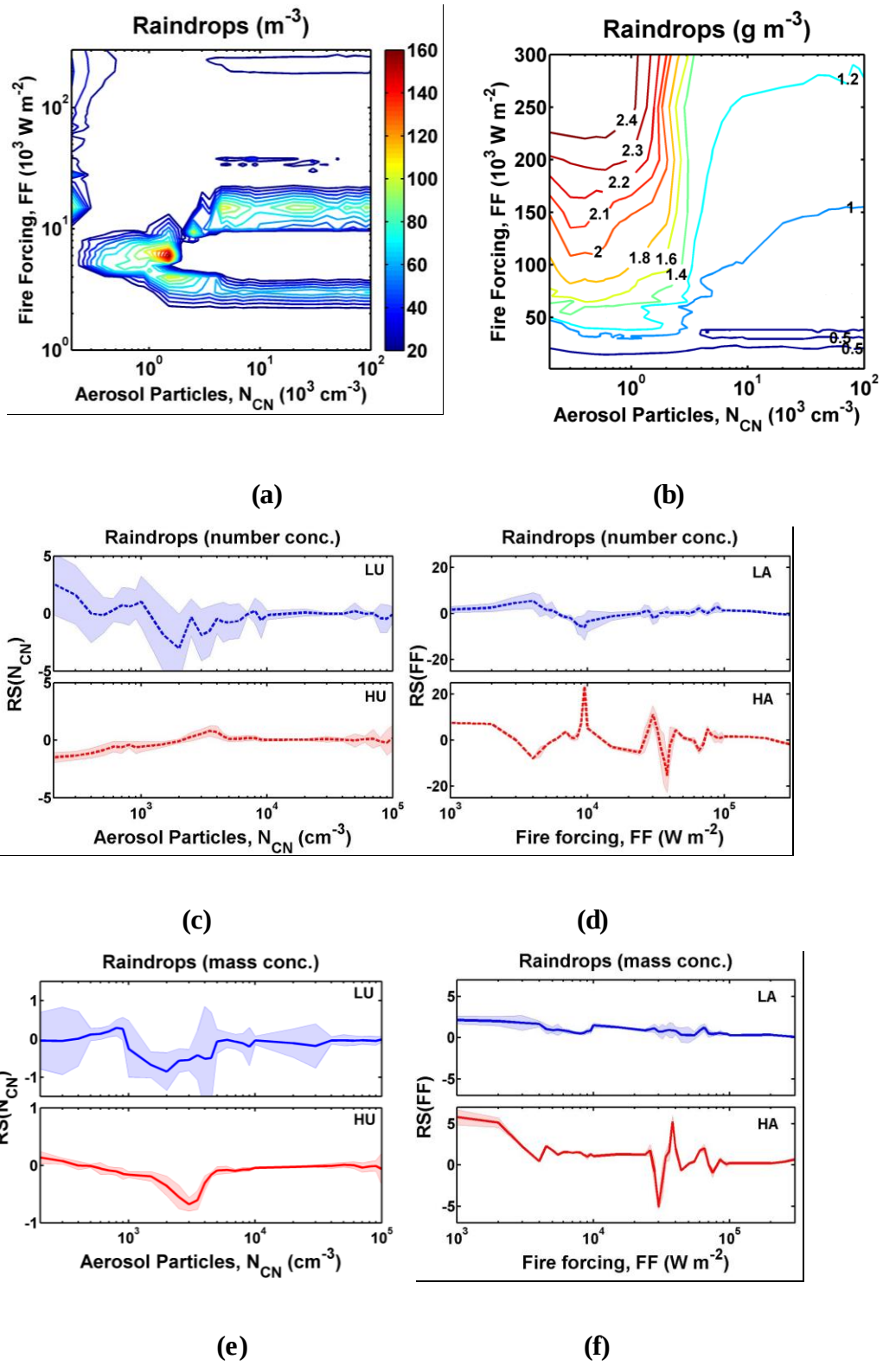

Figure 3.4: *Same as Figure 3.2 but for raindrops.*

3.2.3 Frozen water contents

Within our microphysical scheme, frozen water contents are grouped into four main classes: ice crystals, snow, graupel, and hail (Seifert and Beheng, 2006). The time evolution of frozen water content in Figure 3.5 suggests that the formation of frozen water content usually occurs at a high level (5-9 km for the LU case, and 7-13 km for the HU case), and the height of base layer and top layer decreases over time. Under LU conditions, the appearance of frozen water content is around 35 min, and lasts for ~120 min, with the peak concentration around 50~70 min. Under HU conditions, the frozen particles form around 10 min, and keep in a steady state.

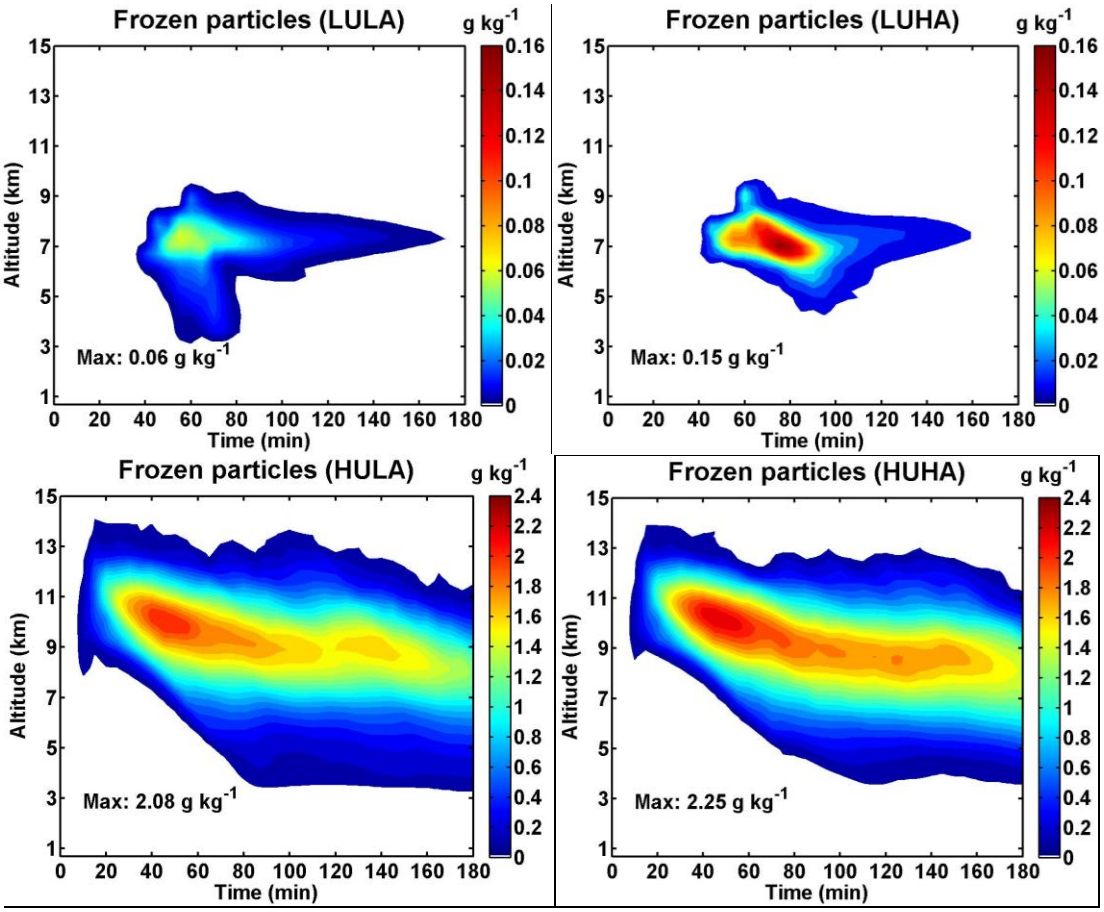

Figure 3.5: *Same as Figure 3.1 but for the frozen particles.*

Aerosols exert influence on the frozen water contents via the process of ice nucleation (*in*), but the processes that convert between the different hydrometeor classes and water vapor play a greater role in changing the concentrations of frozen particles, especially the processes of cloud freezing to form ice (*cfi*) and the vapor depositional growth of ice and snow (*vdi* and *vds* respectively). Figure 3.6 illustrates the percentage mass contributions of the individual frozen hydrometeor classes to the total frozen mass. The percentages of each hydrometeor are calculated based on average values over the entire simulation period. Generally, greater concentrations of aerosols result in more snow and less graupel. This is in agreement with previous studies on convective clouds (Seifert et al., 2012; Lee and Feingold, 2013) and can be explained by the suppression of the warm rain processes under high-aerosol conditions. High N_{CN} delays the conversion of the cloud water to form raindrops, so that more cloud water content can ascend to altitudes with sub-zero temperatures and hence directly freeze into small frozen particles (Rosenfeld et al., 2008). Other research has suggested that elevated aerosols could increase the concentration of large frozen particles (graupel/hail) in the convective system (Khain et al., 2009; Wang et al., 2011), which was attributed to the competing effects of aerosols on graupel formation. Since graupel is mainly formed by the accretion of supercooled droplets by ice or snow, the smaller but more abundant supercooled drops under polluted conditions could be either favorable or unfavorable for graupel formation. The percentage of ice crystals does not change much, contributing approximately 20% on average (Figure 3.6). It is worth noting that stronger *FF* leads to increasing concentration of hail. But compared to other hydrometeors, its contribution is not important and the relative percentage is very low.

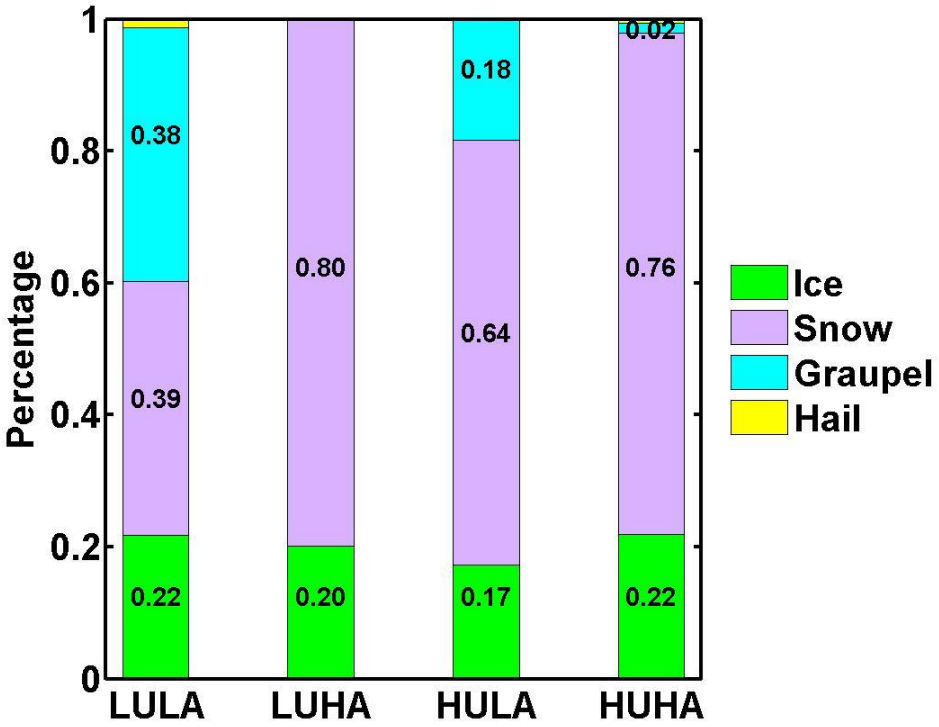

Figure 3.6: *Contributions of individual frozen hydrometeor to total frozen water content under four extreme conditions, which are referred to as (1) LULA: low updrafts (2,000 W m^{-2}) and low aerosols (200 cm^{-3}); (2) LUHA: low updrafts (2,000 W m^{-2}) and high aerosols (100,000 cm^{-3}); (3) HULA: high updrafts (300,000 W m^{-2}) and low aerosols (200 cm^{-3}); and (4) HUHA: high updrafts (300,000 W m^{-2}) and high aerosols (100,000 cm^{-3}).*

The dependence of total frozen particles on *FF* and N_{CN} is summarized in Figure 3.7. With the enhancement in *FF* and N_{CN}, both the number and mass concentrations of the frozen water particles (N_{FP} and M_{FP}, respectively) increase. High $RS(N_{CN})$ and $RS(FF)$ values were found at low-N_{CN} and *FF* conditions, respectively. As N_{CN} or *FF* increases, its impact becomes weaker, as indicated by a decreasing *RS*. According to the ratio of $RS(FF)/RS(N_{CN})$, both N_{FP} and M_{FP} are within the updraft-limited regime. Again, smaller $RS(N_{CN})$ values for M_{FP} compared with N_{CD} illustrate the weaker impact of N_{CN} on the production of frozen particles.

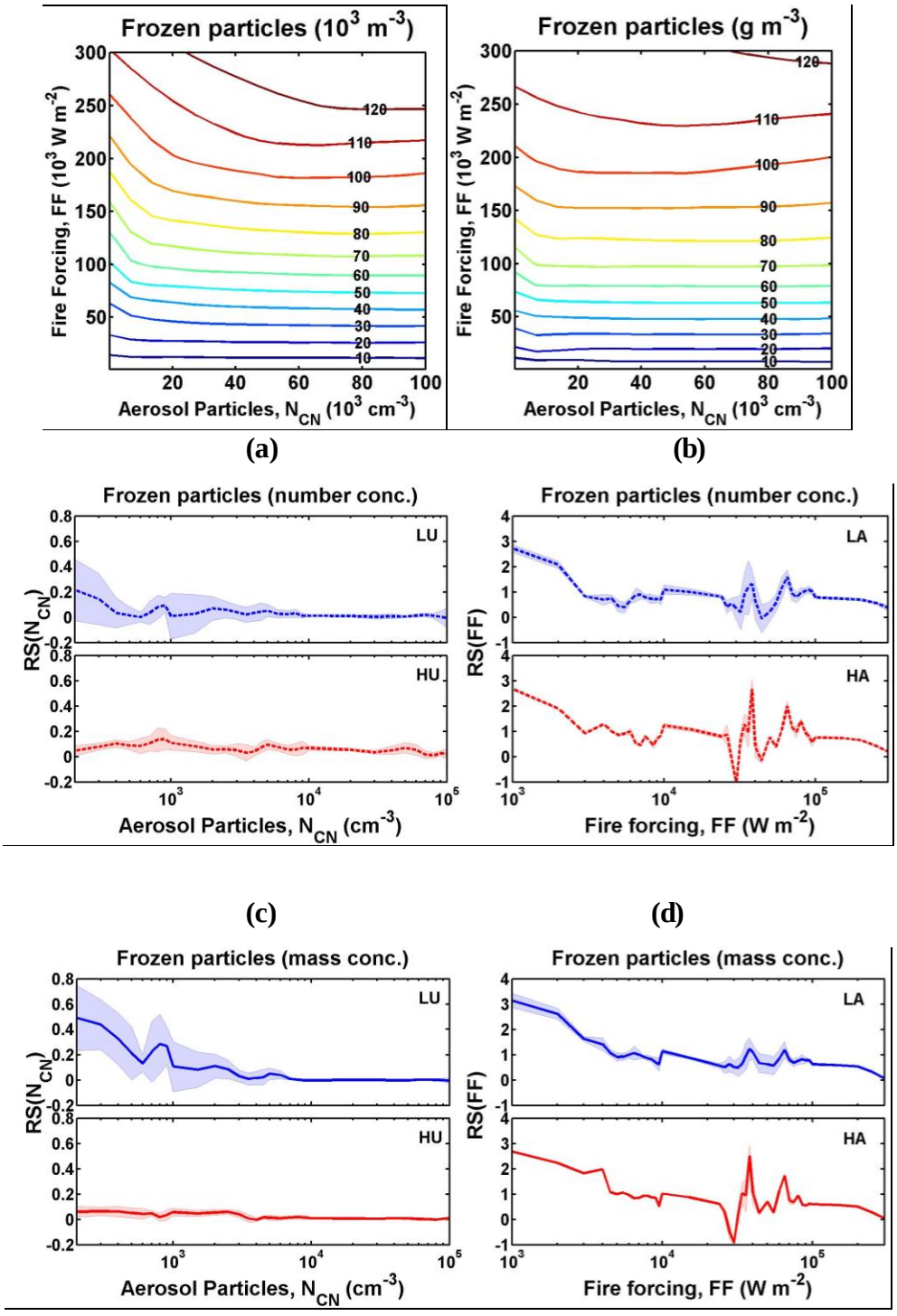

Figure 3.7: *Same as Figure 3.2 but for total frozen particles.*

3.2.4 Precipitation rate

Surface precipitation rate is a key factor in climate and hydrological processes. Many field measurements, remote sensing studies, and modeling simulations have attempted to evaluate the magnitude of aerosol-induced effects on the surface rainfall rate (Rosenfeld, 1999, 2000; Tao et al., 2007; Li et al., 2008; Sorooshian et al., 2009). The response of averaged surface precipitation rate (over 3-h simulations) to *FF* and N_{CN} is shown in Figure 3.8a. The response of surface precipitation to these forcings is similar to that of raindrops (Figure 3.4b). *FF* plays a positive role in the precipitation, and *RS*(*FF*) shows a decreasing trend as *FF* increases (Figure 3.8).

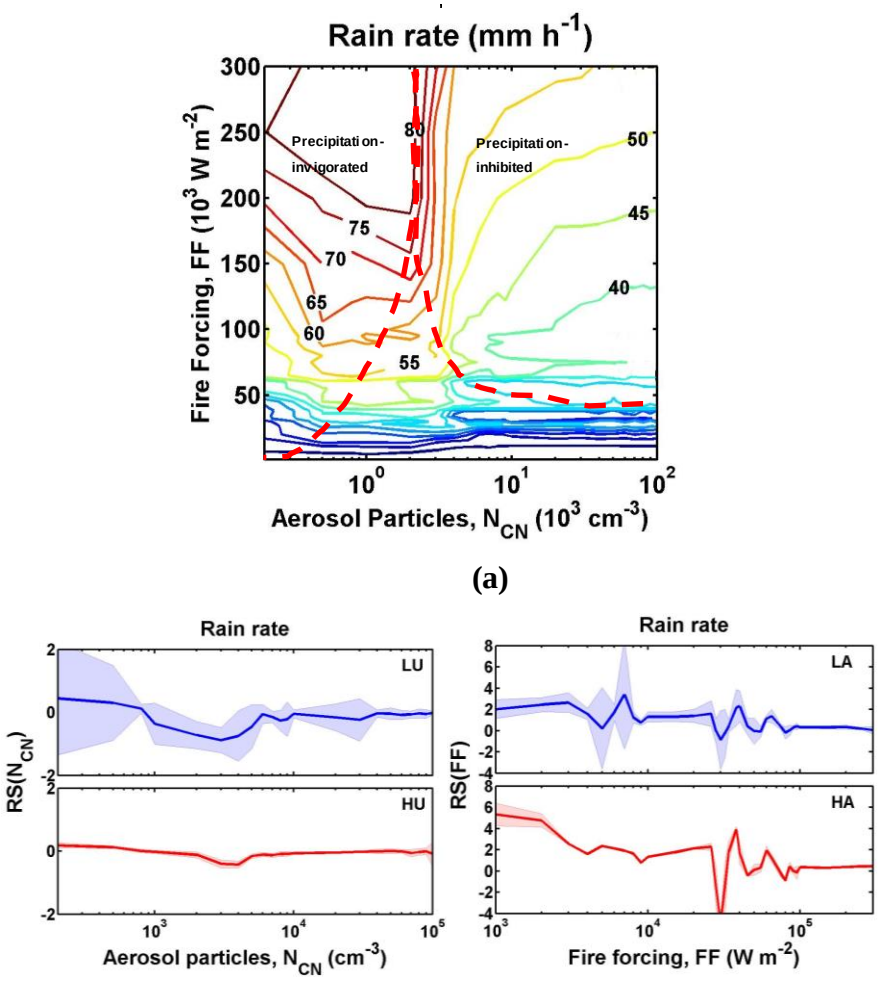

Figure 3.8: *Same as Figure 3.2 but for surface rain rate.*

The effect of N_{CN} is more complex. Both positive and negative RS (N_{CN}) were found in our study. There are generally two different regimes: a precipitation-invigorated regime and a precipitation-inhibited regime. In the precipitation-invigorated regime (N_{CN} < ~1000 cm^{-3}), an increase in N_{CN} leads to an increase in the precipitation rate, and a reduction in RS (N_{CN}) (Figure 3.8b). In the precipitation-inhibited regime (N_{CN} > ~1000 cm^{-3}), aerosols start to reduce the precipitation, which is reflected in a negative $RS(N_{CN})$. Within the precipitation-inhibited regime, there is also an extreme $RS(N_{CN})$ at a value of N_{CN} of a few thousand particles per cubic centimeter (Figure 3.8b). The threshold to distinguish these two regimes is derived from the current simulated pyro-convective clouds. The cumulus cloud investigation in Li et al. (2008) also suggested this non-monotonic trend, with the threshold aerosol value around 3000 cm^{-3}. The existence of threshold N_{CN} in both studies implies that similar cloud types may have a similar regime dependence, of which the exact shape may differ due to difference in the meteorological conditions, aerosol properties, etc.

Based on the ensemble studies, we found that individual case studies result in large uncertainties in evaluating the response of precipitation to perturbations, e.g., N_{CN}. Different selections of the parameter space may result in different or even opposite conclusions. Therefore, our ensemble study over a wide range of parameter space sheds some light on these debates.

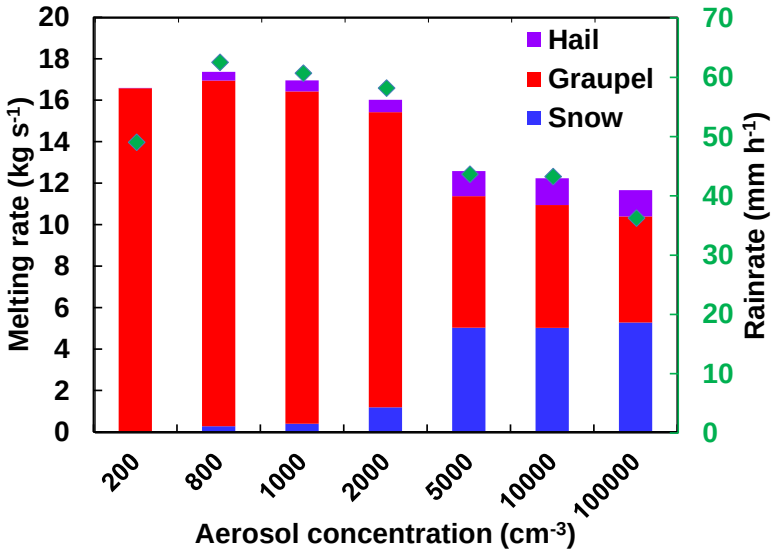

Figure 3.9: *The correlation of rain rate and the melting rate of the frozen particles. The green diamond points are the averaged rain rate under different aerosol concentrations (FF= 10^5 W m^{-2}). The columns represent the integrated melting rate from individual frozen particles.*

Within our simulations, melting of frozen particles is the biggest contributor to precipitation, and the rain rate is well correlated with the melting rate (Figure 3.9). For N_{CN} > 1,000 cm^{-3}, increasing N_{CN} results in more small frozen particles (i.e., snow) with low fall velocities. These small frozen particles cannot fall into the warm areas and melt efficiently, resulting in a reduced melting rate. For N_{CN}< 1,000 cm^{-3}, the ratio between large and small frozen particles is not sensitive to N_{CN} anymore and the vertical distribution of frozen particles becomes important. Increasing N_{CN} leads to earlier formation of frozen particles at low altitude, which evaporate less and result in more rainfall.

In the literature, both positive (Tao et al., 2007) and negative (Altaratz et al., 2008) relationship between aerosols and rain rate have been reported in previous case studies. Our simulations suggest that this apparently contradictory phenomenon might be the expression of the same physical processes under different aerosol and dynamic conditions.

Regarding the temporal evolution, low N_{CN} results in earlier rainfall (Figure 3.10), which is consistent with current understanding, observations (e.g., Rosenfeld, 1999, 2000), and modeling evidence (e.g., the convective cumulus cloud study by Li et al.

(2008)). Note that the general relationship between precipitation and aerosols described in this study is based on simulations over a period of 3 hours. Simulations for a longer period should be carried out in future studies to investigate the influence of aerosols on precipitation over longer time scales as in Fan et al. (2013) and Wang et al. (2014b).

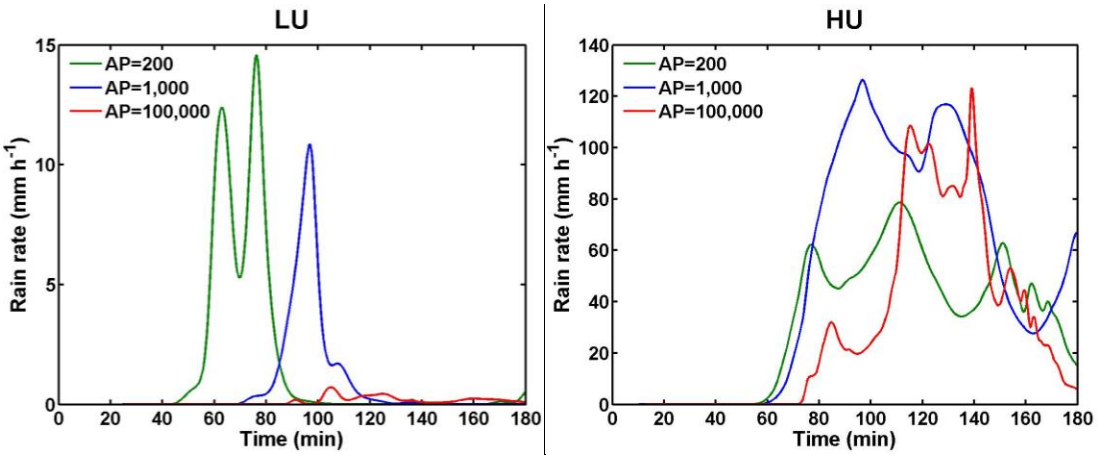

Figure 3.10: *Time evolution of surface rain rates for the three aerosol episodes (N_{CN} = 200, 1,000, and 100,000 cm^{-3}, respectively) under LU (low updrafts, FF=2,000 W m^{-2}) and HU (high updrafts, FF=50,000 W m^{-2}) conditions.*

3.3 Process analysis

The evolution of hydrometeor concentrations is determined by multiple microphysical and dynamical processes. It is often difficult to tell exactly how aerosol particles affect clouds and precipitation. Here we introduce a process analysis method to help understand the aerosol effects.

3.3.1 Clouds

Figure 3.11 summarizes the microphysical processes that act as the main sources (warm colorS) and sinks (cold colorS) for cloud droplets under different aerosol and fire forcing conditions. For N_{CD}, the dominant source term is the cloud nucleation (CCN activation) process, in which aerosols are activated under supersaturated water vapor and form cloud droplets. As cloud nucleation happens mostly at the cloud base and thus is not strongly affected by cloud dynamical feedbacks, the response of N_{CD} shows similar regimes to

cloud parcel models (Reutter et al., 2009). To help explain the regime designation, we divide N_{CD} into two factors: an ambient aerosol number concentration (N_{CN}) and an activated fraction (N_{CD}/N_{CN}). Given the aerosol size distributions, the N_{CD}/N_{CN} ratio is determined approximately by the critical activation diameter (D_c) above which the aerosols can be activated into cloud droplets. The D_c is a function of ambient supersaturation. Stronger updrafts result in higher supersaturation, smaller D_c and hence larger N_{CD}/N_{CN} ratios. Under high-updraft conditions (>15 m s^{-1}), N_{CD}/N_{CN} is already close to unity (Reutter et al., 2009). A further increase in the updraft velocity will still change the supersaturation and D_c, but it will not significantly influence the N_{CD}/N_{CN} ratios and N_{CD}. In this case, N_{CD} is approximately proportional to N_{CN}.

Under weak updrafts, the N_{CD}/N_{CN} ratio is sensitive to ambient supersaturations. In this case, a larger supersaturation induced by stronger updrafts can effectively change the N_{CD}/N_{CN} ratio, and thus N_{CD} is sensitive to the updraft velocity. On the other hand, the stronger dependence of N_{CD}/N_{CN} on the supersaturation also changes the role of aerosols. As more aerosols reduce supersaturation, increasing N_{CN} tends to reduce the activated fraction, N_{CD}/N_{CN}. Taking N_{CN} = 60,000 cm^{-3} (FF = 2,000 W m^{-2}), for example, a 10% increase in N_{CN} causes a 4% decrease in N_{CD}/N_{CN}, whereas a 10% decrease in N_{CN} leads to an 8% increase in N_{CD}/N_{CN}. The impact of changing N_{CN} on the N_{CD}/N_{CN} ratio counteracts partly or mostly the positive effect of N_{CN} on cloud droplet formation.

The changes in M_{CD} are influenced mainly by (sources) (1) the condensation of water vapor on the present cloud droplets (*vdc*) and (2) the cloud nucleation process (*cn*) and by (sinks) (3) cloud droplet evaporation (*cep*), (4) the accretion of cloud droplets (*ac*), and (5) the freezing of cloud droplets to form cloud ice (*cfi*), the latter of which includes heterogeneous (Seifert and Beheng, 2006) and homogeneous freezing processes (Jeffery and Austin, 1997; Cotton and Field, 2002). Concerning their relative contributions, the net change in condensational growth of cloud droplets (*vdc*) and cloud droplet evaporation (*cep*) dominates the change in M_{CD}. As N_{CN} increases, the condensation rate (*vdc*) does not change much, while the evaporation rate (*cep*) is raised greatly owing to increased surface-to-volume ratio of smaller cloud droplets. Condensation increases M_{CD} and evaporation reduces M_{CD}. In our study, the net effects are negative. A similar result

was reported by Khain et al. (2005) for deep convective clouds. They found that high CCN concentrations led to both greater heating and cooling, and that the net convective heating became smaller as CCN increased. However, the cloud nucleation rate is enhanced and the loss of cloud water due to other sinks (accretion for LU conditions, and *cfi* for HU conditions) decreases at the same time. This leads to a positive influence of N_{CN} on the total cloud water content.

Concerning the absolute contribution, increasing *FF* enhances the change rate of the conversion of water vapor to the condensed phase (R_{vdc} and R_{cn}), whose effect is straightforward. In addition, as *FF* increases, the conversion of cloud droplets to frozen particles, especially to ice (the *cfi* process), becomes increasingly important.

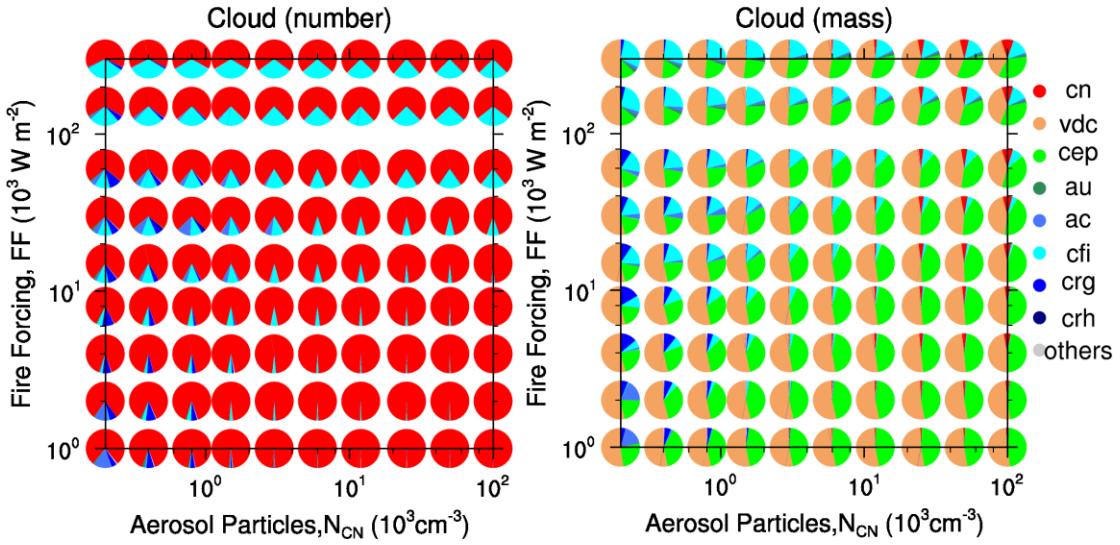

(a) (b)

Figure 3.11: *The pie charts summarize the relative percentage of the microphysical processes involving cloud droplets as a function of N_{CN} and fire forcing (a: number concentration; b: mass concentration). Colors within each pie chart reflect the contribution of processes under the specific condition. Warm colors denote the sources, while cold colors denote the sinks. Abbreviations are as follows: cn, cloud nucleation; vdc, condensational growth of cloud droplets; cep, evaporation of cloud droplets; au, autoconversion; ac, accretion; cfi, freezing of cloud droplets to form ice crystals, including homogeneous and heterogeneous nucleation; crg/h, riming of cloud droplets to form graupel/hail.*

The contribution of the microphysical processes in each modeling grid can be observed from the pie charts in Figure 3.12 (taking HUHA (w = 27 m s^{-1}; N_{CN}=100,000 cm^{-3})

for example, which is representative of the pyro-convective clouds). Each plot shows the vertical cross sections of the averaged change rate of main processes contributing to cloud water content over 30 simulation minutes. Colors within each pie chart reflect the percentage of contributions in each grid. CCN activation usually starts at cloud base, followed by condensational growth by water vapor deposition in the center of cloud. Towards both sides, cloud droplets convert to water vapor via evaporation. It is worth noting that the pie charts only represent the relative importance of each process at individual simulation grid, not the absolute amount. Though there are fewer *vdc*-dominated grids than *cep*-dominated grids, the total cloud formation rate from *vdc* is still similar to or higher than the *cep* processes. At cloud top with sub-freezing temperature, cloud droplets are frozen to ice crystals via homogeneous and heterogeneous nucleation. At the beginning stage of the cloud (30 min), the cloud droplets concentrate at the center of the modeling domain. As the cloud evolves, it starts to expand, and at the same time the margin area dissipates due to the sink processes (i.e., *cep*, *cfi*, and *ac*).

We are aware that the exact process rates may vary depending on the microphysical schemes used in the simulation (Muhlbauer et al., 2010). Therefore, we stress that the process analysis here is based on the Seifert microphysical scheme (Seifert and Beheng, 2006). In the future, further observations from laboratory and field measurements are needed to improve the understanding of aerosol-cloud interactions and to better constrain microphysical parametrizations.

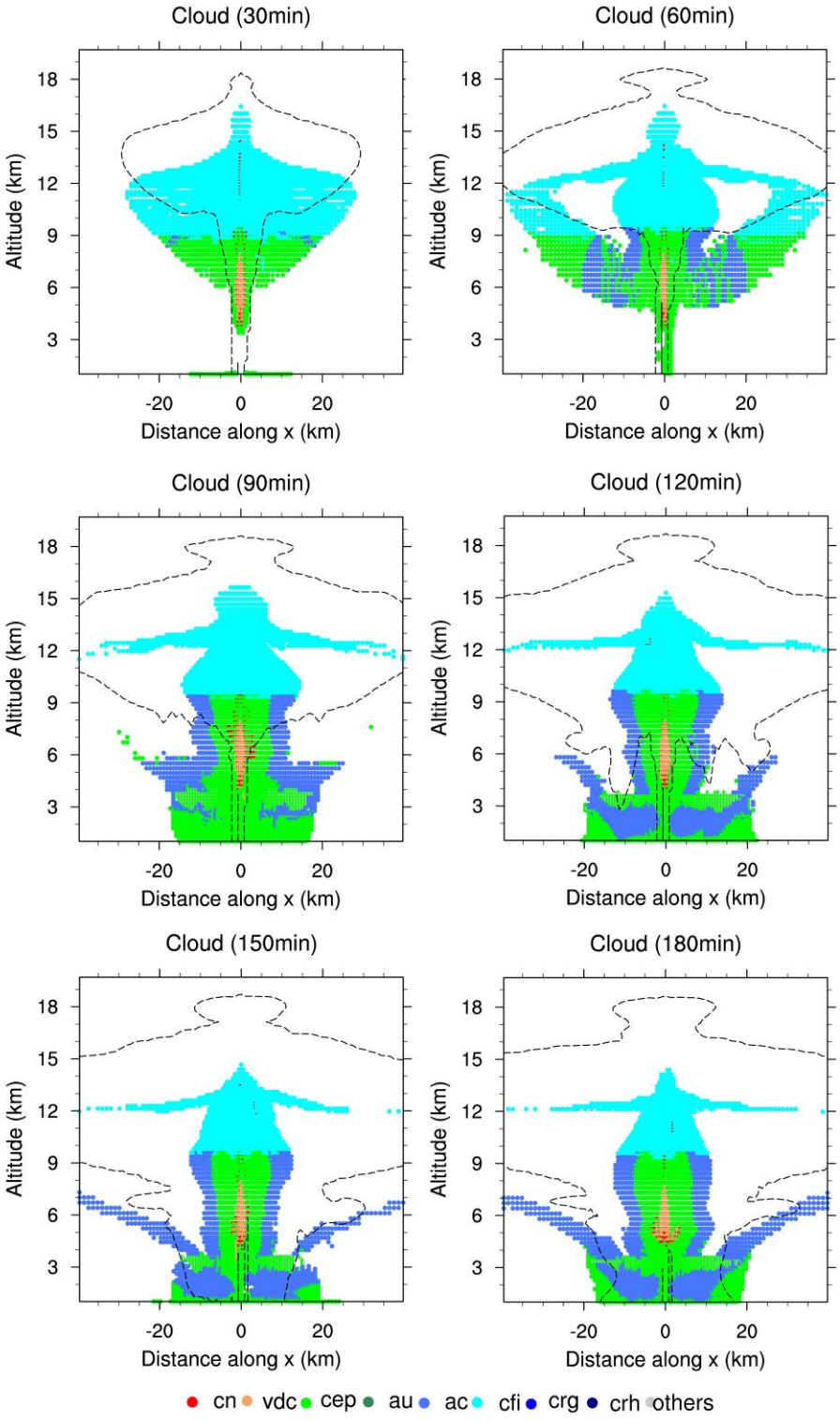

Figure 3.12: *The pie charts summarize the vertical cross sections of the change rate of main microphysical processes contributing to cloud water content. Each pie chart shows the averaged contribution over the past 30 min. Colors within each pie chart reflect the percentage of processes in each grid. The black dashed line is the 0.1 μg kg^{-1} isoline of*

the interstitial aerosol, indicating the shape of smoke plume. The meaning of the acronyms is the same as in Figure 3.11. Warm colors denote the source, while cold colors denote the sink.

3.3.2 Rain

Dynamic conditions strongly influence the pathways of rain formation and dissipation. For weak updraft cases, the warm rain processes, i.e., autoconversion (*au*) and accretion (*ac*), play a big role. Together with melting of snow (*smr*) or graupel (*gmr*), they are the main sources for raindrops (Figure 3.13). Under this condition, raindrops may appear at altitudes as high as 5–7 km (e.g., Figure 3.3a). For high updraft cases, strong updrafts deliver cloud droplets to higher freezing altitudes (Figure 3.1). The cloud droplets then turn directly into frozen particles (cloud→ice crystals), without formation of raindrops as an intermediate stage (cloud→rain→larger frozen particles; Figure 3.13). Most raindrops are formed from melted frozen droplets, and consequently they appear below ~4 km (Figure 3.3c, d). The weaker cloud→rain conversion with higher updrafts also influences the conversion of rain to frozen particles and is the reason why the *rrg* process (riming of raindrops to form graupel) under HULA becomes relatively less important as *FF* increases under low-aerosol conditions.

The aerosols also modify the pathways of rain formation. Taking weak updraft cases, for example, the accretion process (*ac*) dominates the cloud→rain conversion under low aerosol concentrations but is replaced by autoconversion (*au*) under high aerosol concentrations (Figure 3.13). The reason for this is that *au* is the process that initializes rain formation. Once rain embryos are produced, accretion of cloud droplets by raindrops is triggered and becomes the dominant process of rainwater production, as observed for shallow clouds (Stevens and Seifert, 2008) and stratiform clouds (Wood, 2005). High aerosol loading reduces *au*, inhibiting the initialization of rain and the following accretion processes at the early stage (0–100 min). Melted frozen particles are also a major source of raindrops. Under low-aerosol conditions, most of them form from melted graupel particles, whereas under high-aerosol conditions, they are converted mainly from snowflakes.

This is consistent with the aerosol impact on the relative abundance of frozen particles shown in Figure 3.6. A higher aerosol concentration leads to a higher fraction of smaller frozen particles (ice crystals and snowflakes). The main difference between low and high updrafts is that cloud conversion is the main source in the former case, whereas melted graupel/snow particles become the main contributors in the latter case.

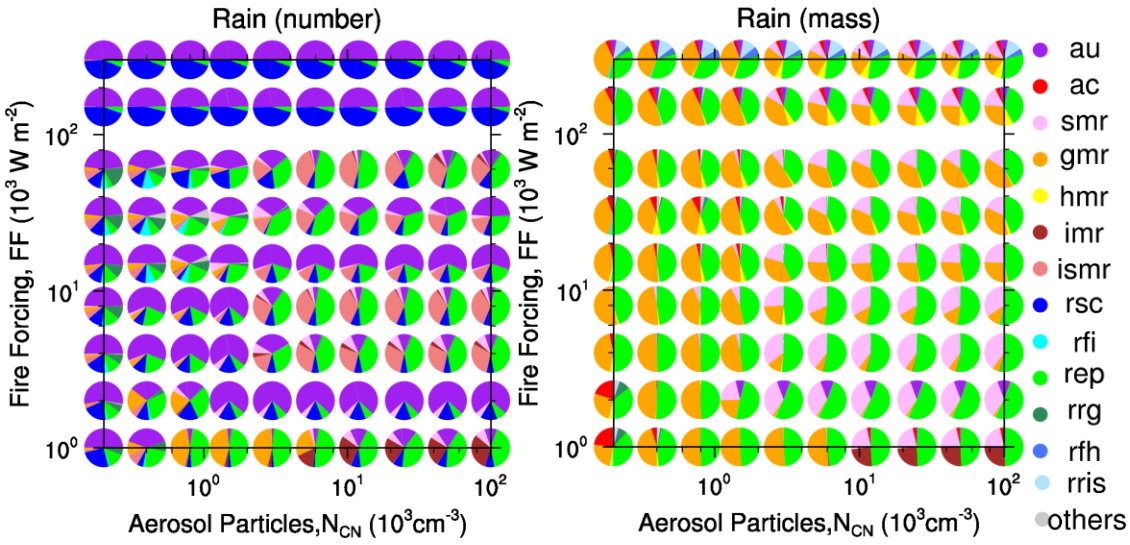

(a) (b)

Figure 3.13: *Same as Figure 3.11 but for raindrops. Abbreviations are as follows: au, autoconversion; ac, accretion; i/s/g/hmr, melting of ice/snow/graupel/hail to form raindrops; rsc, self-collection of raindrops; ismr, melting of ice and snow to form raindrops; rfi/h, freezing of raindrops to form ice crystals/hail; rep, raindrop evaporation; rrg, riming of raindrops to form graupel; rris, riming of raindrops to form ice and snow.*

Figure 3.14 illustrates the temporal evolution of the contribution of each process at individual simulation grid (HUHA case). As mentioned before, the warm rain process is quite unimportant under strong *FF* conditions (Figure 3.13b). However, it is observed that the warm rain process is the leading source of raindrops at the beginning stage (60 min). The raindrops formed from *au* and *ac* are relatively small, and can easily evaporate. The melting of frozen particles to form raindrops becomes more significant after ~90 min, which dominates the production of raindrops. As shown in Figure 3.14, although the pro-

cesses still continue at 180 simulation minutes, the microphysics have already fully developed during this simulation period. Thus our three simulation hours could cover the characteristics of the formation and evolution of the pyro-convective clouds. What is more, attention should be paid to the fact that long-term simulation may conceal some detailed information, leading to the bias in prediction of hydrometeors.

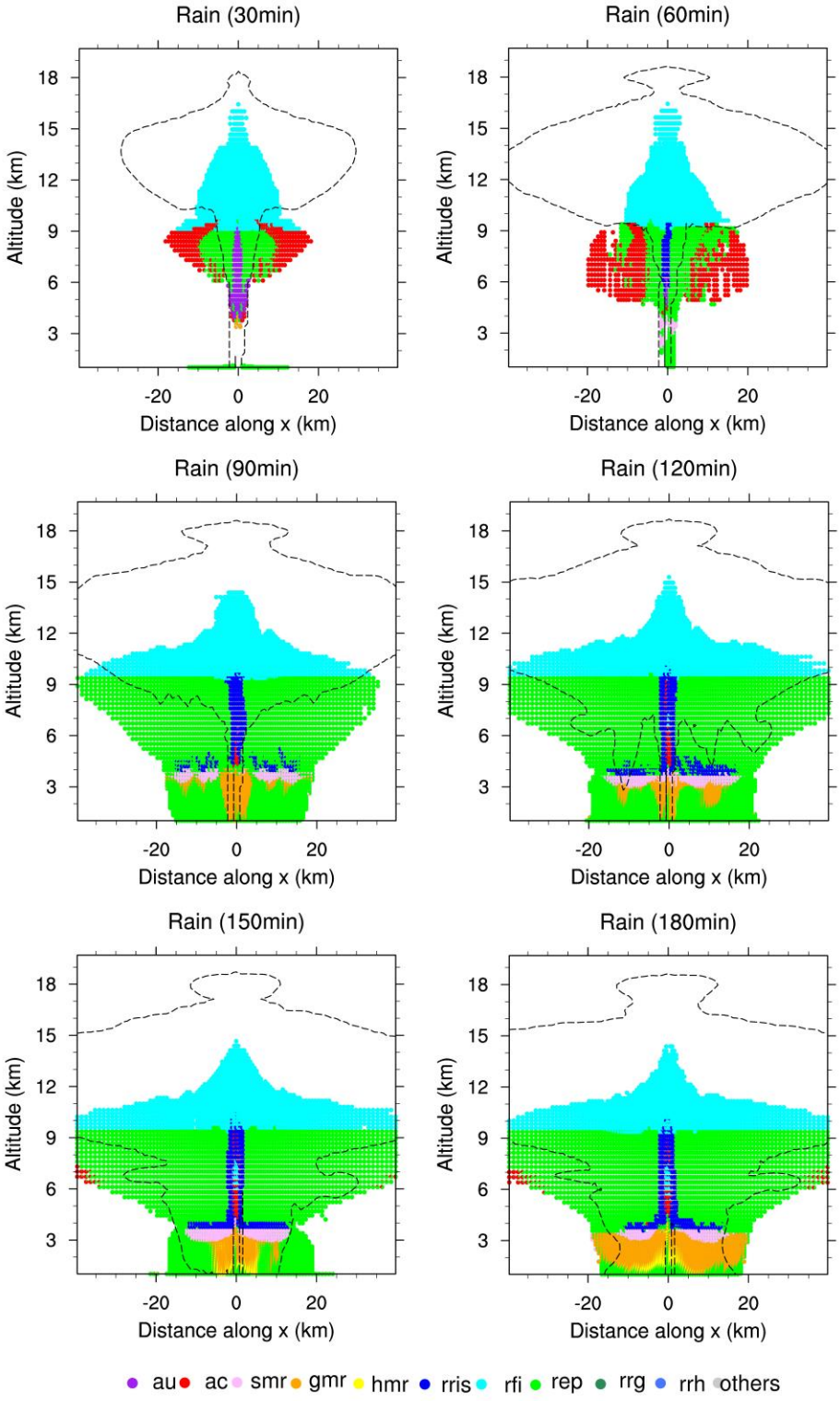

Figure 3.14: *Same as Figure 3.12 but for raindrops.*

The sensitivity of raindrops to aerosols mainly depends on autoconversion parameterization, the melting processes, etc. All those parameterizations have very large uncertainties, especially with bulk microphysical parameterizations. For example, most of the autoconversion schemes were developed or evaluated for stratocumulus clouds, which may not be appropriate for convective clouds. Based on the simulations during the convective phase of squall-line development, van Lier-Walqui et al. (2012) presented the uncertainty in the microphysical parameterization by the posterior probability density functions (PDFs) of parameters, observations, and microphysical processes. With the purpose to improve the representation of microphysics, it is of significance to quantify the parameterization uncertainty by using observation data to constrain parameterization.

3.3.3 Frozen water content

In this section, we only focus on the interactions between liquid water phase and solid water phase. As the self-collection and internal conversion between different frozen hydrometeors could also cause the change in number concentration of total frozen particles, the process analysis for its number concentration is not discussed. As shown in Figure 3.15, the effect of *FF* is straightforward, boosting vapor deposition (*vdi*) and cloud droplet freezing on ice (*cfi*). The *vdi* is always the most important pathway for the formation of frozen particles in our simulations, whereas *cfi* show comparable contributions in the HULA cases. Over a wide range of aerosol concentrations and updraft velocities, our results have extended and generalized the results of Yin et al. (2005), in which *vdi* and *cfi* were suggested as the dominant processes controlling the formation of ice crystals in individual mixed-phase convective clouds. Although snow is the dominant constituent of frozen particle mass (Figure 3.6), the deposition of vapor on ice (*vdi*) rather than on snow is the major pathway for frozen particles. The increase of snow mass is mostly caused by collecting of ice (*ics*) and ice self-collection (coagulation of ice particles, *iscs*), which are internal conversions not counted as either a source or a sink of frozen water content. The ice crystals used for conversion to snow derive mostly from the *vdi* process. Increasing *FF* enhances the upward transport of water vapor and liquid water to higher altitudes, where frozen particles can be formed effectively through *vdi* and *cfi*. On the other hand,

stronger *FF* reduces the residence time of cloud droplets in the warm environment (to form raindrops), which could explain the attenuation of *rrg* (riming of raindrops to form graupel) as fire forcing increases under low-aerosol conditions.

Positive relationship between aerosols and the frozen water content have been demonstrated in Sect. 3.2.3. As shown in Figure 3.15, the increase in frozen water content is achieved through the enhancement of the *vdi* process. The depositional growth rate R_{vdi} is a function of the number concentration (N_{ice}) and size (D_{ice}) of ice, together with the ambient supersaturation over ice (S_{ice}). In our simulations, the averaged S_{ice} and D_{ice} are not sensitive to the aerosol disturbance; it is N_{ice} that has been increased significantly because of elevated aerosol concentrations. Higher N_{ice} provides a larger surface area for water vapor deposition on the existing ice crystals and increases R_{vdi}. Lee and Penner (2010) suggested similar mechanisms for cirrus clouds, based on the double-moment bulk representation of Saleeby and Cotton (2004).

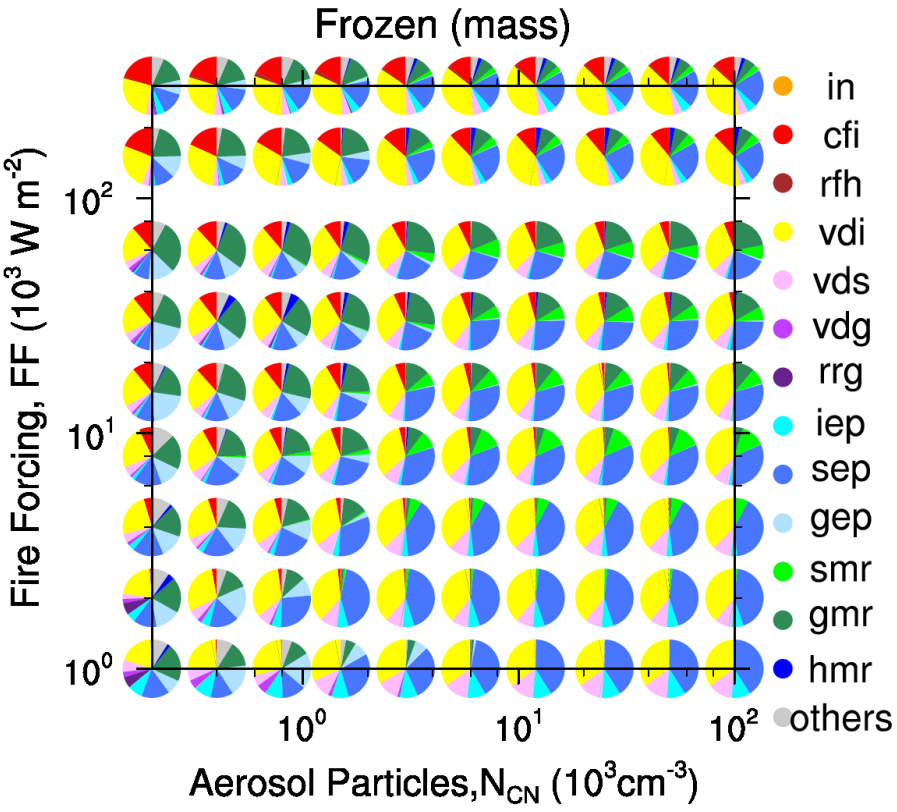

Figure 3.15: *Same as Figure 3.11 but only for the mass concentration of the frozen particles. Abbreviations are as follows: in, ice nucleation; cfi, freezing of cloud droplets to*

form ice crystals, including homogeneous and heterogeneous nucleation; rfh, freezing of raindrops to form hail; vdi/s/g, condensational growth of ice crystals/snow/graupel by water vapor; rrg, riming of raindrops to form graupel; i/s/gep, evaporation of ice/snow/graupel; s/g/hmr, melting of snow/graupel/hail to form raindrops.

The process of the formation and dissipation of frozen water content in the modeling area is illustrated in Figure 3.16. The ice crystals form firstly at a higher height, followed by the snow production at a lower level. Downdrafts in the margin region are caused mainly by evaporation and melting. Massive melting takes place at the late stage (after 90 min), when large frozen particles (i.e., graupel) form. This is in agreement with the fact that the raindrops appear at a late stage and at a lower altitude under strong *FF* conditions (Figure 3.3c and d).

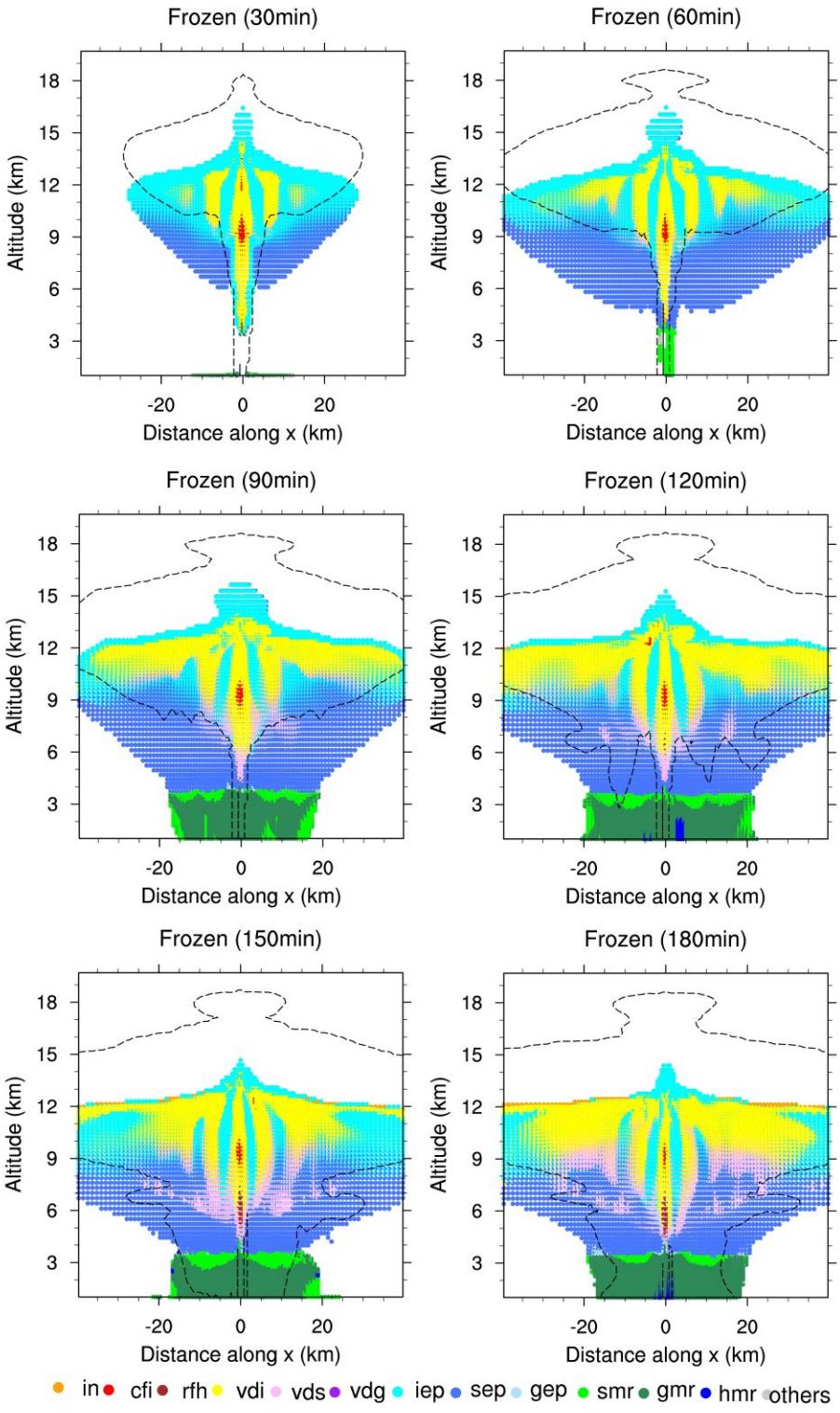

Figure 3.16: *Same as Figure 3.12 but for frozen particles.*

As shown aforementioned, drop freezing parameterizations and ice nucleation parameterizations influence frozen water content dramatically, which involve large uncertainties. Ice microphysics are significantly more complicated due to the wide variety of ice particle characteristics. On the one hand, the intensities of these processes differ greatly among different microphysical schemes. Eidhammer et al. (2009) compared three different ice nucleation parameterizations and found that different assumptions could result in similar qualitative conclusions although with distinct absolute values. The parameterization with observational constraints agrees well with the measurements. On the other hand, van Lier-Walqui et al. (2012) suggested the processes contributing to frozen particles are dependent on both particle size distribution and density parameters. Parameterization improvement based on observations could help to reduce the uncertainties.

3.3.4 Contribution of individual microphysical processes

ATHAM consists of tens of microphysical processes. However, based on the calculation of their relative contributions, only a few processes play dominant roles in regulating the number and mass concentrations of cloud hydrometeors, suggesting a possibility for the simplification of microphysical schemes.

For the number concentration of cloud droplets, the cloud nucleation (*cn*) and *cfi* (freezing of cloud droplets to form ice) processes contribute most to its budget, while other processes together account for less than 10%. For the mass concentration, the net change in *vdc* (condensational growth of cloud droplets by deposition) and *cep* (evaporation of cloud droplets) processes determines the variations in the cloud water content. The *cfi* process could contribute ~50% of the sink under LUHA conditions. Therefore, when we simulate the mass of cloud droplets, four microphysical processes, i.e., *cn*, *vdc*, *cep*, and *cfi*, account for a large fraction of the budget.

The dominant processes that contribute ~90% to the raindrop number concentration under specific conditions are autoconversion (*au*); self-collection (*rsc*); evaporation (*rep*); and melting of ice, snow, and graupel (*imr*, *smr*, and *gmr*). For the raindrop mass

concentration, the contribution of three processes accounts for ~90% under most conditions, which are rain evaporation (*rep*) and melting of snow and graupel (*smr*, and *gmr*).

For the frozen water content, under weak fire forcing conditions, *vdi* (condensational growth of ice crystals by deposition) and *sep* (snow evaporation) contribute ~90% of the source and sink respectively. Under strong fire forcing conditions, *vdi* and *cfi* together contribute 90% of the source, while *sep* and *gmr* together are the most important sink (90%).

These major processes can capture most of the qualitative and quantitative features of pyro-convection processes and this complex model can thus be simplified for many purposes to improve the computational capacity. Comparison between the comprehensive model and simplified framework will be performed and validated in future studies.

3.4 Uncertainties due to nonlinearity

Aerosol-cloud interactions are regarded as nonlinear processes. In this case, the local aerosol effects on a cloud-relevant parameter Y, i.e., $d\mathrm{Y}/dN_{\mathrm{CN}}$ can be different from $\Delta\mathrm{Y}/\Delta N_{\mathrm{CN}}$, the dependence derived from two case studies. Figure 1.4 has shown such an example: depending on the case selection, a positive (or negative) $d\mathrm{Y}/dN_{\mathrm{CN}}$ can correspond to a $\Delta\mathrm{Y}/\Delta N_{\mathrm{CN}}$ of 0. The question then arises of how much difference can be expected between $d\mathrm{Y}/dN_{\mathrm{CN}}$ and $\Delta\mathrm{Y}/\Delta N_{\mathrm{CN}}$. In the following, we take the responses of the precipitation to aerosols as an example to address this issue.

Figure 3.17 shows the statistics of the relative difference between $\Delta\mathrm{Y}/\Delta N_{\mathrm{CN}}$ and $d\mathrm{Y}/dN_{\mathrm{CN}}$ under LU and HU conditions, in which *Y* represents the precipitation rate. As precipitation is insensitive to aerosols for N_{CN} >10,000 cm^{-3}, only the cases with N_{CN} of 200~10,000 cm^{-3} are chosen in the calculation. The relative difference is defined as:

$$\text{Relative difference} = \frac{\frac{\Delta Y}{\Delta N_{CN}} - \frac{dY}{dN_{CN}}}{\frac{dY}{dN_{CN}}} \tag{6}$$

and $\frac{\Delta Y}{\Delta N_{CN}}$ is calculated as $\frac{\Delta Y}{\Delta N_{CN}} = \frac{Y(2N_{CN}) - Y(N_{CN})}{2N_{CN} - N_{CN}}$, in which the aerosol effect is determined by the difference between the reference case and that after doubling N_{CN}. $\frac{dY}{dN_{CN}}$ is the derivative of the precipitation rate at each N_{CN}, representing the local dependence of precipitation on N_{CN}.

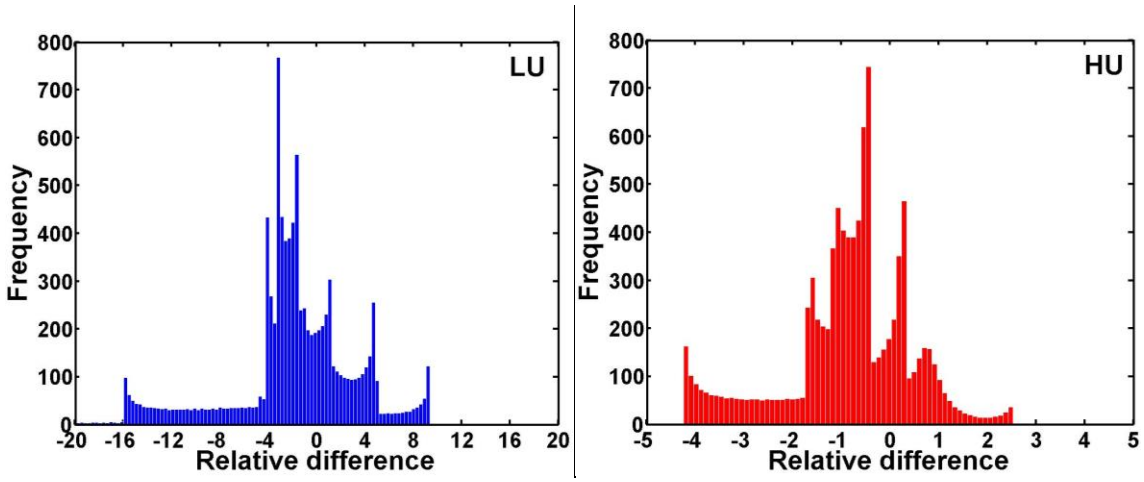

Figure 3.17: *Histograms of the relative difference between* $\frac{\Delta Y}{\Delta N_{CN}}$ *and* $\frac{dY}{dN_{CN}}$ *under LU and HU conditions, where Y here denotes precipitation rate.* $\frac{\Delta Y}{\Delta N_{CN}} = \frac{Y(2N_{CN}) - Y(N_{CN})}{2N_{CN} - N_{CN}}$, *and* $\frac{dY}{dN_{CN}}$ *is the derivative of the precipitation rate along the variable* N_{CN}.

The histograms in Figure 3.17 demonstrate that $\frac{\Delta Y}{\Delta N_{CN}}$ can deviate considerably from $\frac{dY}{dN_{CN}}$, not only for the absolute value but also for the sign. Statistically, most of the relative differences are in the range of −3.7~0.9 (the 25th and 75th percentiles respectively, with the average difference of -3.0) under LU conditions, while they are between −1.5 and 0.04 (the 25th and 75th percentiles respectively, with the mean value of 0.02) under HU conditions. The fact that individual case studies may not reveal local aerosol effects demonstrates the importance of ensemble studies in determining the real responses of clouds to aerosol perturbations.

3.5 Summary

Within this chapter, we employed the ATHAM model with full microphysics to investigate how a pyro-convective cloud responds to the change of aerosols (acting as CCN) and fire forcing (representing updraft velocity). A series of 2-D simulations (over 1000) were performed over a wide range of N_{CN} and dynamic conditions. The results show that: (1) the three regimes for cloud condensation nuclei (CCN) activation in the parcel model (namely aerosol-limited, updraft-limited, and transitional regimes) still exist within our pyro-cloud simulations. The production of raindrops and frozen particles is mostly controlled by updrafts, and insensitive to CCN concentrations. (2) Generally, elevated aerosols enhance the formation of cloud droplets and frozen particles. The response of raindrops and precipitation to aerosols is more complex and can be either positive or negative as a function of aerosol concentrations. The most negative effect was found for values of N_{CN} of ~1000 to 3000 cm^{-3}. (3) The involvement of nonlinear (dynamic and microphysical) processes leads to a more complicated and unstable response of clouds to aerosol perturbation compared with the parcel model results. Therefore, conclusions drawn from limited case studies might require caveats regarding their representativeness, and high-resolution ensemble studies over a wide range of aerosol concentrations and updraft velocities are strongly recommended.

The PA provided further insight into the mechanisms of aerosol−cloud interactions. By calculating the contribution of the associated processes to an individual hydrometeor, the PA revealed the dominant factors responsible for the changes in hydrometeor number and mass. (1) Cloud nucleation (*cn*) initializes cloud droplet formation and is the major factor that controls the number concentration of cloud droplets. As expected, the increase in cloud droplet mass can be mostly attributed to the condensational growth (*vdc*). (2) Under weak *FF*, autoconversion (*au*) and accretion (*ac*) are the main sources of rain droplets. Under strong *FF*, the major source is the melting of frozen particles. (3) For the frozen content, water vapor deposition on existing ice crystals (*vdi*) is the most important contributor. In addition to CCN activation, the PA also highlights the significance of other microphysical processes in regulating pyro-cloud formation, which is worthy of detailed parameterization.

Chapter 4 IN effects on cloud and precipitation

4.1 Introduction

Ice microphysical processes in mixed-phase clouds are of significance to cloud radiative and optical properties and precipitation production. The ice phase scheme consists of the primary ice nucleation, ice crystal growth by water vapor deposition, freezing and riming of cloud droplets to form ice crystals, ice aggregation, multiplication, melting, etc. (Seifert and Beheng, 2006). The understanding of ice formation mechanisms, especially heterogeneous ice nucleation is one of the key questions of theoretical and applied physics of clouds. Compared to cloud nucleation, ice nucleation is more complicated and much less understood. Large uncertainties exist in the representation of ice nucleation processes in models, and aerosol effects on mixed-phase clouds due to the complicated interaction. In Sect. 4.2, in combination with process analysis (PA), we focus on the statistical behavior of the response of each hydrometeor to changing IN number concentration (fixed CCN) and fire forcing (*FF*). In addition, the joint effect of CCN and IN on pyro-clouds is also simulated and presented in Sect. 4.3.

4.2 Dependence of hydrometeors on IN and fire forcing

4.2.1 Cloud droplets

Figure 4.1 displays the isopleths of cloud droplets as a function of initial aerosol concentrations (N_{CN}) and fire forcing. As expected, fire forcing exerts positive influence in the formation of cloud droplets. When fire forcing is low, both N_{CD} and M_{CD} are very sensitive to the change of fire forcing. When fire forcing gets higher, N_{CD} and M_{CD} become less sensitive to fire forcing. Different from the effect of CCN concentration, cloud droplets have negative relationship with the variation in IN concentrations. A higher IN concentration (high N_{CN}) leads to less M_{CD}, especially under high updraft (HU) condition. This is consistent with previous finding, which also denotes an increase in IN leads to a decline in cloud liquid water because of more efficient freezing (Seifert et al., 2012). Under low updraft (LU) condition, changing IN concentration hardly has influence on the cloud formation with $RS(N_{CN})$ around zero.

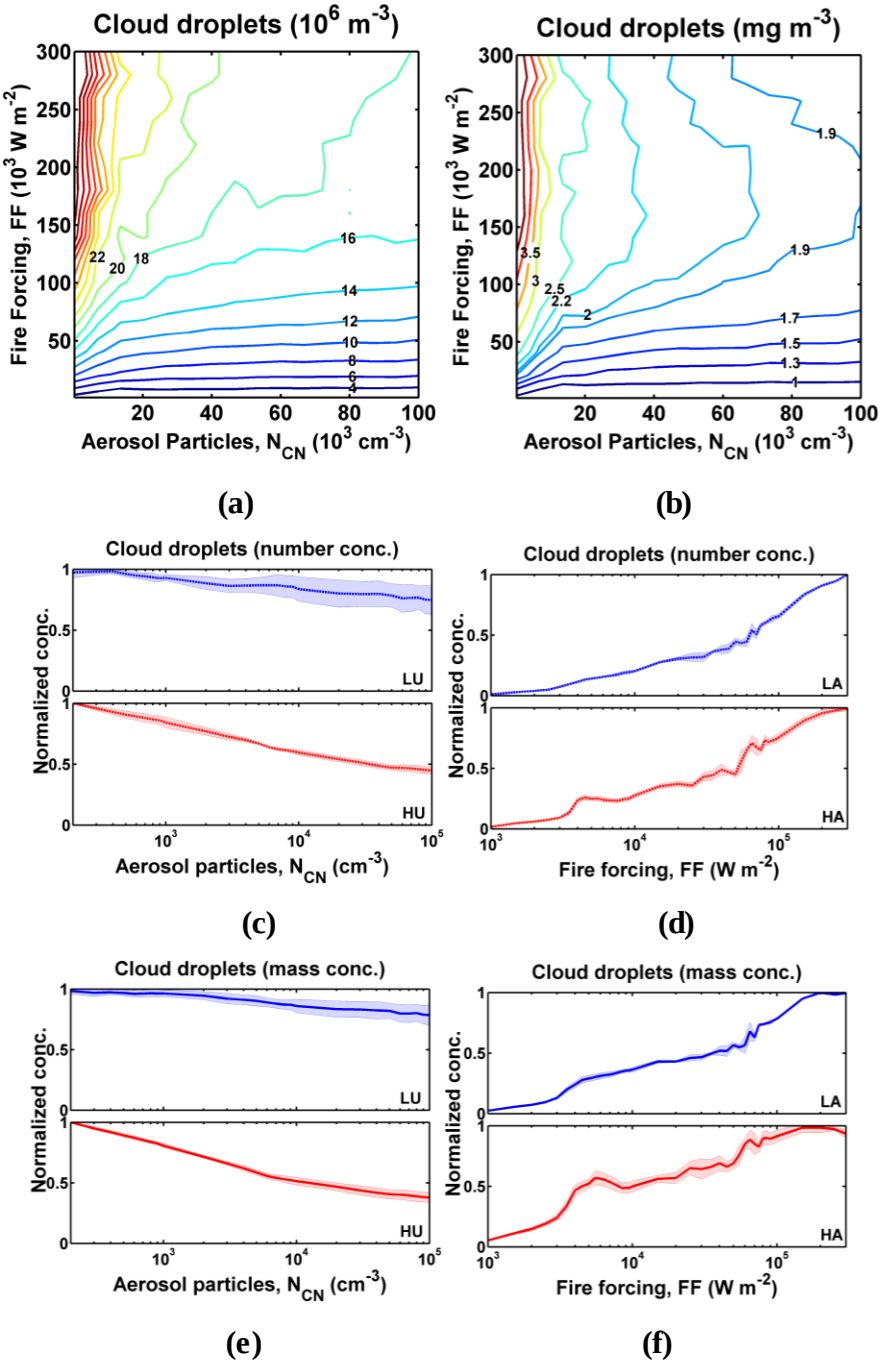

Figure 4.1: *Domain averaged number (a) and mass concentrations (b) of cloud droplets calculated as a function of aerosol number concentrations (N_{CN}) and fire forcing (FF). Normalized cloud droplet number concentration (relative to the maximum value) as a function of N_{CN} (c) and FF (d); and normalized mass concentrations as a function of N_{CN} (e) and FF (f).*

The evolution of cloud water content also demonstrates the suppression of cloud water due to IN from qualitative aspect (Figure 4.2). More IN results in a great decline in the liquid-phase cloud top height and hence shallower liquid-phase cloud depth (defined as the height between cloud base and cloud top). This is consistent with previous convective-scale model studies (Seifert et al., 2012). As shown in Figure 4.3, similar with the process analysis for cloud droplets in Sect. 3.3.1, the major contributor to N_{CD} is cloud nucleation, and freezing of cloud droplets (including homogeneous and immersion freezing) is the dominant sink. The net change of cloud droplet growth by vapor deposition (*vdc*) and droplet evaporation (*cep*) governs the variation in M_{CD} except for HULA case, in which homogeneous freezing of cloud droplets plays a great role.

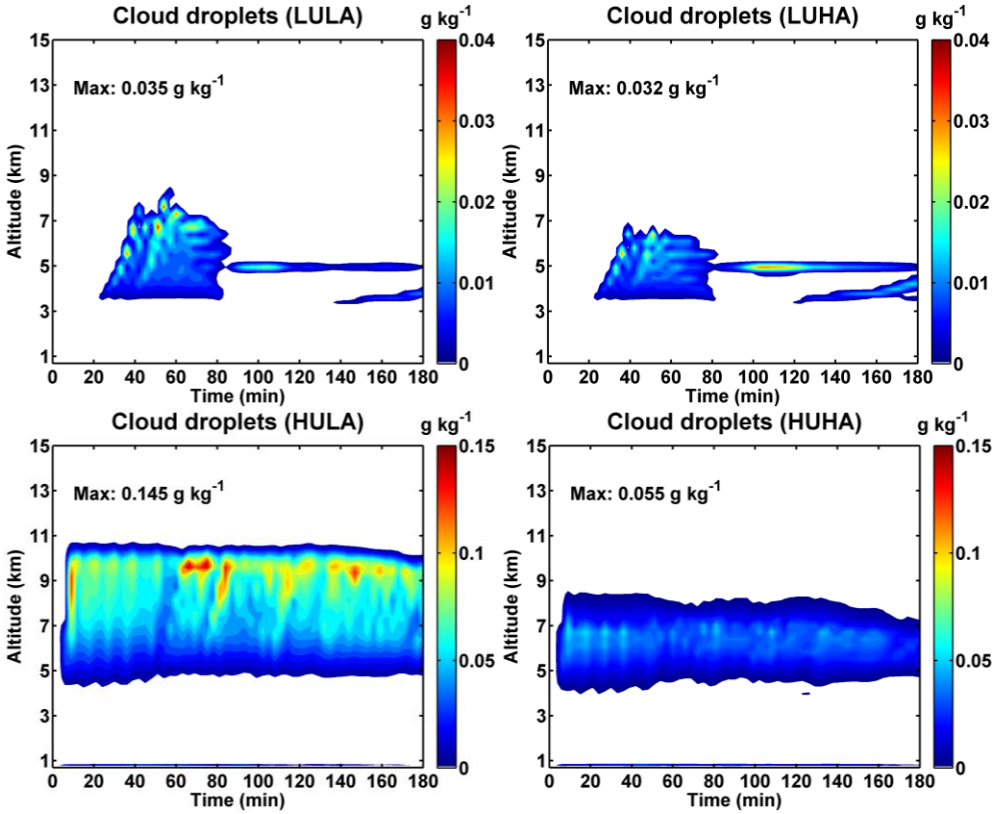

Figure 4.2: *Time evolution of horizontally-averaged cloud water content (g kg^{-1}) as a function of altitude for four extreme cases, which are referred to as (1) LULA: low updrafts (2,000 W m^{-2}) and low aerosols (200 cm^{-3}); (2) LUHA: low updrafts (2,000 W m^{-2}) and high aerosols (100,000 cm^{-3}); (3) HULA: high updrafts (300,000 W m^{-2}) and low aerosols (200 cm^{-3}); (4) HUHA: high updrafts (300,000 W m^{-2}) and high aerosols (100,000 cm^{-3}). Maximum values for each episode are also shown.*

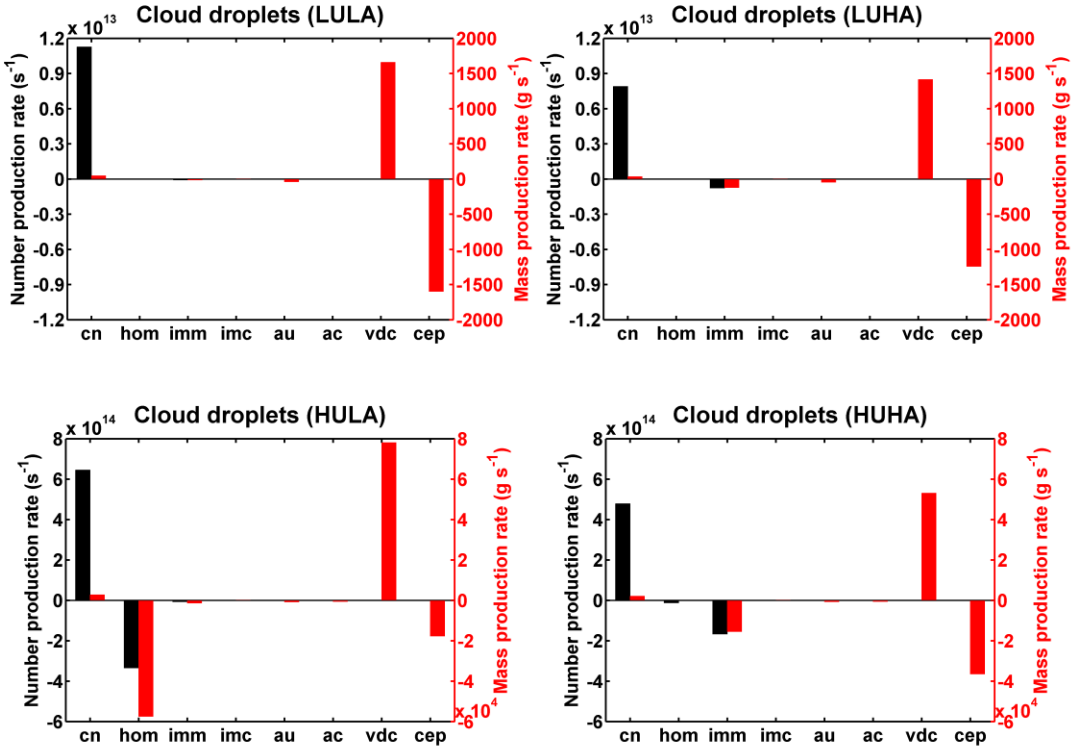

Figure 4.3: *Comparisons of the time-averaged rates of change in cloud droplet concentration resulting from main processes, which were obtained from the domain-integrated values. Histograms indicate contributions of processes to number concentration (black) and mass concentration (red). Sources are plotted as positive values, and sinks are negative. The acronyms indicate cn: cloud nucleation; hom: homogeneous freezing of cloud droplets; imm: immersion freezing of cloud droplets; imc: melting of ice crystals to form cloud water; au: autoconversion; ac: accretion; vdc: vapor depositional growth of cloud droplets; cep: the evaporation of cloud droplets, which is the opposite process of vdc.*

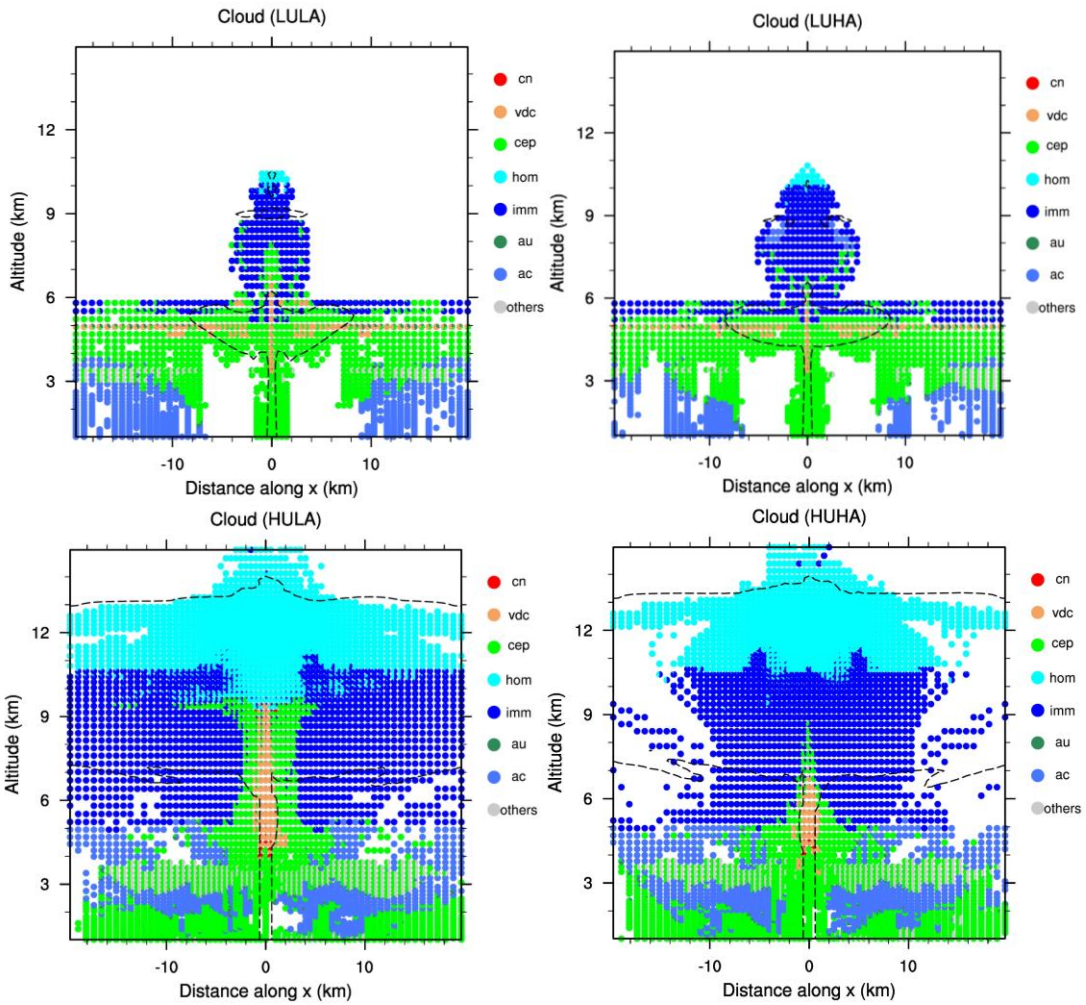

Figure 4.4: *The pie charts summarize the vertical cross sections of the time-averaged change rate of main microphysical processes contributing to cloud water. Colors within each pie chart are reflective of the percentage of processes in each grid. The black dashed line is the 0.1 μg kg^{-1} isoline of the interstitial aerosol, indicating the shape of smoke plume. The meaning of the acronyms is the same as in Figure 4.3. The warm color denotes the source, while the cold color denotes the sink.*

The pie charts in Figure 4.4 summarize the spatial distribution of the time-averaged change rate of main microphysical processes contributing to cloud water under four extreme conditions. It is worth noting that the colored pie charts just reflect the percentage of the contribution of individual process to each modeling grid. Immediately fol-

lowing the formation of cloud droplets through cloud nucleation (*cn*) at cloud base, cloud droplets proceed to grow by the process of vapor deposition (*vdc*) at the center of cloud with updrafts. The evaporation (*cep*) usually occurs at both sides of *vdc* with downdrafts. At cloud top with subfreezing temperature, cloud droplets could be frozen to ice crystals via homogeneous and heterogeneous (immersion) freezing nucleation. At the margin of the cloud, each grid is usually dominated by one major process; while at the center area, several processes could occur in a same grid point at the same time, representing the transition between different microphysical processes.

As shown in Figure 4.5, increasing IN under same fire forcing conditions could suppress vapor deposition on cloud droplets (*vdc*), and accelerate cloud droplet evaporation (*cep*). The growth of cloud droplets is based on the difference between water vapor mixing ratio and saturation specific humidity. Adding IN leads to more efficient heterogeneous (immersion) freezing, and hence more ice embryos (but much lower than CCN number density). The evaporation of small cloud droplets at cloud top could provide more water vapor, leading to a higher supersaturation with respect to ice and enhanced growth of ice embryos by vapor deposition. At the same time, the consumption of water vapor could reduce the water saturation, thereby further boosting the evaporation of cloud droplets. This implies at the same subfreezing temperature, the ice embryos could gain mass via vapor deposition at the expense of the cloud droplets that would lose their mass through evaporation. This is so-called Wegener-Bergeron-Findeisen (WBF) process. Owing to this process, the water vapor cannot condense on cloud droplets at a high altitude with more IN, whereas the evaporation would occur earlier at a lower level (Figure 4.5b, d).

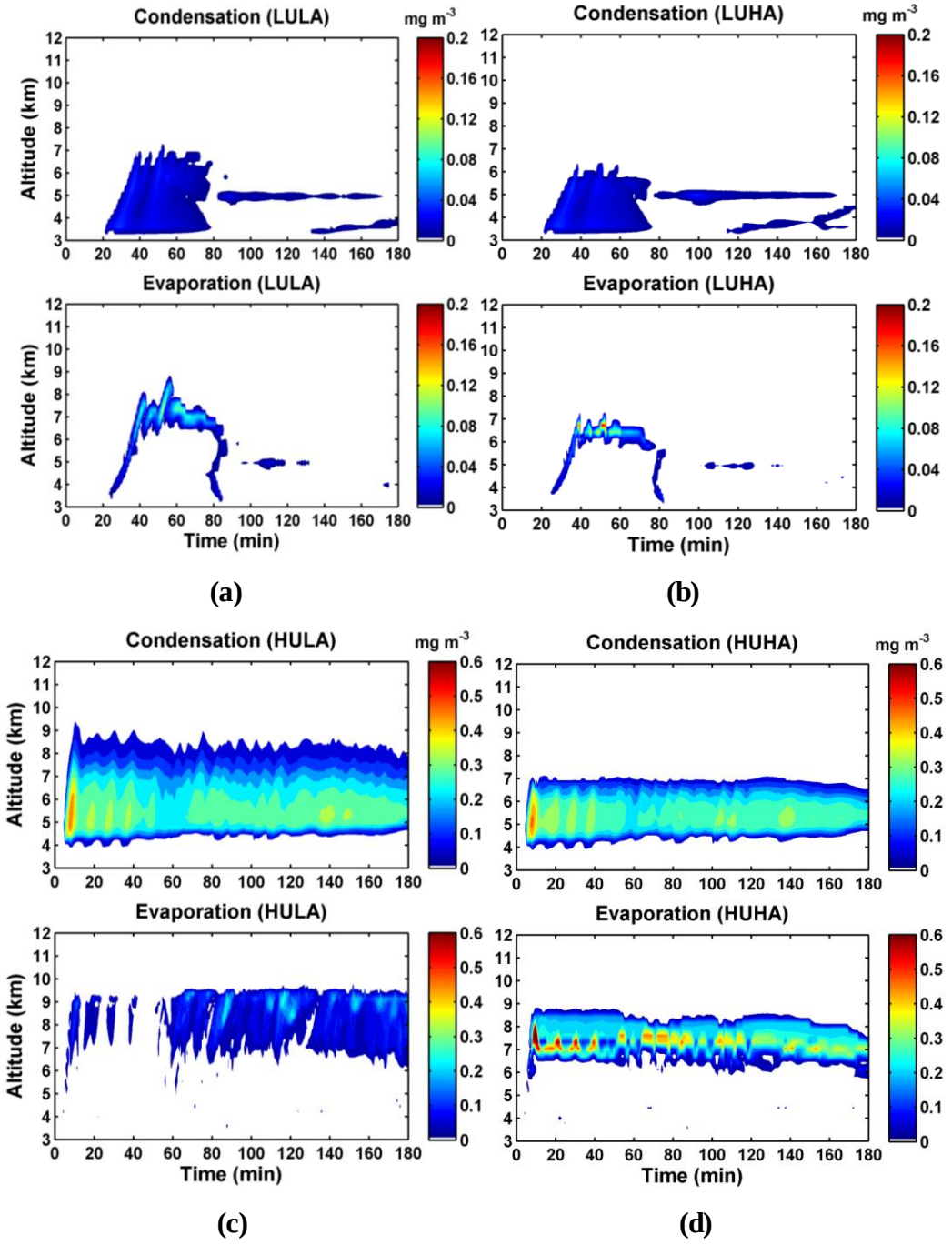

Figure 4.5: *Time evolution of horizontally-averaged rate of vdc (condensation) and cep (evaporation) as a function of altitude for four extreme cases.*

4.2.2 Raindrops

The isopleths of the number and mass concentration of raindrops as a function of aerosol concentrations and fire forcing could be seen in Figure 4.6. Based on the calculated $RS(N_{CN})$ to $RS(FF)$ ratio, the formation of raindrops is mainly controlled by the fire forcing. For mass concentration (M_{RD}), M_{RD} and fire forcing are positively correlated, and $RS(FF)$ is extremely high with weak fire forcing. An increase in aerosols could slightly boost the production of raindrops when N_{CN} is very low. This is consistent with regional-scale modeling studies (Seifert et al., 2012). For the number concentration (N_{RD}), N_{RD} is maximum around fire forcing of 300,000 W m^{-2}. The aerosol (acting as IN) effect on N_{RD} is nearly negligible within this study.

The tempo-spatial distribution of raindrops in Figure 4.7 also shows that the effect of IN under the same fire forcing condition is very small. When fire forcing is very strong, the distribution of raindrops usually occur at a very low elevation with temperature above 0 ℃. When fire forcing is weak, raindrops could be observed in a higher altitude. The reason for this phenomenon will be explained through the PA results.

The contribution of major microphysical processes involving raindrops is compared in Figure 4.8, and their governing region could be observed in Figure 4.9. For mass concentration of raindrops (M_{RD}), autoconversion plays an important role under LU condition, as well as melting of snow (*smr*). Under HU condition, the contribution of autoconversion to M_{RD} is very small, most of which is from melting of graupel, snow and hail that occurs at temperature above 0 ℃. This can be ascribed to the inhibition of warm rain processes (e.g., autoconversion, accretion) with strong fire forcing, which leads cloud droplets are prone to be converted to frozen particles rather than to raindrops. The raindrops at the center could be directly rimed to small frozen particles, which is not so important under LU condition. The loss of M_{RD} is mostly through the process of evaporation (*rep*), which mainly occurs in the margin of cloud and beneath the melting layer.

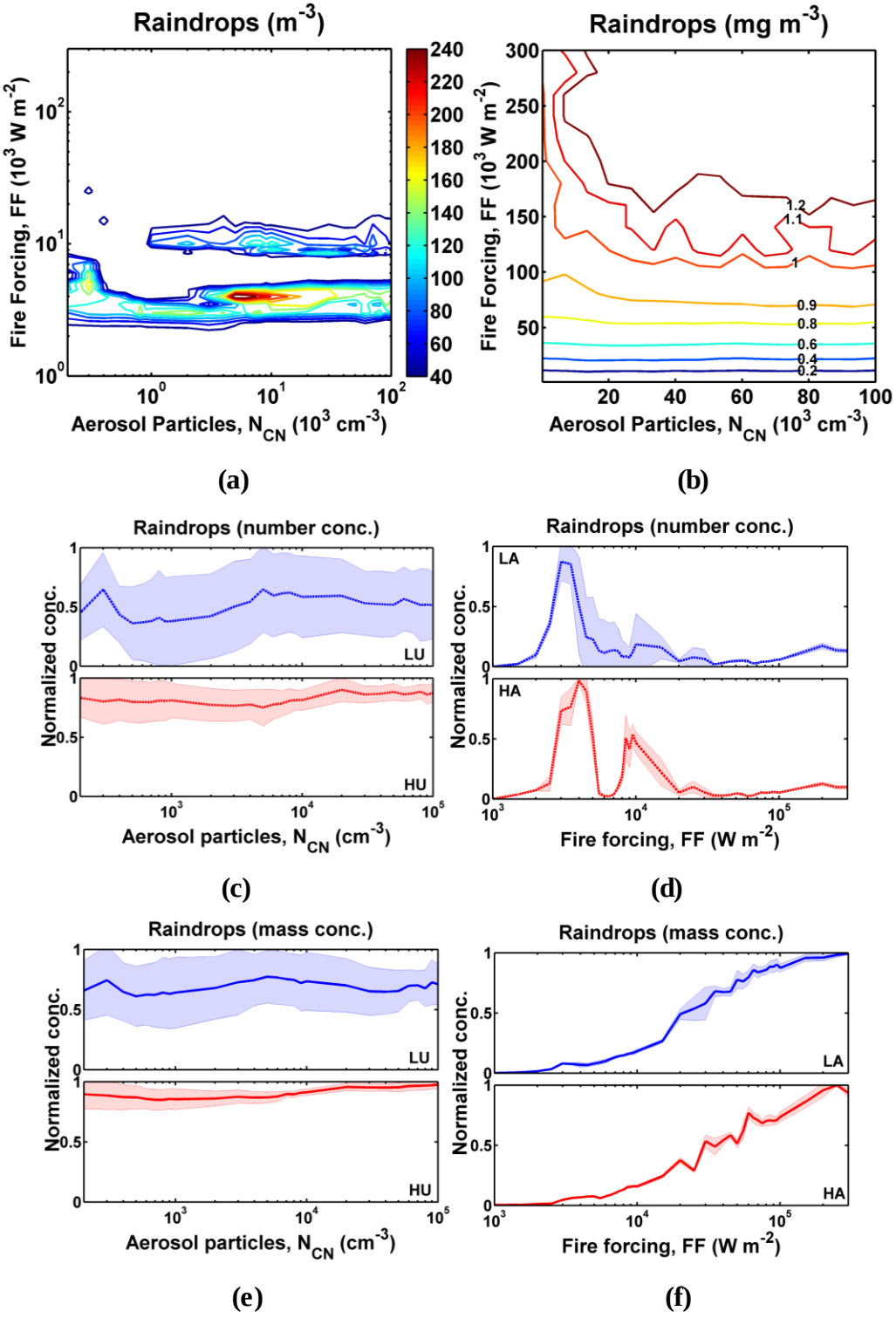

Figure 4.6: *Same as Figure 4.1 but for raindrops.*

For number concentration of raindrops (N_{RD}), autoconversion serves as the major source for all conditions, which occurs around cloud base. Freezing of raindrops to form ice crystals (*rfi*), which takes place at cloud top with sub-zero temperature, is the leading sink under LU condition, and the selfcollection of raindrops (*rsc*) is the dominant sink under HU condition. As a matter of fact, the absolute change rate of *rfi* is enhanced under HU condition. However, in comparison with raindrop selfcollection (*rsc*) rate which increases greatly due to enormous production of rain water from melting of frozen particles, the contribution of *rfi* becomes not so important.

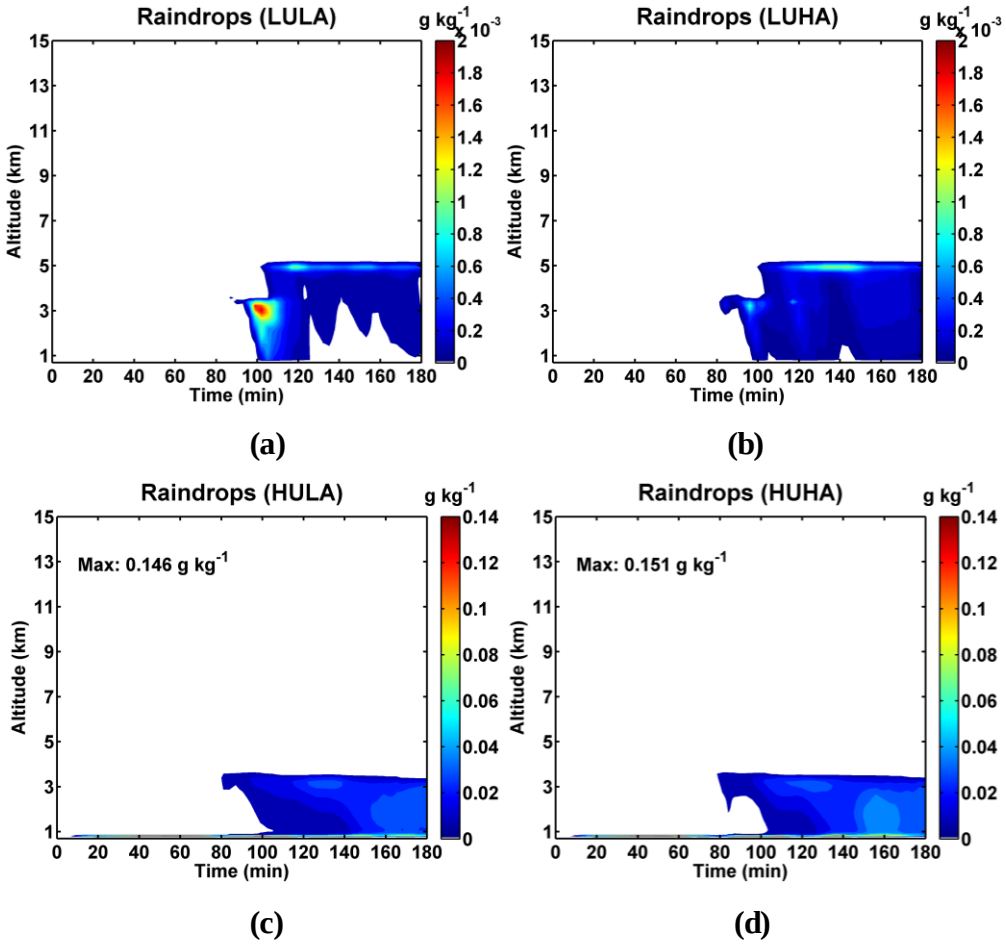

Figure 4.7: *Same as Figure 4.2 but for raindrops.*

Combining with process analysis, we found the formation of raindrops at a high elevation (~5km, Figure 4.7a, b) is associated with autoconversion and accretion of cloud droplets; while the appearance of raindrops at a low elevation (~3km, Figure 4.7c, d) is attributed to the melting of frozen particles (i.e., graupel, snow and hail). The first peak of raindrops in Figure 4.7a, b is associated with the important contribution of snow melting (Figure 4.8a, b).

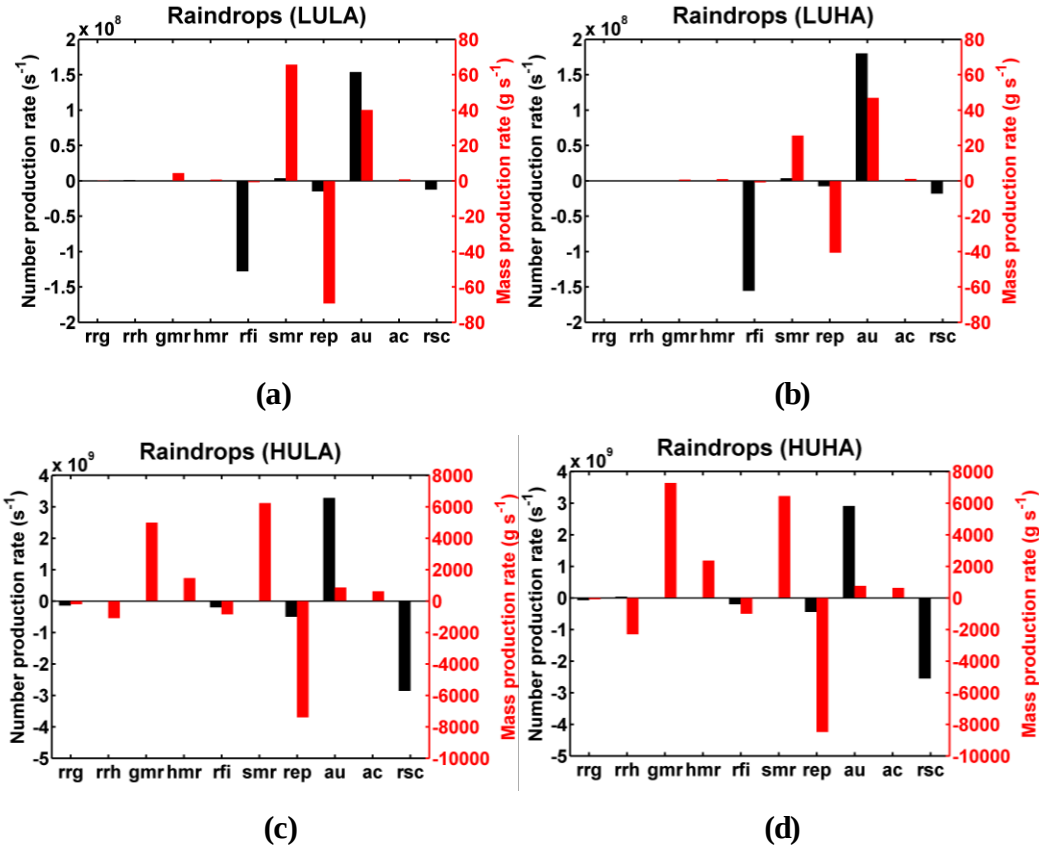

Figure 4.8: *Same as Figure 4.3 but for raindrops. The acronyms indicate rrg/h: riming of rain to form graupel/hail; g/h/smr: melting of graupel/hail/snow to form raindrops; rfi: freezing of raindrops to form ice crystals; rep: evaporation of rain; au: autoconversion; ac: accretion; rsc: self-collection of raindrops.*

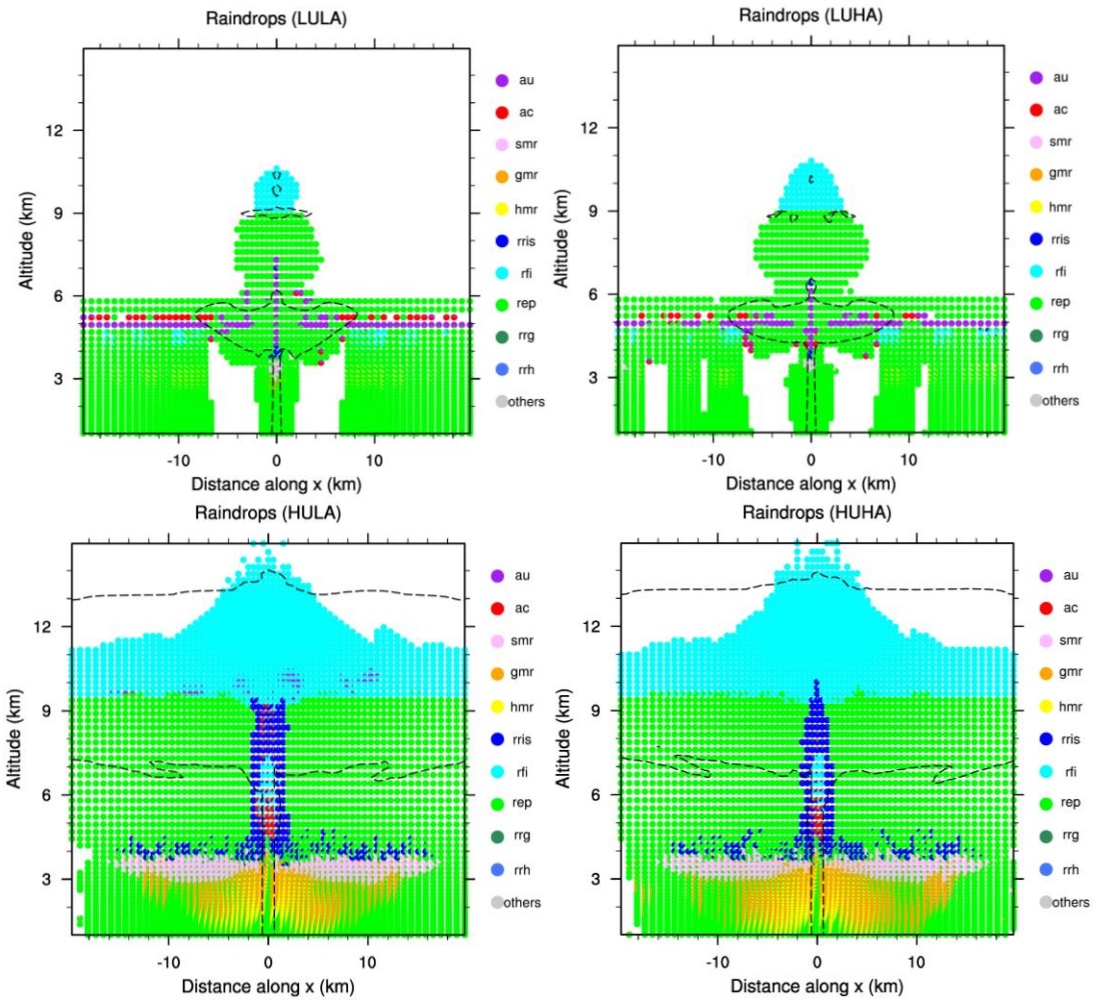

Figure 4.9: *Same as Figure 4.4 but for raindrops (rris: riming of raindrops to form ice and snow; the meaning of other acronyms is the same as in Figure 4.8).*

4.2.3 Cloud ice

As IN affects the cloud formation through the direct interaction between IN and ice crystal, besides the total frozen particles, the results concerning cloud ice are also presented and discussed. Figure 4.10 shows the dependence of number and mass concentration of ice crystals (N_{ice} and M_{ice}) on aerosols and fire forcing. In general, the effect of fire forcing overwhelms the influence of aerosol concentrations. When fire forcing is weak, cloud ice (both N_{ice} and M_{ice}) is very sensitive to the change of fire forcing; when fire forcing is stronger, N_{ice} and M_{ice} is less sensitive to fire forcing. The influence of IN concentration

(N_{CN}) is in general very weak. An increase in the IN concentration by a factor of 500 would result in less than 50% change in N_{ice} and ~20% change in M_{ice}. Our results also suggest a non-monotonic relationship between aerosols and M_{ice}. When fire forcing is weak (LU condition), it seems adding more potential IN gives rise to a slight increase on M_{ice}. When fire forcing is strong (HU condition), IN plays a negative role in M_{ice}.

The time evolution of cloud ice (Figure 4.11) exhibits that as IN increases, the cloud ice depth (which is defined as the height between the base and top of cloud ice) becomes deeper. Weaker fire forcing significantly delay the initiation of ice crystals, compared to strong fire forcing. This spatio-temporal distribution also demonstrates the positive effect of IN on cloud ice under LU condition and negative impact under HU condition.

The main contributors to N_{ice} and M_{ice} are shown in Figure 4.12 for four extreme scenarios. For N_{ice}, except the HULA case, immersion freezing (*imm*) is the dominant source, and adding more IN leads to a great increase in the averaged freezing rate (Figure 4.13). This agrees well with parcel model study in Eidhammer et al. (2009), convective-scale model investigation in Seifert et al. (2012), and a global model research in Yun and Penner (2012), which focused on the IN impact on heterogeneous ice nucleation. This is not surprising that the contribution of deposition freezing nucleation is nearly negligible, which is in agreement with Wang et al. (2014a).

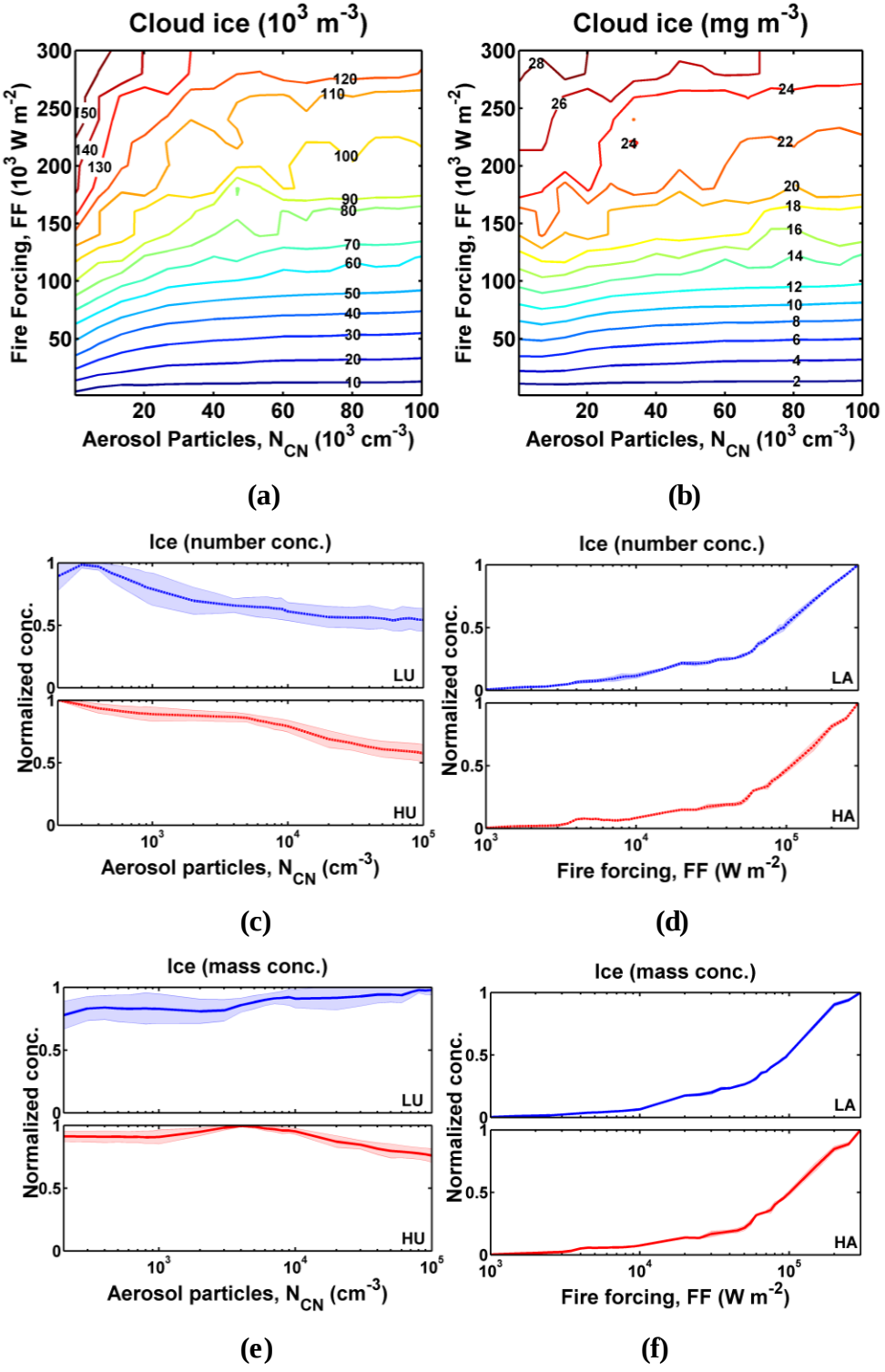

Figure 4.10: *Same as Figure 4.1 but for ice crystals.*

However, under HULA condition, the homogeneous freezing rate is remarkable, which is only temperature-dependent in ATHAM model (Jeffery and Austin, 1997; Cotton and Field, 2002). We found under such condition, the homogeneous freezing occurs at the altitude higher than ~10 km (Figure 4.14c), where the temperature is down to -50 ℃. As low IN inhibits the conversion between cloud droplet and ice phase, this allows lots of cloud droplets still existing in this high region (Figure 4.2c), which will be homogeneously frozen to be ice. Therefore, homogeneous nucleation dominates the production of N_{ice} for this case. However, under HUHA condition, the cloud top significantly descends below 10 km (Figure 4.2d) due to strong evaporation (see Sect. 4.2.1) and fast conversion into the ice phase, leading to very little cloud water available for homogeneous freezing (Figure 4.14d). Under LU condition, the homogeneous freezing is negligible compared to heterogeneous freezing (Figure 4.14a, b).

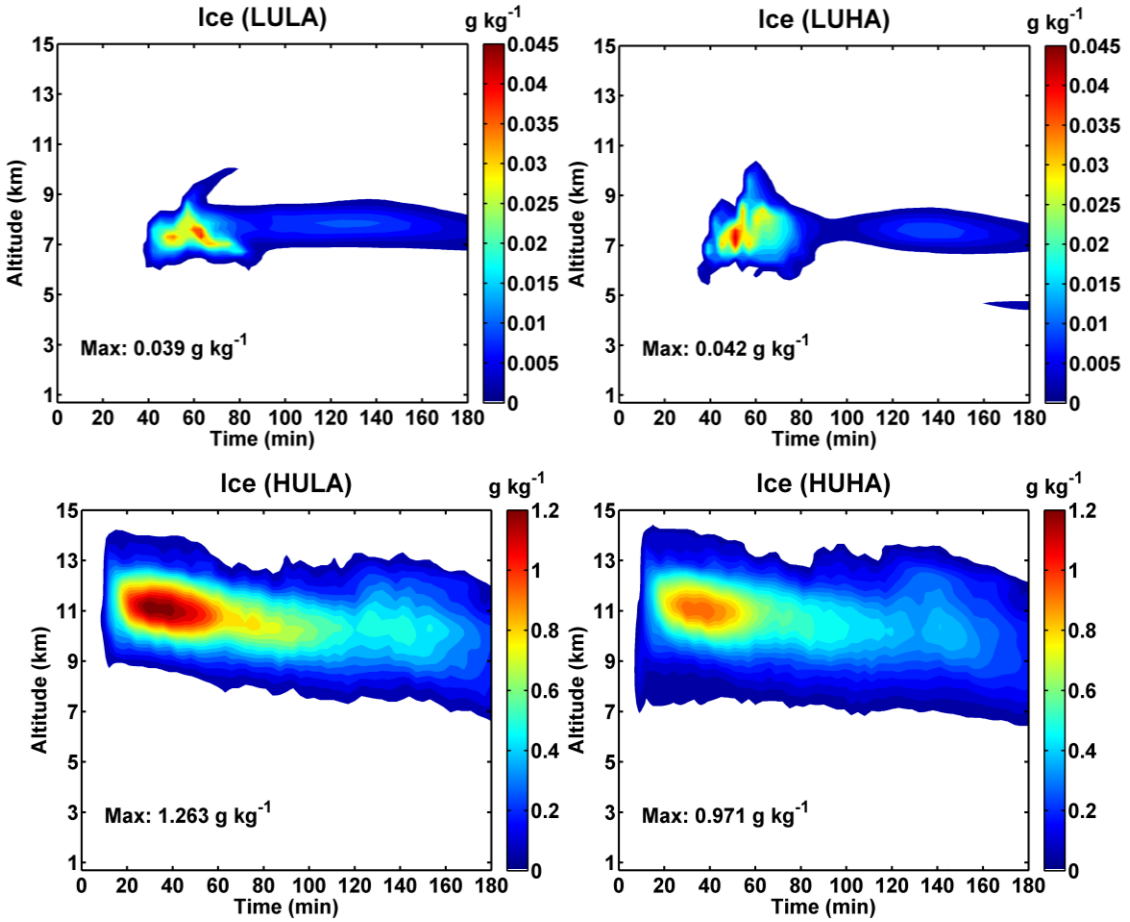

Figure 4.11: *Same as Figure 4.2 but for ice crystals.*

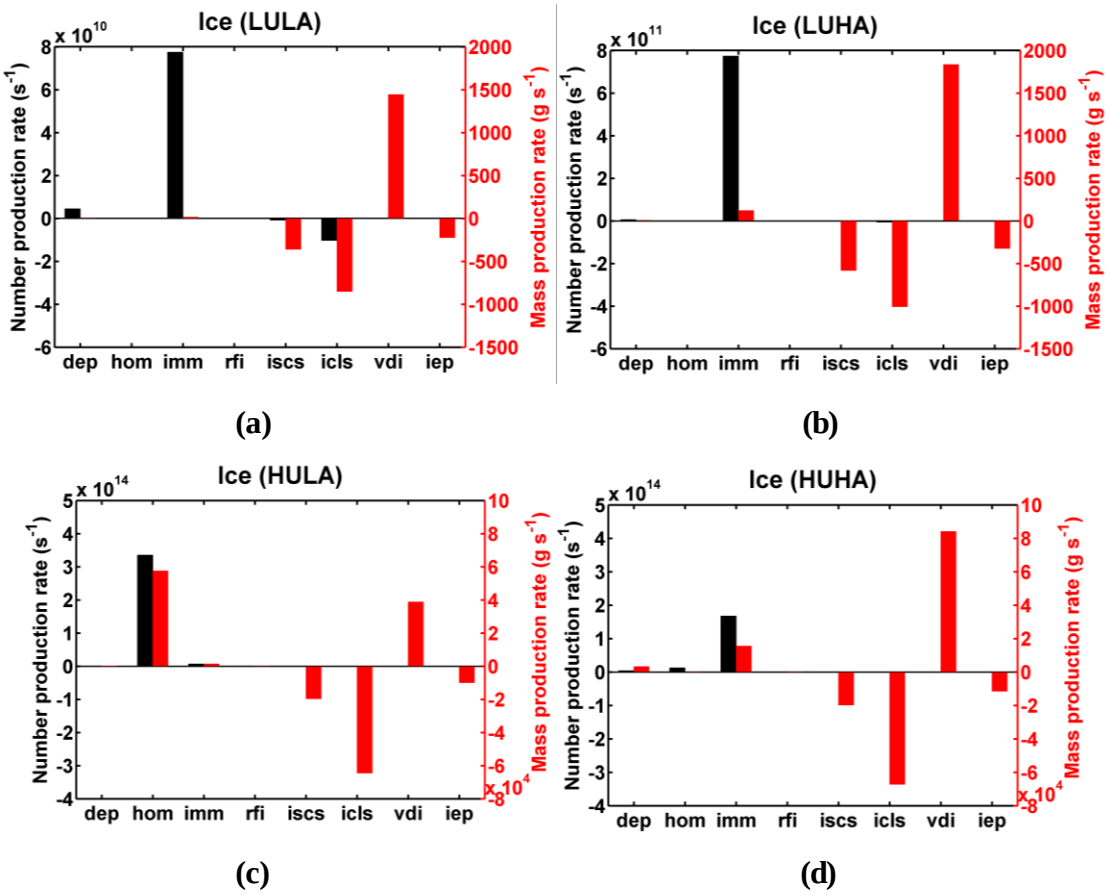

Figure 4.12: *Same as Figure 4.3 but for ice crystals. The acronyms indicate dep: deposition ice nucleation; hom: homogeneous ice nucleation; imm: immersion ice nucleation; rfi: freezing of raindrops to form ice crystals; isc: ice selfcollection; icls: collection of ice to form snow; vdi: depositional growth of ice crystals; iep: evaporation of ice crystals.*

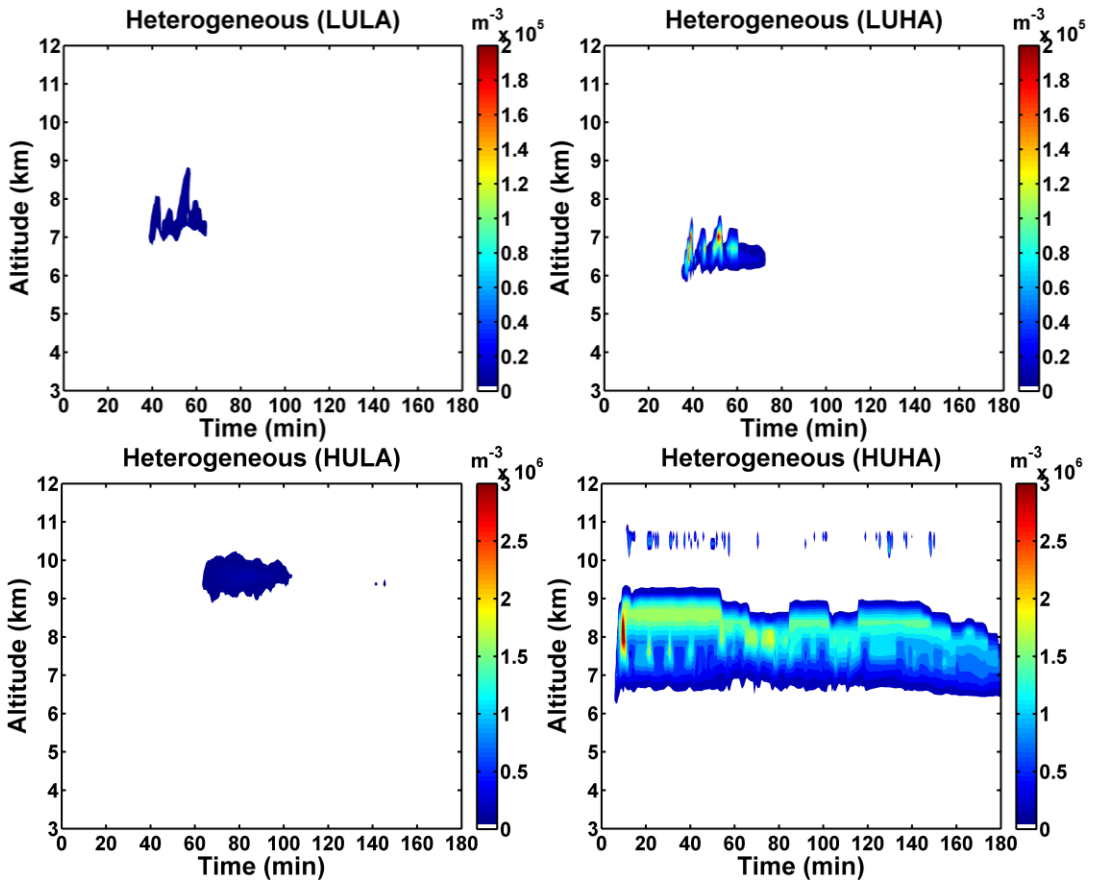

Figure 4.13: *Time evolution of horizontally-averaged heterogeneous freezing (immersion) rate (m^{-3}) as a function of altitude for four extreme cases.*

For ice mass concentration (M_{ice}), the leading source is from depositional growth of ice crystals from water vapor (*vdi*) except for HULA case in which both *vdi* and homogeneous freezing of cloud water are the main sources (the explanation for this exception is the same as for N_{ice}). As described in Sect. 4.2.1, the ice crystals and cloud droplets in mixed-phase cloud are processed in accordance with the Wegener-Bergeron-Findeisen (WBF) mechanism. Adding more IN leads to more water vapor evaporating from cloud droplets, which serves to feed ice crystals. The main sink of M_{ice} is due to the collection and selfcollection of ice (*icls* and *isc*), which increase slightly with enhanced IN concentrations.

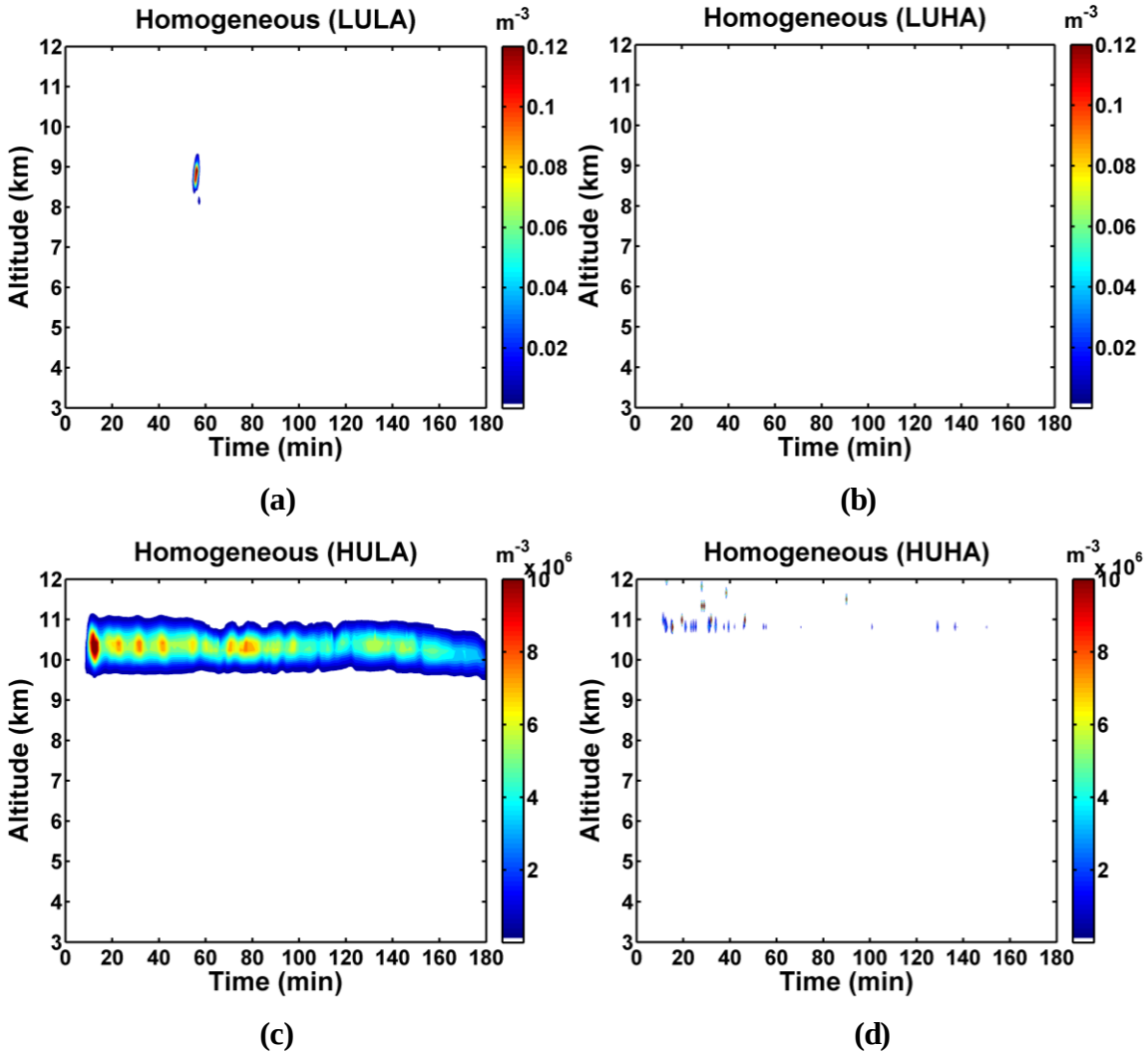

Figure 4.14: *Time evolution of horizontally-averaged homogeneous freezing rate (m^{-3}) as a function of altitude for four extreme cases.*

4.2.4 Frozen water contents

The contours of frozen particles (including ice, snow, graupel and hail) as a function of N_{CN} and fire forcing indicate that the production of frozen particles is in general controlled by fire forcing (Figure 4.15). Similar to other hydrometeors, $RS(FF)$ decreases as fire forcing gets stronger. The impact of IN concentration on the mass concentration (M_{FP}) is very small with $RS(N_{CN})$ around zero. For number concentration (N_{FP}), an increase in aerosols (N_{CN}) leads to a decline in N_{FP}, particularly when N_{CN} is in a low level.

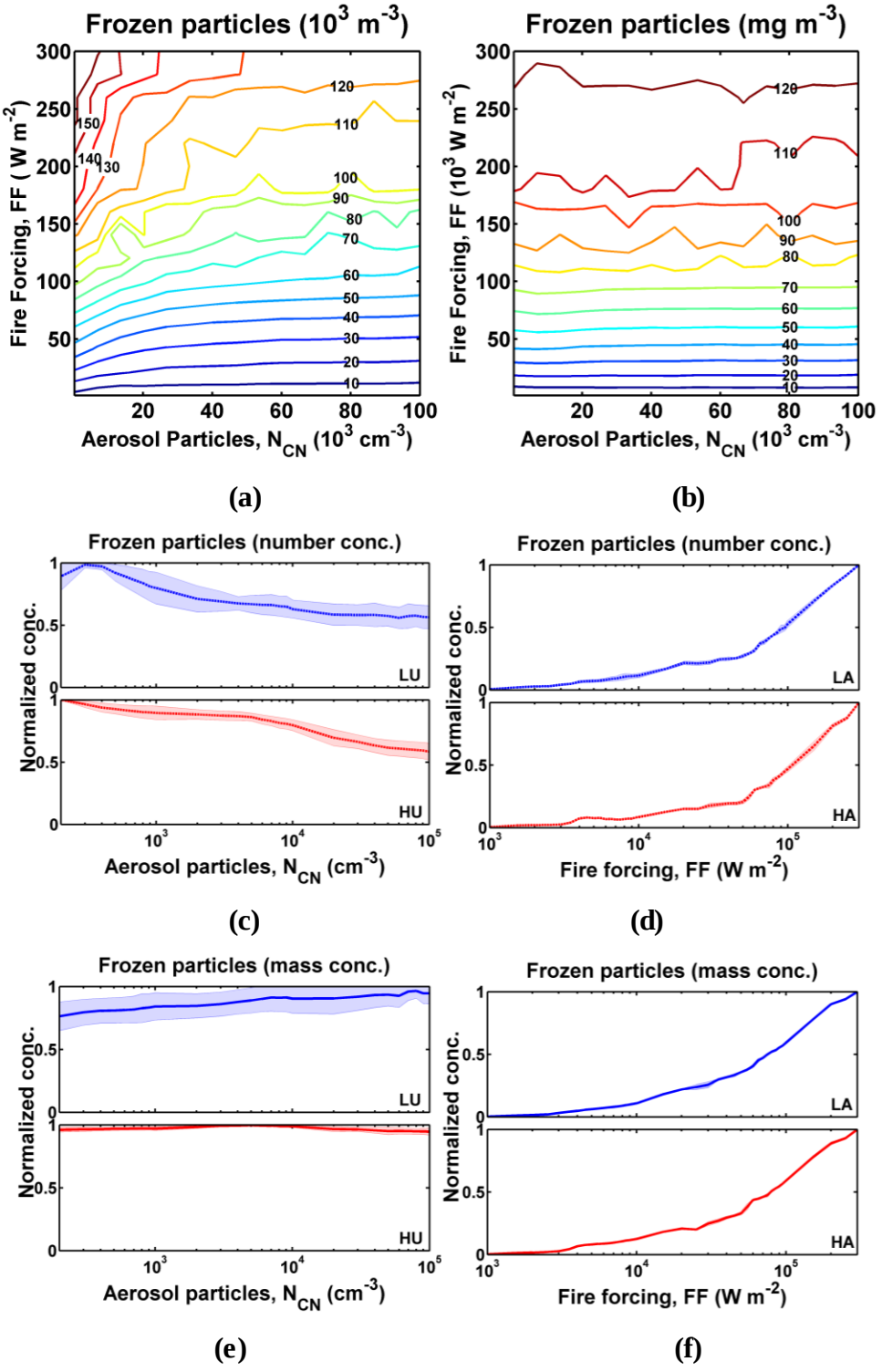

Figure 4.15: *Same as Figure 4.1 but for the total frozen particles (including ice, snow, graupel, and hail).*

The time series of horizontal-integrated total frozen water content (M_{FP}) is demonstrated in Figure 4.16, approximate 80% of which is comprised of snow (Figure 4.17). Therefore, the characteristic of M_{FP} is dominated by that of snow. Weak fire forcing significantly delay the appearance of frozen particles, while strong fire forcing could deliver the frozen particles to a very high altitude. Even aerosol concentration increases by a factor of 500, there is no obvious change in M_{FP}.

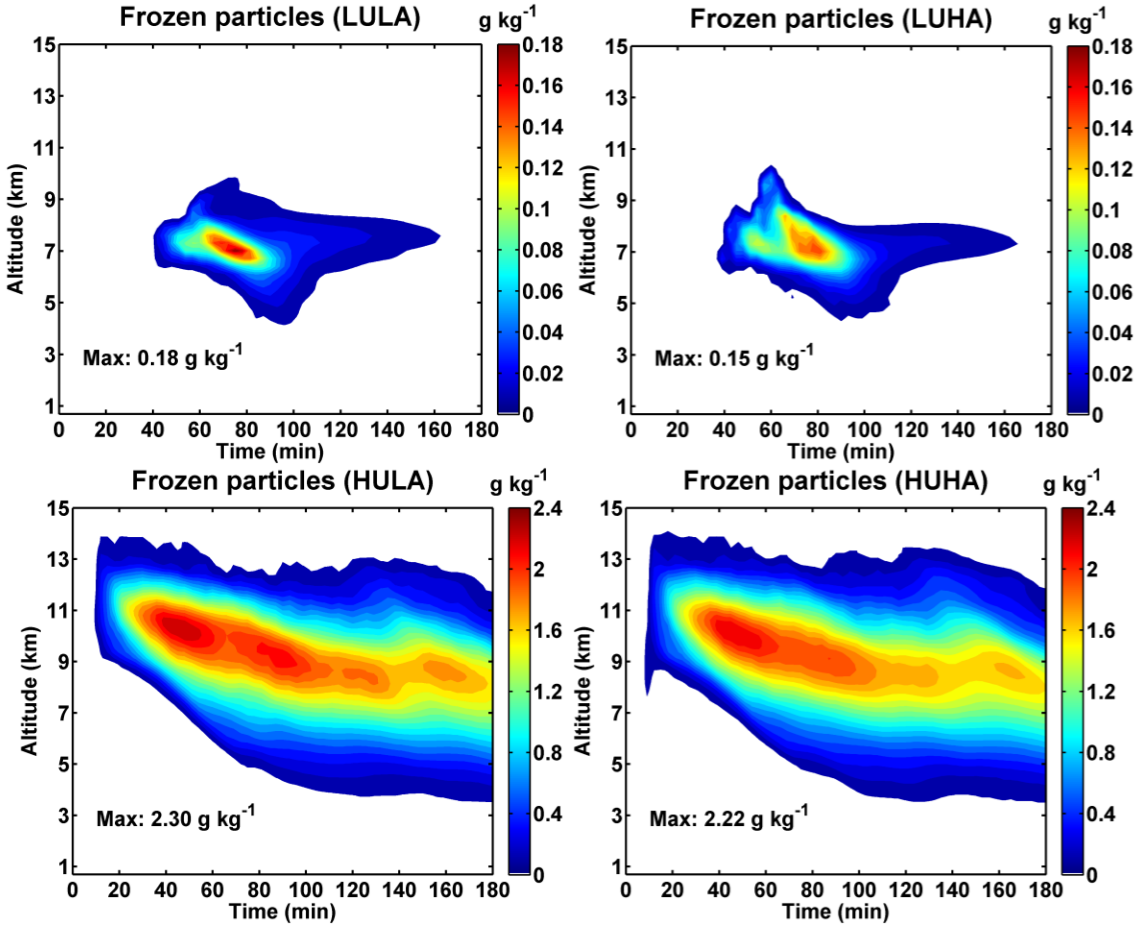

Figure 4.16: *Same as Figure 4.2 but for the total frozen water content.*

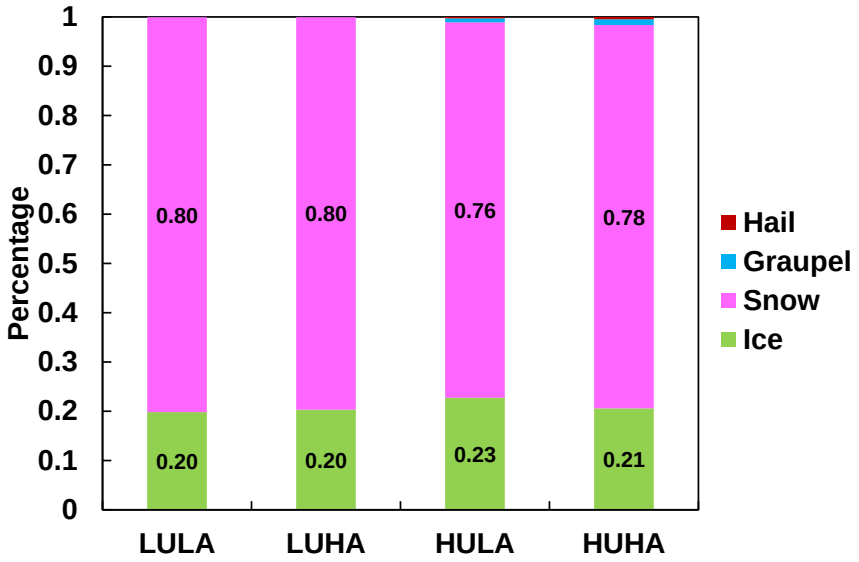

Figure 4.17: *Contributions of individual frozen hydrometeor to the total frozen water content under four extreme.*

Similar to the PA discussion in Sect. 3.3.3, only the major contributors to M_{FP} are illustrated in Figure 4.18, as this section focuses on the interactions between liquid water phase and frozen water phase. Except HULA case, the growth of ice crystals via vapor deposition (*vdi*) is the leading source for M_{FP}, and the ice crystals could efficiently collide and coalesce to snow. Snow evaporation (*sep*) is the major sink of the total frozen particles. For HULA case, the contribution of homogeneous nucleation is of significance.

Although the total frozen water content is insensitive to IN concentrations, it is obtained from Figure 4.18 that the leading processes that produce frozen particles and their intensities do change greatly. The leading source of frozen water content under LU condition is from ice growth by vapor deposition (*vdi*), and IN plays a positive role in *vdi* change rate. At the same time, the major loss pathway (via snow evaporation) is enhanced as well. Therefore, the net change of total frozen water content remains unchanged. Under HU condition, both homogeneous freezing (*hom*) and *vdi* process are the main sources. The process of *hom* is significant for LA case, as cloud droplets could ascend to a very high altitude, which could efficiently freeze to ice crystals via homogeneous nucleation. The change rate of *vdi* is enhanced via WBF process for HA case, which

thereby reduces the cloud water available for the homogeneous nucleation. The snow evaporation does not change much under such condition. As a result, the IN effect on the total frozen water content is not important.

The significance of each process in different cloud region could be obtained in Figure 4.19. The processes contributing to the formation and dissipation of ice crystals usually occur in the upper level with low temperature. The activities of other frozen particles (i.e., snow, graupel, and hail) take place in a low elevation with a higher temperature. When temperature is warmer than 0 ℃, the frozen hydrometeors would melt to raindrops. Under HU condition, intensive melting still exists even near the surface (Figure 4.20c, d), which is owing to large frozen particles (graupel and hail) with bigger size and faster terminal velocity.

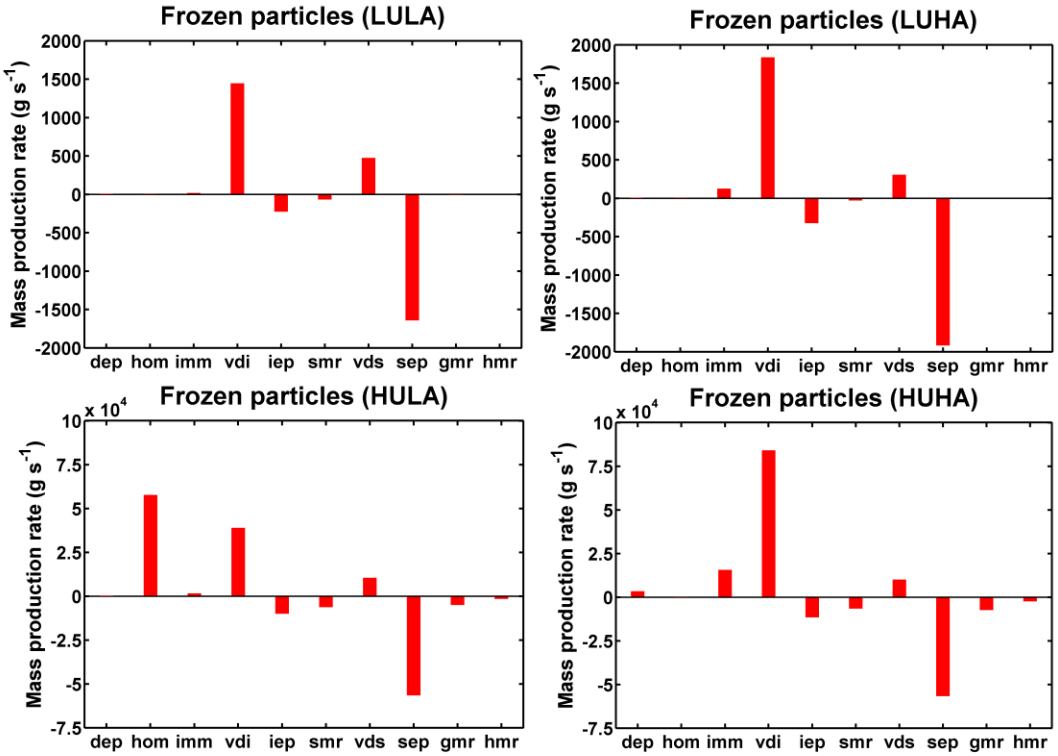

Figure 4.18: *Same as Figure 4.3 but only for the mass concentration of total frozen particles (ice, snow, graupel, and hail). The acronyms indicate dep: deposition ice nucleation; hom: homogeneous ice nucleation; imm: immersion ice nucleation; vdi/s: depositional growth of ice crystals/snow; i/sep: evaporation of ice/snow; s/g/hmr: melting of snow/graupel/hail to form raindrops.*

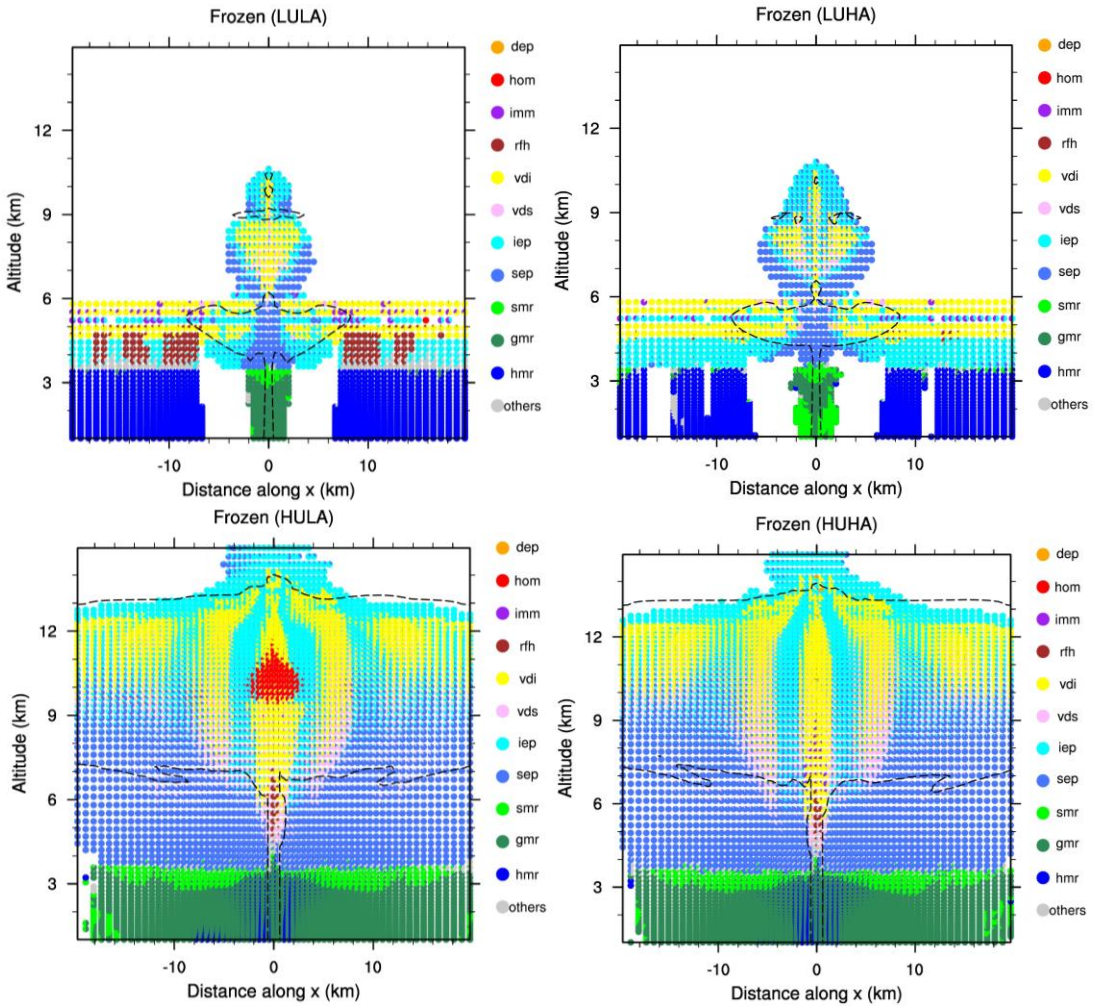

Figure 4.19： *Same as Figure 4.4 but for the total frozen particles (rfh: freezing of raindrops to form hail; the meaning of other acronyms is the same as in Figure 4.18).*

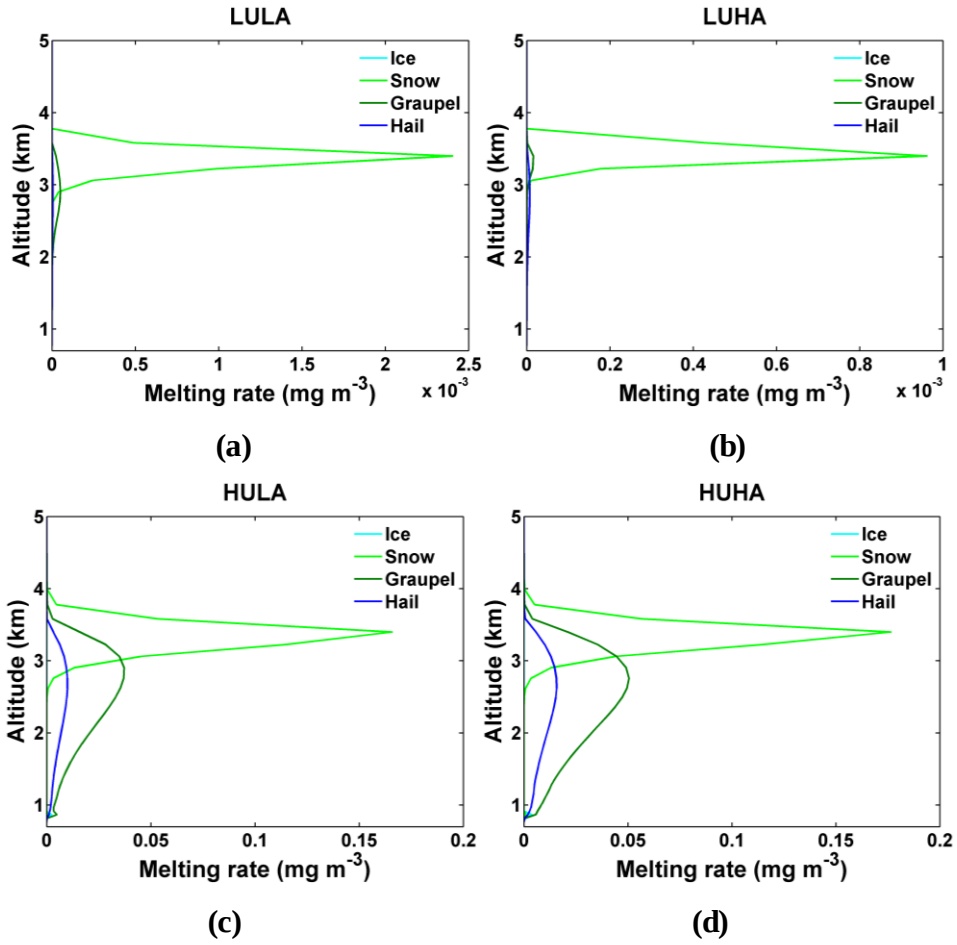

Figure 4.20: *Vertical profiles of time-averaged melting rate of individual frozen particles under four extreme conditions.*

4.2.5 Precipitation rate

The generation of precipitation is a fundamental process for the Earth's hydrological cycle, and understanding precipitation-aerosol relationships remains a challenging question. Within this work, the precipitation rate is also dominated by the fire forcing, especially when fire forcing is very weak (Figure 4.21a). As fire forcing gets stronger, precipitation rate gets less sensitive to the change of fire forcing. More potential IN could spur the precipitation rate slightly, which is probably owing to the intensified dynamics caused by freezing-released latent heat. Some previous convective studies also reported independently enhancing IN could produce more surface precipitation (van den Heever et al., 2006; Seifert et al., 2012).

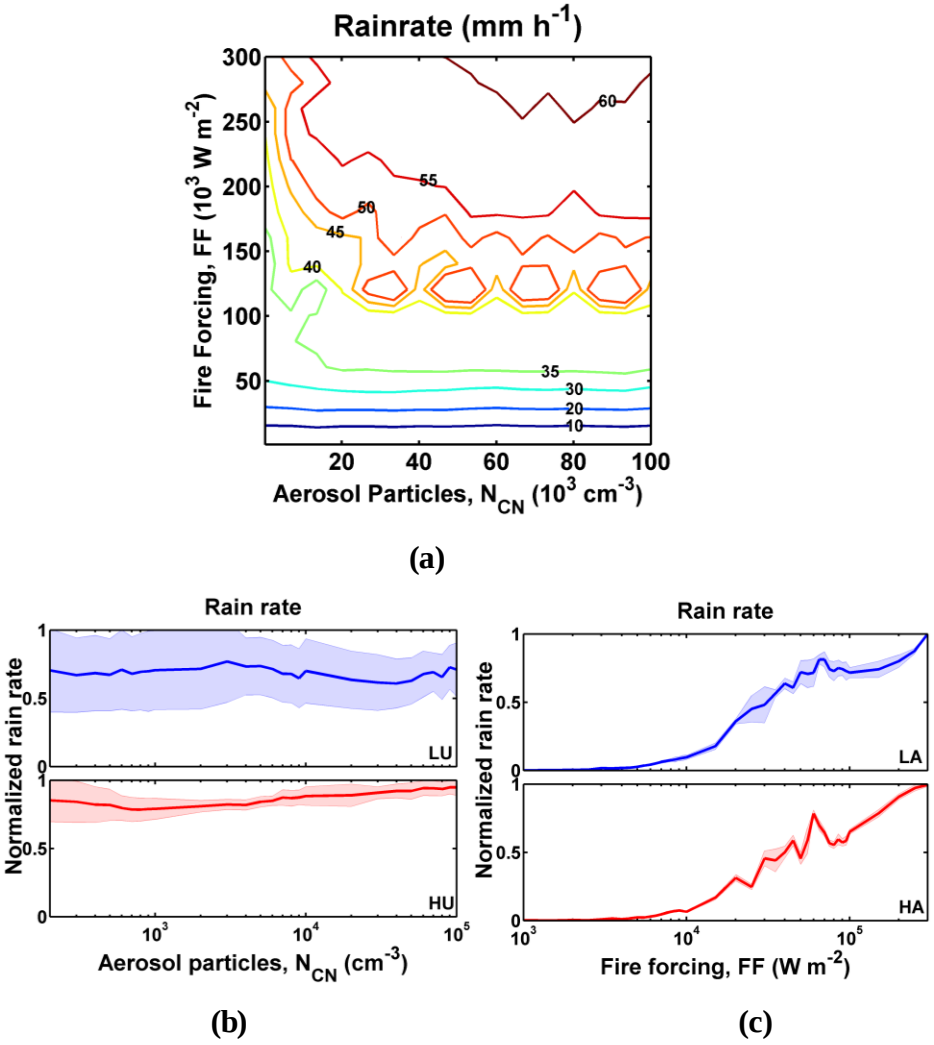

Figure 4.21: *Isopleths of precipitation rate calculated as a function of N_{CN} and fire forcing (a). Normalized precipitation rate (relative to the maximum value) as a function of N_{CN} (b) and FF (c).*

Different from the CCN impact on precipitation, it seems more potential IN particles cannot delay the appearance of surface rainfall or decrease the precipitation amount (Figure 4.22). In contrast, extremely high IN could slightly promote the production of precipitation. However, some research based on a synergy between observations and models concluded that wet scavenging is a principle driver of precipitation-aerosol relationship for convective precipitation at a global scale (Grandey et al., 2014), which is not taken into account in our simulations. In the future study, the inclusion of aerosol scav-

enging may be necessary to deduce more reliable results concerning aerosol effect on rainfall production.

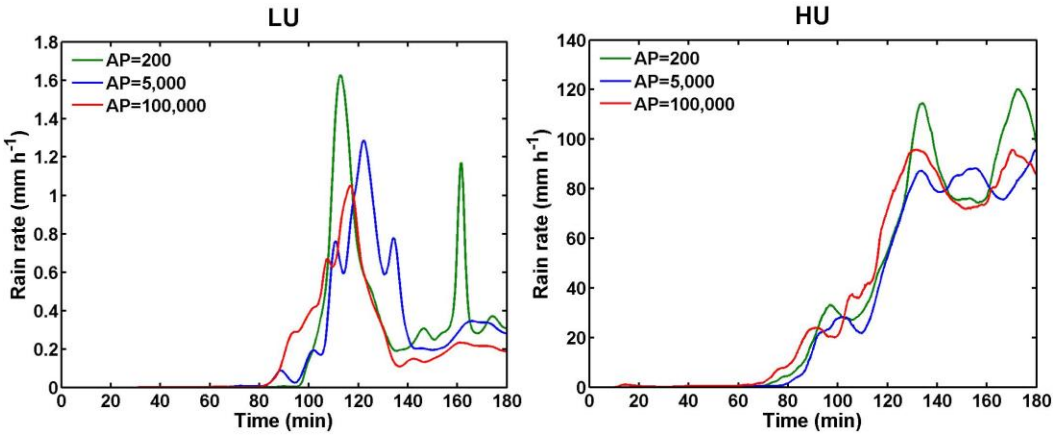

Figure 4.22: *The surface rain rate as a function of time for three aerosol levels (N_{CN} = 200; 5,000; and 100,000 cm^{-3}) under LU (1,000~3,000 W m^{-2}) and HU (80,000~100,000 W m^{-2}) conditions respectively. The solid lines represent the averaged values under individual condition.*

4.3 Joint effects of CCN and IN

In the real atmosphere, there is hardly any case where the change of total aerosol concentration will only change the CCN concentration but not the IN concentration (and vice versa). Increasing/decreasing the aerosol concentrations often lead to corresponding changes in both CCN and IN. In this section, we present and discuss how the cloud hydrometeors react to the variations in aerosols acting as both CCN and IN under different fire forcing conditions. The CCN and IN are both functions of total aerosol concentrations, and are determined by an empirical lookup table (Reutter et al., 2009) and newly-developed ice nucleation schemes as detailed in Sect. 2.4.2, respectively.

As shown in Figure 4.23a, there are three different regimes for the isolines of N_{CD}, which is quite similar to Figure 3.2a: an aerosol-limited regime in the upper left sector, a

fire forcing-limited regime in the lower right sector, as well as a transitional regime between the two other regimes. This is because N_{CD} is governed by CCN activation, which has nothing with IN effect. The isolines of M_{CD} (Figure 4.23b) resulting from simultaneous variation in CCN and IN are more complicated: when fire forcing is very weak (<20,000 W m^{-2}), M_{CD} is mainly dependent on fire forcing and aerosols play a slightly positive role in M_{CD} (upper panel in Figure 4.23e); while fire forcing gets stronger (>20,000 W m^{-2}), M_{CD} is negatively correlated to aerosols. The non-monotonic effect of aerosols is because under LU condition, the interaction between cloud droplets and frozen particles is unimportant, as discussed in Sect. 3.3.1. The main loss of cloud droplets is through conversion to raindrops, which will be suppressed with more aerosols (more CCN). This leads to the positive relationship between aerosols and M_{CD} under LU condition. Under HU condition, the conversion to frozen particles (i.e., ice crystals) becomes the leading sink of cloud droplets, and the IN impact gets remarkable, which plays a negative role in M_{CD} (see Sect. 4.2.1).

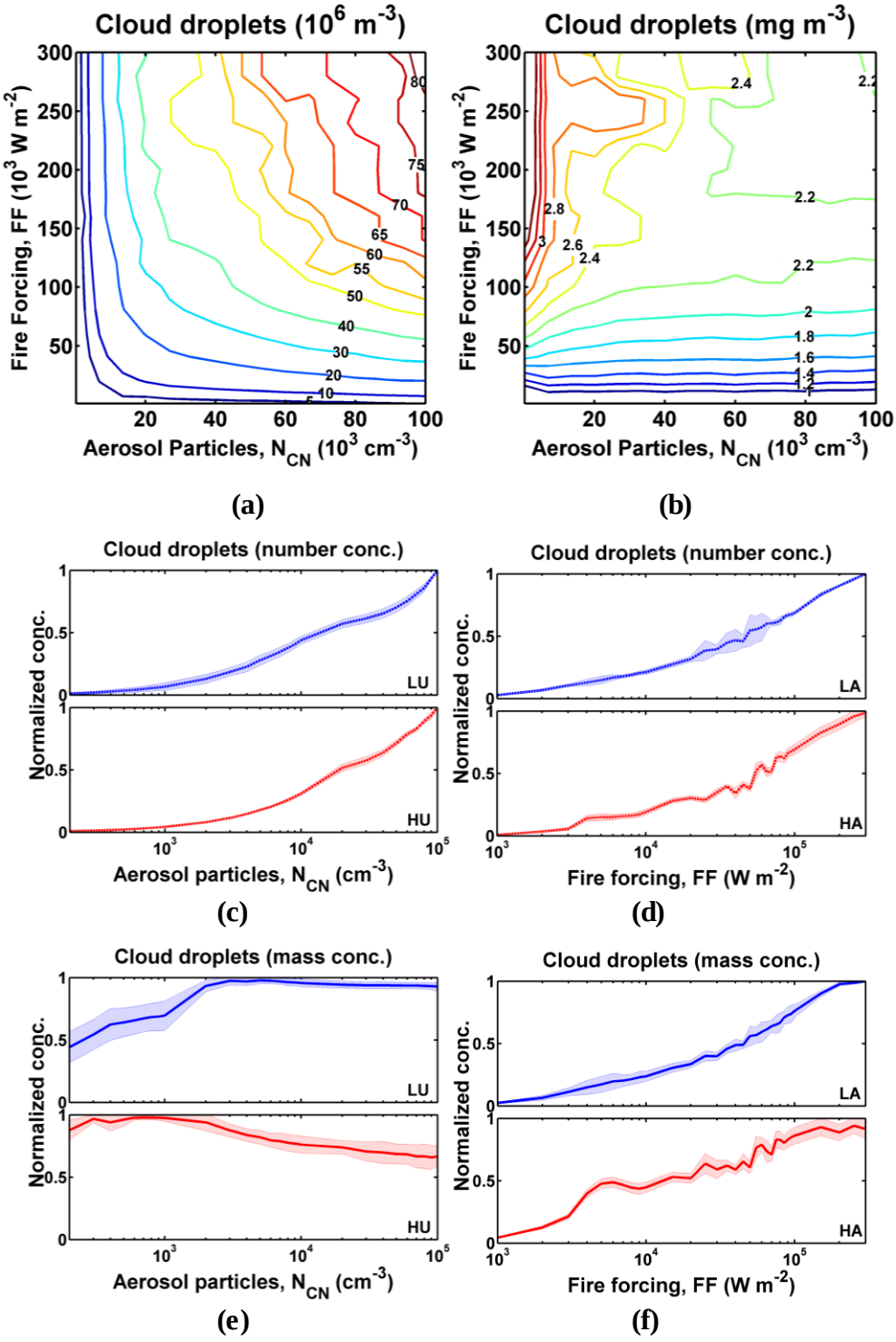

Figure 4.23: *Same as Figure 4.1.*

The contours of number concentration of raindrops (N_{RD}) is in agreement with Figure 3.4a, which is also dominated by fire forcing (Figure 4.24a). Increasing fire forc-

ing within a certain range (~<5,000 W m^{-2}) could produce more N_{RD}, while further increase will result in reduction in N_{RD} (Figure 4.24d). The impact of aerosols on N_{RD} should be discussed separately under LU and HU conditions (Figure 4.24c). Under LU condition, enhanced aerosols could either promote N_{RD} (N_{CN}<700 cm^{-3}) or suppress N_{RD} (N_{CN}>700 cm^{-3}), while N_{RD} decreases monotonically as aerosols increase under HU condition. The shape of the isopleths of mass concentration (M_{RD}) is more alike with Figure 3.4b, which shows a slight positive effect of aerosols with very weak fire forcing, and negative effect with strong fire forcing. Strong fire forcing leads to more M_{RD}, which is in a larger size owing to reduced N_{RD} under HU condition. This implies that the regulation of raindrops due to CCN overwhelms the IN influence.

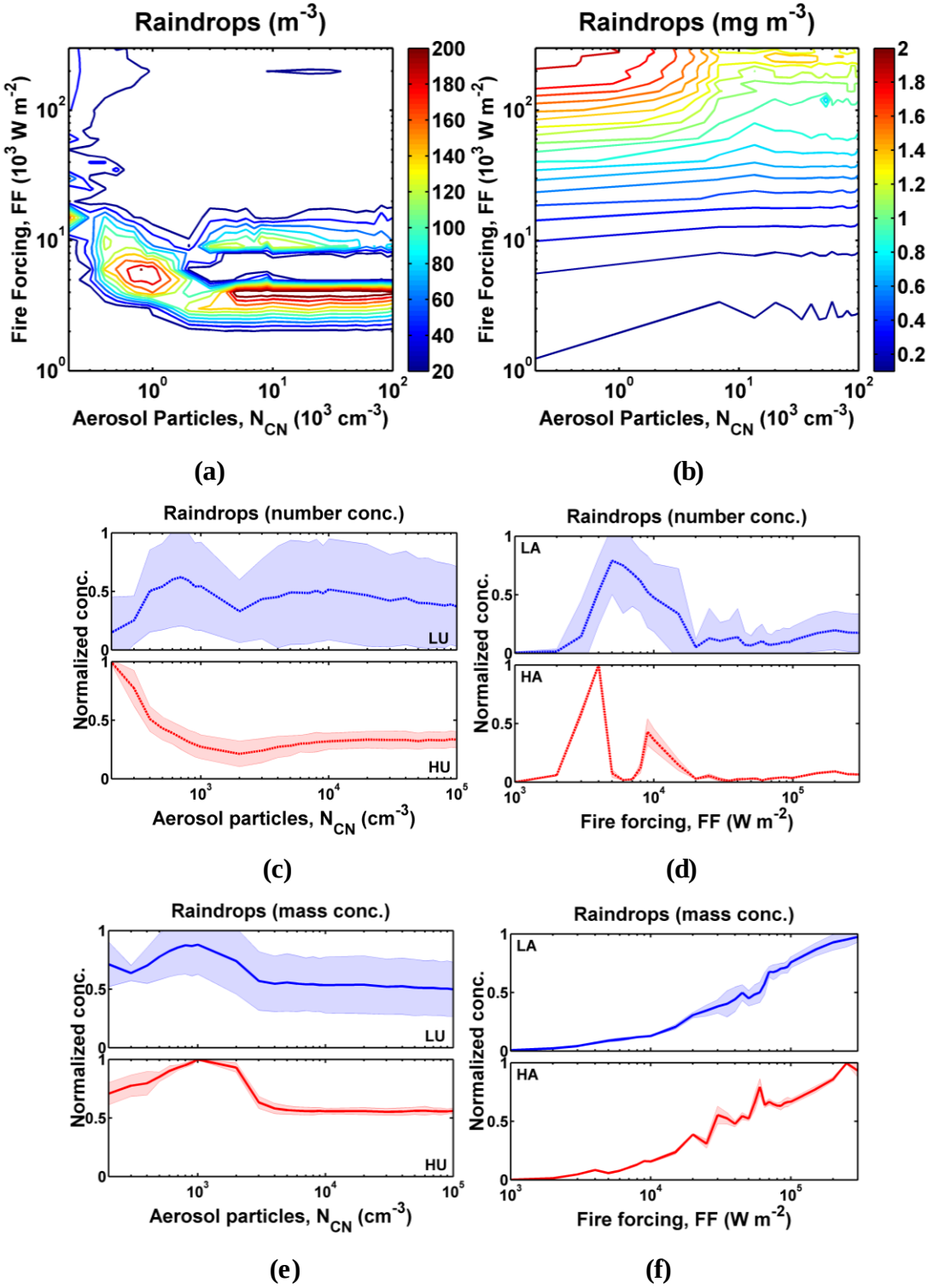

Figure 4.24: *Same as Figure 4.6.*

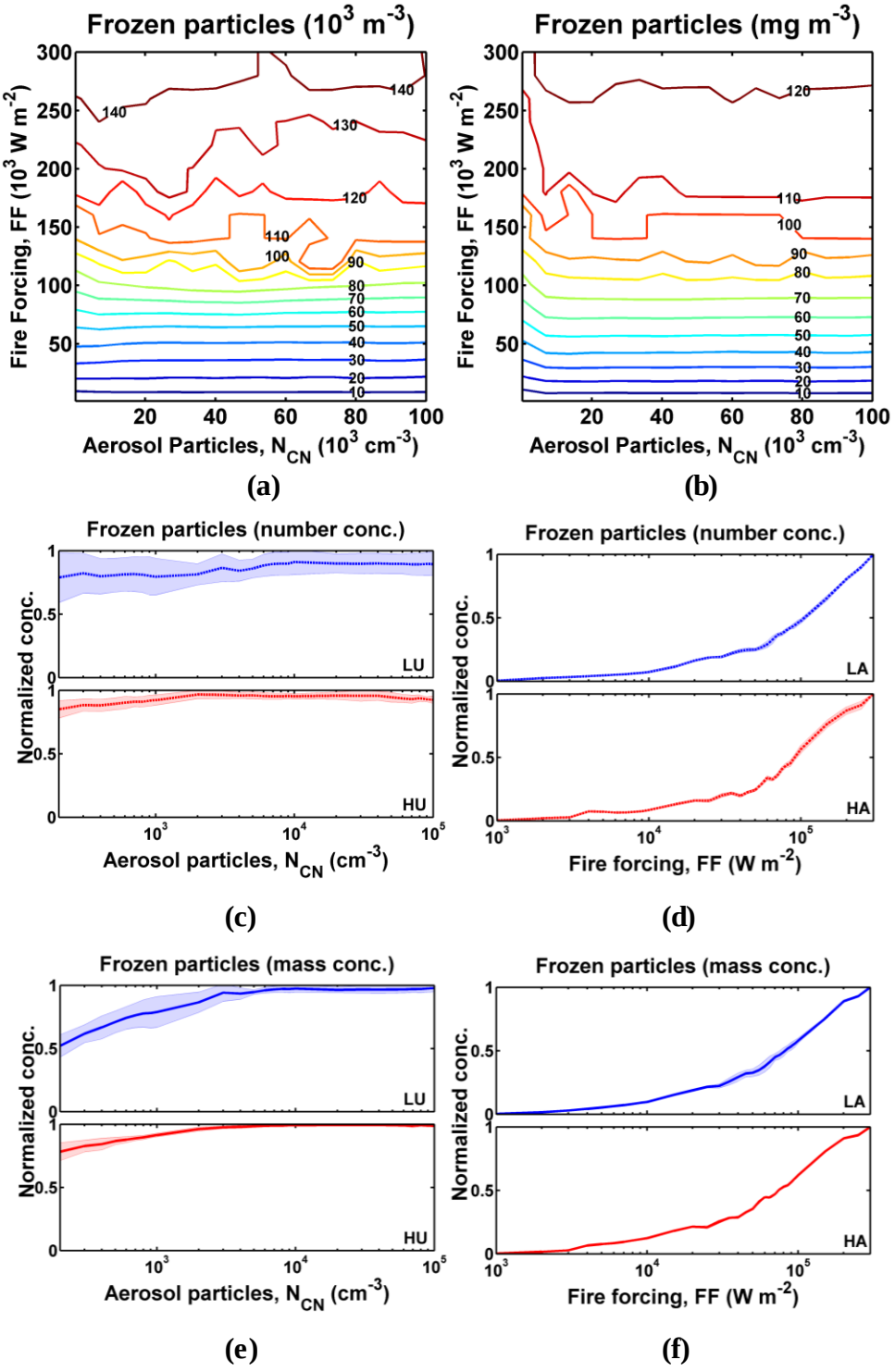

Figure 4.25: *Same as Figure 4.15.*

Figure 4.25a, b shows the dependence of the number and mass of frozen particles (N_{FP} and M_{FP} respectively) as a function of aerosols and fire forcing. It appears the aerosol effect on N_{FP} is negligible, and M_{FP} increases slightly with simultaneous enhancement of CCN and IN. In chapter 3, we find increasing CCN (fixed IN) plays a positive role in N_{FP} and M_{FP}; while in chapter 4, more IN (fixed CCN) leads to a slight decrease in N_{FP}, while the effect on M_{FP} is quite small. According to Figure 4.25, it appears that the negative effect of IN on N_{FP} counteracts the positive effect of CCN, resulting in nearly negligible effect of aerosols on N_{FP}. The microphysical effects of CCN on M_{FP} are bigger than that of IN, leading the contours are similar to Figure 3.7b: enhanced aerosols causes a slight increase in frozen water content.

The isopleths of precipitation rate with simultaneous variation in CCN and IN are shown in Figure 4.26a, which is more similar to the CCN effects in Figure 3.8a. In general, rain rate is reduced with increasing aerosols under LU condition (Figure 4.26b); while under HU condition, rain rate is enhanced when aerosol concentration is lower than 2,000 cm^{-3}, and then suppressed with further increase in aerosols. Such characteristic illustrates the dominant effects of CCN on precipitation relative to IN.

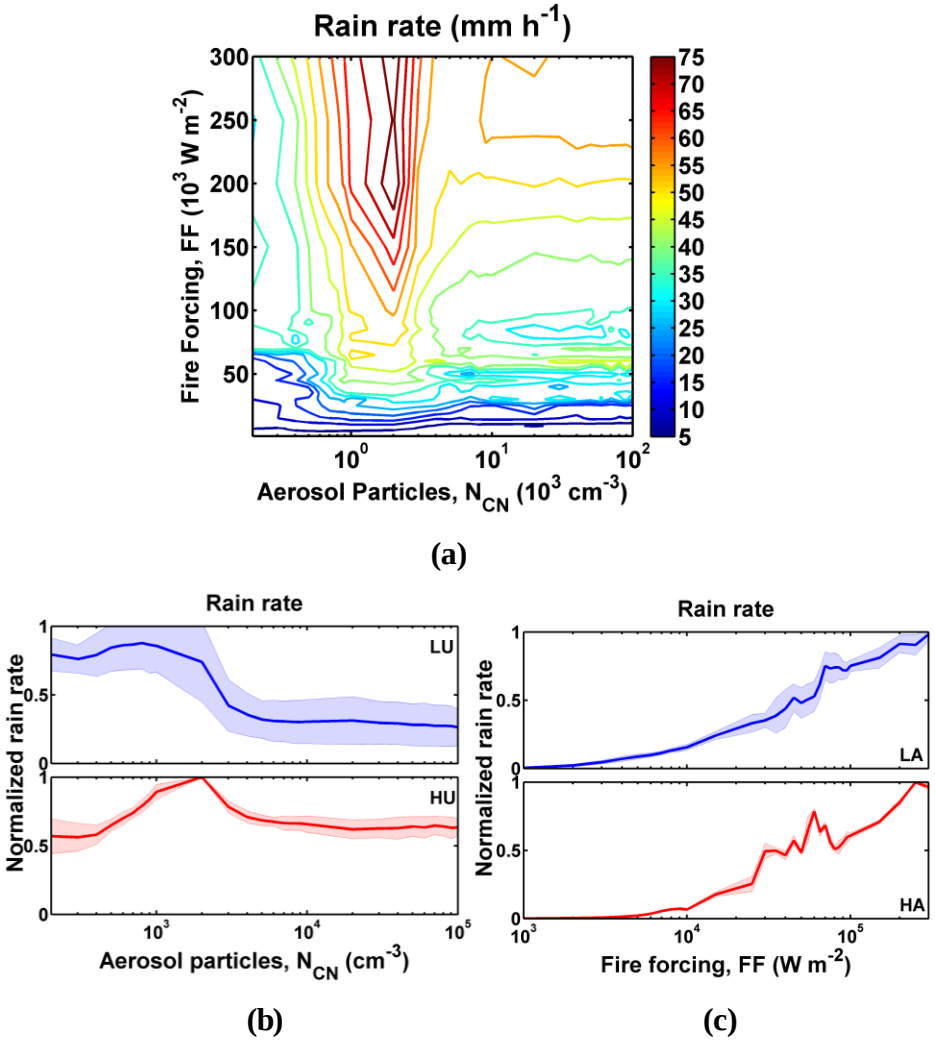

Figure 4.26: *Same as Figure 4.21.*

4.4 Summary

In this chapter, we have examined cloud properties such as liquid and solid water contents, and their relationship, with the purpose of gaining insights to reveal the influence of changing IN (with fixed CCN or changing CCN separately) on the formation and evolution of pyro-convective clouds.

When the aerosol effect only acting as IN is considered, the formation of all cloud hydrometeors is mainly within updraft-limited regime, and is insensitive to aerosol concentrations. Specifically, IN plays a negative role in the production of cloud water con-

tents, which is opposite to the CCN effect. An increase in IN leads to more water vapor condensed onto existing small ice crystals, which will promote the evaporation of cloud droplets and hence reduce its mass concentration. Compared to the influence of fire forcing, IN effect on the number and mass concentrations of raindrops (N_{RD} and M_{RD}) is very small. Both N_{RD} and M_{RD} involve large variations under LU condition; while enhanced IN plays a slightly positive role in N_{RD} and M_{RD} under HU condition. In general, the influence of IN on the total frozen water contents is nearly negligible, which is mostly comprised of snow. Different from CCN impact, the initiation and the amount of surface precipitation is also insensitive to the variation in IN concentration.

The simulations of pyro-convective clouds when both CCN and IN effects are taken into account are also performed. For this scenario, only the production of cloud number concentration displays three different regimes: an aerosol-limited regime in the upper left sector, an updraft-limited regime in the lower right sector, as well as a transitional regime between the two other regimes. This is because cloud number concentration is dominated by CCN activation. For cloud mass concentration (M_{CD}) and other hydrometeors (i.e., raindrops and frozen water contents), only updraft-limited regime is observed. When fire forcing is weak, M_{CD} is mainly controlled by CCN effect, because of the importance of warm rain process. When fire forcing is strong, the IN effect overwhelms the CCN effect, resulting in a decrease in M_{CD} with more aerosols. The response of raindrops and surface precipitation to aerosols is non-monotonic and could be either positive or negative as aerosol concentrations increase. The aerosol effect on the total frozen particles is nearly negligible, especially for the number concentration. Increasing aerosols play a slightly positive role in the mass concentration, which is similar to the change trend when only CCN effect is only considered.

Chapter 5 Conclusions and Outlook

5.1 Summary

The major objective of the modeling work presented in this dissertation was to evaluate the effect of aerosol particles by serving as CCN and IN on pyro-convective clouds over a wide range of dynamical conditions. For this purpose, over 3000 simulations (CCN, IN, CCN+IN) of the pyro-clouds that developed over the Chisholm fire in May 2001 were performed over 3 simulation hours and sensitivity studies were conducted. The numerical experiments yield valuable insights for the interpretation of the formation and evolution of pyro-convective clouds.

In general, there are multiple regimes for the cloud number concentration. For cloud mass concentration and other hydrometeors (including raindrops, and frozen particles), fire forcing (*FF*) plays a dominant role and the aerosol effect is of relatively less importance. The CCN and IN effects on individual hydrometeor are summarized as follows:

The CCN effect (fixed IN):

(1) As N_{CN} and *FF* increase, the number concentration of cloud droplets increases. There are three distinct regimes for the cloud number concentration: an updraft-limited regime (high $RS(FF)/RS(N_{CN})$ ratio), an aerosol-limited regime (low $RS(FF)/RS(N_{CN})$ ratio), and a transitional regime (intermediate $RS(FF)/RS(N_{CN})$ ratio), which agrees well with the regimes derived from a parcel model. The cloud mass concentration is less sensitive to aerosols, and there are two regimes for mass concentration: an updraft-limited regime, and a transitional regime.

(2) The production of rain water content (i.e., M_{RD}) was enhanced with increase in updrafts, and the aerosols could either slightly increase M_{RD} with low N_{CN} or decrease M_{RD} with large N_{CN}. The N_{CN} plays a mostly negative role in M_{CD} under intermediate N_{CN} conditions (N_{CN} of several 1000 cm^{-3}). M_{RD} was generally within an updraft-limited regime, i.e., M_{RD} was very sensitive to changes in updrafts, but insensitive to aerosol con-

centrations ($RS(FF)/RS(N_{CN})>4$). The aerosol and *FF* effects on raindrop number concentrations (N_{RD}) are quite complicated; both of them play the non-monotonic role in the N_{RD}.

(3) As updrafts and aerosols increase, the domain-averaged number and mass concentrations of frozen particles (N_{FP} and M_{FP} respectively) were enhanced. N_{FP} and M_{FP} were also within the updraft-limited regime, which is characterized by large $RS(FF)/RS(N_{CN})$ ratio. In this regime, N_{FP} and M_{FP} were directly proportional to fire forcing, and independent of aerosols.

(4) Larger *FF* resulted in more precipitation, whereas the effect of aerosols on precipitation was complex and could be either enhance or suppress the production of precipitation. The suppression on the precipitation is due to the change in the fraction of small frozen particles and total melting rate of frozen particles. The enhancement on the precipitation resulting from increasing N_{CN} under low aerosol condition is a result of changes in the vertical distribution of frozen particles and its evaporation process.

(5) In addition, when N_{CN} and *FF* became too large, their impact became weaker, as indicated by a decreasing relative sensitivity.

The IN effect (fixed CCN):

(1) The formation of cloud droplets is mostly within updraft-limited regime, and the IN effect is very small. An increase in IN results in a reduction in cloud water content, opposite to the CCN effect. This is because enhanced IN leads to more efficient growth of ice crystals by vapor deposition, which accelerates the evaporation of cloud droplets and hence decrease its amount.

(2) IN effect on raindrops is much smaller relative to fire forcing. Both number (N_{RD}) and mass (M_{RD}) concentrations involve large variations with weak fire forcing, and both the warm rain process and melting process are important for the raindrop production; while enhanced IN plays a slightly positive role in N_{RD} and M_{RD} with strong fire forcing, which mostly results from melting of frozen particles at a low altitude.

(3) Generally, the influence of IN on total frozen water contents is nearly negligible. When fire forcing is weak, the leading source of frozen water content is through ice

growth by water vapor deposition (*vdi*), which increases with more IN. At the same time, the snow evaporation, as a major sink, is also enhanced. As a result, the net change of total frozen water content is very small. When fire forcing is very strong, both homogeneous and *vdi* processes are the main sources. The former source is significant with fewer IN, as cloud droplets could ascend to a very high elevation, leading to enormous cloud water available for homogeneous freezing. The latter one is enhanced with more IN via WBF process, which in turn decreases the cloud water available for the homogeneous nucleation. The snow evaporation does not change much under HU condition. Consequently, the response of the total frozen water content to IN concentrations is not obvious.

(4) The IN impact on the precipitation at the surface is also very small compared to the effect of fire forcing. Different from CCN effect, increased IN cannot delay or suppress the precipitation rate at surface; on the contrary, it causes a slight increase in precipitation efficiency when fire forcing is very strong.

Joint effects of CCN and IN:

(1) The production of cloud number concentration (N_{CD}) displays three different regimes, similar to the CCN effect because N_{CD} is dominated by the CCN activation process. For cloud mass concentration (M_{CD}), the effect of fire forcing is dominant, and M_{CD} is insensitive to aerosols. M_{CD} is controlled by the CCN effect under LU condition, due to the efficient warm rain process (i.e., autoconversion and accretion), and weak conversion between cloud droplets and ice phase. Increasing aerosols could inhibit autoconversion and accretion and hence enhance M_{CD}. When fire forcing is strong, the main loss pathway of cloud droplets changes from autoconversion and accretion (conversion to raindrops) to freezing nucleation and WBF process (conversion to cloud ice). Therefore, the IN effect overwhelms the CCN effect, resulting in a decrease in M_{CD} with more aerosols.

(2) The production of both raindrops and surface precipitation is within the updraft-limited regime, and the CCN effect is larger than IN effect, leading to the isopleths of raindrops and precipitation are similar to that when only CCN is changed. The response of raindrops and precipitation to aerosols is complex and can be either positive or negative as a function of aerosol concentrations.

(3) The production of total frozen particles is nearly independent of aerosol concentrations. The negative effect of IN could weaken and even counteract the positive CCN effect on the mass (M_{FP}) and number (N_{FP}) concentrations, respectively. This causes that N_{FP} is insensitive to the change of aerosols, and M_{FP} is weakly susceptible to aerosols.

Process analysis (PA):

The PA gives further insight into the underlying mechanisms of aerosol-cloud interactions. By evaluating the contribution of the relevant microphysical processes to the formation of an individual hydrometeor, the PA revealed the dominant factors responsible for the changes in hydrometeor number and mass. (1) Cloud nucleation (*cn*) initializes cloud droplet formation and is the major factor that affects the number concentration of cloud droplets. As expected, the increase in cloud droplet mass can be mostly attributed to the net result of condensational growth (*vdc*) and droplet evaporation (*cep*). (2) Under weak *FF*, autoconversion (*au*) and accretion (*ac*) are the main sources of rain droplets. Under strong *FF*, the major source is through the melting process of frozen particles. (3) Aerosols alter the properties of the frozen water contents via heterogeneous ice nucleation process. It is not surprising that more IN leads to more efficient heterogeneous freezing nucleation. Water vapor deposition on existing ice crystals (*vdi*) is the most important contributor to the mass concentration. Homogeneous ice nucleation plays a great role when numerous supercooled cloud droplets exist in a very high altitude. In addition to CCN activation, the PA also highlights the importance of other microphysical processes in regulating cloud evolution, which is worthy of further scrutiny.

Furthermore, the PA clearly illustrates that aerosols could significantly alter the microphysical pathways (as shown in Figure 2.5) and their intensities. Although the change in individual microphysical process is very remarkable, the net result of all processes is not obvious and even insusceptible to aerosol perturbations. For example, the major pathway that produces cloud ice in HU case switches from homogeneous nucleation to *vdi* (ice growth by vapor deposition) process as more aerosols are added. At the same time, homogeneous freezing rate is greatly suppressed, while *vdi* process is enhanced due to efficient WBF mechanism under high aerosol condition. This is especially obvious when we consider the aerosol effect (only acting as CCN) on rain water: it is ob-

served that as aerosols is enhanced by a factor of 500, the intensities of the source processes only increase by a factor of 100; however, there is only a two-fold increase in the net rain water content. This implies that the cloud microphysics itself is a self-regulatory system, which can produce equilibrium and buffers the effect of aerosol disturbance (negative feedback).

While the general trend is clear, the inclusion of nonlinear (dynamic and microphysical) processes leads to a complex and unstable response of clouds to aerosol perturbations. This applies to the response of all hydrometeors and precipitation, as indicated by the large standard deviation of relative sensitivities (*RS*). This should also hold when variations in other parameters (e.g., meteorological conditions) are introduced. Compared with our results, the *RS* derived from cloud parcel modeling is much smoother (Figure 8 in Reutter et al. (2009)). The difference is probably caused by complex interactions between cloud microphysics and dynamics (Khain et al., 2008; Fan et al., 2009). These highly nonlinear processes result in a more unstable and chaotic response of cloud evolution to aerosol and dynamic perturbations. Because of this nonlinearity, sensitivities of clouds based on limited case studies may require caveats, because they may not be as representative as expected, and therefore cannot safely be extrapolated to conditions outside of the range explored. To better understand the role of aerosols in cloud formation, we recommend high-resolution ensemble sensitivity studies over a wide range of dynamic and aerosol conditions.

5.2 Perspectives

Current general understanding and global modeling studies suggest that, for cloud droplet number concentration, the updraft-limited regime may be more characteristic of continental clouds, while the aerosol-limited regime may be more characteristic of marine clouds (e.g., Karydis et al., 2012), suggesting that aerosol effects are generally more important for the marine environment. For this case study of pyro-convective clouds, then, we conclude that aerosol effects on cloud droplet number concentrations and cloud droplet size are likely more important than effects on precipitation, since precipitation is far less sensitive to N_{CN} than to updraft velocity. This is in agreement with other studies (e.g., Seifert et al., 2012). A recent long-term convective cloud investigation found that micro-

physical effects driven by aerosol particles dominate the properties and morphology of deep convective clouds, rather than updraft-related dynamics (Fan et al., 2013). Therefore, whether this conclusion applies to other cloud types and over longer timescales still needs to be determined.

In this study, we demonstrate the performance of ensemble simulations in determining the regime dependence of aerosol effects. The use of such regime dependence requires caveats because it may differ for different cloud types, aerosol properties, meteorological conditions, and model configurations (e.g., microphysical schemes, dynamic schemes, and dimensionality).

Therefore, (1) it must still be determined whether this conclusion applies to other cloud types with other meteorological or atmospheric conditions; (2) The results within this work are derived over 3 simulation hours, which may not cover a whole cloud life time under some specific conditions. Thus, investigating the cloud response to aerosols over longer timescales is very necessary (Van Den Heever and Cotton, 2007), as different observational scales could introduce biases into the quantification of aerosol effects on clouds (McComiskey and Feingold, 2012); (3) Future work is still needed to evaluate the relative contribution of microphysical and dynamic effects to cloud buffering effects (Stevens and Feingold, 2009; Seifert et al., 2012); (4) This work only considers soot particles acting as efficient IN, similar simulations would be performed to study other IN type, e.g., biological aerosols, which could be activated as efficient IN at a very low updraft condition; (5) This study has an emphasis on the dynamic effect on pyro-clouds, and two-dimensional dynamics is very different from three-dimensional. In the future work, investigations based on three-dimensional simulations are required and may draw some different conclusions. In addition, it is also necessary to extend our study from the column of a single cloud to a regional scale.

Appendix A: Seifert microphysical scheme

This appendix provides a brief description of the two-moment microphysical parameterization (Seifert and Beheng, 2006) used in ATHAM model. The scheme parameterizes the interactions between six hydrometeor types (i.e., cloud droplets, raindrops, ice crystals, graupel and hail), and predict their mass and number densities (Seifert and Beheng, 2006; Blahak, 2008). Here the main processes to predict the hydrometeor are included.

1. Autoconversion

Autoconversion process initiates the raindrop formation via self-collection of cloud droplets, and is the major process in the initial stage of the evolution. Explicit rate equation for autoconversion is formulated using Long's piecewise polynomial collection kernel and universal functions following a fundamental similarity relationship (Seifert and Beheng, 2001):

$$\frac{\partial L_r}{\partial t}\Big|_{au} = \frac{k_{cc}}{20x^*}\frac{(\nu_c+2)(\nu_c+4)}{(\nu_c+1)^2}\times L_c^2\bar{x}_c^{-2}\left[1+\frac{\phi_{au}(\tau)}{(1-\tau)^2}\right]\frac{\rho_0}{\rho} \qquad \text{(A1)}$$

Where L_r and L_c is the mass densities of raindrops and cloud droplets (in kg m^{-3}) respectively, the drop mass x^* separates cloud portion (with $x < x^*$) from raindrop portion, and equals to 2.6×10^{-10} kg corresponding to a separating radius of 40 um. For cloud droplets, a Γ-distribution with a constant width parameter ν_c is assumed, $\bar{x}_c$ is the mean droplet mass (in kg). The dimensionless internal time scale $\tau = 1-\frac{L_c}{L_c+L_r}$, and the universal function ($\phi_{au}(\tau) = 400\tau^{0.7}(1-\tau^{0.7})^3$) is estimated by numerically solving the stochastic collection equation. In order to consider the increase in terminal fall velocity with reduced air density, the factor $\frac{\rho_0}{\rho}$ (ρ is the air density, and the air density at surface condition ρ_0 =1.225 kg m^{-3} is) is added as the correction. The collision efficiency (k_{cc}) of cloud droplets is the leading factor dominating the collision rate, which is assumed to be fixed (4.44×10^9 m^3 kg^{-2} s^{-1}), and is derived from Pinsky et al. (2001). However, this factor in-

volves large uncertainty as it varies with height, drop size, and different calculation approaches.

2. Accretion

The accretion of cloud droplets becomes the main pathway for the growth of raindrops once small raindrops form. The accretion rate is derived from the application of the improved kernel:

$$\frac{\partial L_r}{\partial t}\Big|_{ac} = k_{cr} L_c L_r \phi_{ac}(\tau)\left(\frac{\rho_0}{\rho}\right)^{1/2} \tag{A2}$$

Where L_r and L_c is the mass densities of raindrops and cloud droplets (in kg m^{-3}) respectively, the universal function $\phi_{au}(\tau) = (\frac{\tau}{\tau + 5\times 10^{-5}})^4$. Similar correction ($\times\frac{\rho_0}{\rho}$) is also taken into account as for autoconversion rate. The collision efficiency (k_{cr}) is assumed to be 5.25×10^9 m^3 kg^{-2} s^{-1} (Pinsky et al., 2001).

3. Selfcollection of liquid droplets

Selfcollection is the process in which cloud droplets (raindrops) collide and stick together, but still remaining in the same hydrometeor class. The selfcollection rate of cloud droplets is calculated according to the following equation:

$$\frac{\partial N_c}{\partial t}\Big|_{sc} = -k_{cc} L_c^2 \frac{(\nu_c + 2)}{(\nu_c + 1)}\left(\frac{\rho_0}{\rho}\right) - \frac{\partial N_c}{\partial t}\Big|_{au} \tag{A3}$$

k_{cc} is the constant in cloud-cloud kernel, which is 4.44×10^9 m^3 kg^{-1} s^{-1}.

Raindrops are assumed to be exponential distribution, and the selfcollection rate is expressed by:

$$\frac{\partial N_r}{\partial t}\Big|_{sc} = k_{rr} N_r L_r \left(1 + \frac{\kappa_{rr}}{\lambda_r}\right)^{-9}\left(\frac{\rho_0}{\rho}\right)^{1/2} \tag{A4}$$

Where k_{rr}=7.12 m^3 kg^{-1} s^{-1}, and κ_{rr}=60.7 $kg^{-1/3}$. λ_r is the slope in raindrop size distribution.

4. Collisional breakup

The generation of raindrops via collisional breakup can be coupled to the raindrop selfcollection rate by the expression:

$$\frac{\partial N_r}{\partial t}\Big|_{br} = -[\Phi_{br}(\Delta\overline{D}_r)+1]\frac{\partial N_r}{\partial t}\Big|_{sc} \tag{A5}$$

Here $\Delta\overline{D}_r = \overline{D}_r - \overline{D}_{eq}$, $\overline{D}_r$ is the mean volume diameter of raindrops, and $\overline{D}_{eq}$ is the constant equilibrium diameter (=0.9 $\times 10^{-3}$ m). When $\overline{D}_r$ <0.3 $\times 10^{-3}$ m, the breakup process is negligible, with $\Phi_{br}(\Delta\overline{D}_r) = -1$; when 3×10^{-3} m $\leq \overline{D}_r \leq \overline{D}_{eq}$, $\Phi_{br}(\Delta\overline{D}_r) = k_{br}\Delta\overline{D}_r$ with k_{br} =1000 m^{-1}; when $\overline{D}_r$ > 0.9 $\times 10^{-3}$ m, $\Phi_{br}(\Delta\overline{D}_r) = 2\exp(\kappa_{br}\Delta\overline{D}_r) - 1$, with κ_{br} =2.3×10^3 m^{-1}.

5. Nucleation and growth of cloud droplets

The nucleation process of cloud droplets is derived from a look-up table from parcel model, which links the CCN number density with different aerosol number concentrations and updraft velocities (Reutter et al., 2009).

The condensational growth of cloud droplets is realized via standard saturation adjustment technique. This adjustment will be made at the end of each time step, after calculating all other microphysical processes. The remaining supersaturation is added to the cloud droplet class. Cloud droplets start to evaporate under subsaturation condition until the water saturation level is reached.

6. Nucleation of cloud ice

The nucleation of ice crystals mainly refers to the deposition freezing process, via which ice particles form by diffusion of water vapor on the dry ice nucleus. The number density of ice nuclei is parameterized according to the deposition-condensation nucleation formula from Meyers et al. (1992):

$$N_{IN} = N_{M92}\exp(a_{M92} + b_{M92}S_i) \tag{A6}$$

Where N_{M92}=1×10^3 m^{-3}, a_{M92}=-0.639, and b_{M92}=12.96, S_i is the supersaturation with respect to ice. The ice crystal number density calculated based on modified Fletcher formula (Reisner et al., 1998) is used as the limitation to avoid very low number concentrations.

7. Freezing of water drops

The freezing nucleation mainly includes the heterogeneous (immersion) and homogeneous freezing processes. The heterogeneous freezing of raindrops follows the classical work of Bigg (1953), and is predicted by a stochastical model. Assuming an exponential size distribution for raindrops, the freezing rate is a function of temperature:

$$\frac{\partial N_r}{\partial t}\Big|_{het} = -N_r \overline{x_r} J_{het}(T) \tag{A7}$$

$$\frac{\partial L_r}{\partial t}\Big|_{het} = -20 L_r \overline{x_r} J_{het}(T) \tag{A8}$$

Where N_r and L_r is the number and mass densities of raindrops (in m^{-3} and kg m^{-3}) respectively, $\overline{x_r}$ is the mean mass of raindrops (in kg), $J_{het}(T)$ is the temperature (T, in K) function for heterogeneous freezing (in kg^{-1} s^{-1}):

$$J_{het}(T) = 0.2\exp[0.65(273.15 - T) - 1]. \tag{A9}$$

Heterogeneous freezing of cloud droplets is treated in a similar way, assuming a Γ-distribution for size distribution.

The homogeneous freezing of cloud droplets is established based on Jeffery and Austin (1997) and Cotton and Field (2002). Once the temperature is lower than -40 ℃, all the cloud water content in this region could be homogeneously frozen to be ice crystals:

$$\frac{\partial N_c}{\partial t}\Big|_{\hom} = -N_c \overline{x_c} J_{\hom}(T) \tag{A10}$$

$$\frac{\partial L_c}{\partial t}\Big|_{\text{hom}} = -\frac{\nu_c + 2}{\nu_c + 1} L_c \overline{x}_c J_{\text{hom}}(T) \tag{A11}$$

Here $J_{\text{hom}}(T)$ is the homogeneous freezing rate per unit volume of water droplets (in $\text{kg}^{-1}\ \text{s}^{-1}$), and is calculated based on Cotton and Field (2002):

$$\log(J_{\text{hom}}(T_c)) = -7.63 - 2.996(T_c + 30) \qquad T_c > -30°\text{C};$$

$$\log(J_{\text{hom}}(T_c)) = -243.4 - 14.75T_c - 0.307T_c^{\,2} - 0.00287T_c^{\,3} - 0.0000102T_c^{\,4}$$

$$T_c <= -30°\text{C}. \tag{A12}$$

Here $T_c = T - 273.15$. Homogeneous freezing of raindrops is not included, due to their efficient heterogeneous freezing.

8. Growth of ice crystals by vapor deposition

The mechanism which causes ice particles to grow by diffusion of water vapor is called deposition. The growth rate is complicated to estimate, because different habits or shapes of ice particles can significantly influence the rate, which varies with different temperature, ice supersaturation, and falling velocities (Cotton et al., 2010). The growth of a single frozen particle by vapor deposition is treated similarly, by using a general growth equation:

$$\frac{\partial L_i}{\partial t} = \frac{4\pi}{c_i} G_{iv}(T,P) D_i(\overline{x}) \overline{F}_{v,1} S_i \tag{A13}$$

Where c_i is constant in capacity for cloud ice (π); $D_i(\overline{x})$ is the diameter of ice particles; S_i is supersaturation with respect to ice; $G_{iv}(T,P)$ is a thermodynamic function. $\overline{F}_{v,1}$ is the ventilation coefficient, which depends on the habit of the ice particles (Cotton et al., 2010). The calculation of deposition is firstly done for ice crystals, and then the ice supersaturation is added to snow. After the calculation of deposition for snow crystals, the growth of graupel and hail by vapor deposition will be predicted sequentially.

9. Melting process

When the temperature is above 0 ℃, frozen particles start to melt. Take graupel for example, the melting rate could be calculated based on Pruppacher and Klett (1997):

$$\frac{\partial M_g}{\partial t} = -\frac{2\pi}{L_{il}} D_g N_g \left[K_T (T - T_3) F_h + \frac{D_v L_{iv}}{R_v} \left(\frac{p_v}{T} - \frac{p_{lv}(T_3)}{T_3} \right) F_v \right] \tag{A14}$$

Where T_3=273.16K, the latent heat of melting L_{il} is 0.333×10^6 J kg^{-1}. D_g is the diameter of graupel (in m), and N_g is the number density of graupel (in m^{-3}). K_T is the conductivity of heat (2.5×10^{-2} J m^1 s^{-1} K^{-1}), D_v is the diffusivity of water vapor (3.0×10^{-5} m^2 s^{-1}), the latent heat of sublimation L_{iv} is 2.834×10^6 J kg^{-1}. R_v is the specific gas constant for water vapor (461.51 J kg^{-1} K^{-1}), p_v and p_{lv} is the pressure and saturation vapor pressure over liquid water (Pa), respectively. The ventilation coefficients for heat and water vapor are calculated by:

$$F_v = a_{v,g} + b_{v,g} N_{Sc}^{1/3} N_{\mathrm{Re}}^{1/2} \tag{A15}$$

$$F_h = \frac{D_T}{D_v} F_v = \frac{K_T}{c_p \rho_0 D_v} F_v . \tag{A16}$$

Where $a_{v,g}$ and $b_{v,g}$ is the constant in ventilation coefficient, N_{Sc} and N_{Re} is Reynolds number and Schmidt number, D_T is the diffusivity of heat in m^2 s^{-1}. Similar calculation is applied to other frozen particle types.

10. Collection processes

The collection processes (e.g., aggregation, riming) between each hydrometeor classes includes collision and coagulation phases. When a bigger drop and a smaller drop collide, they will either join together to form a single larger droplet or be separate. If the colliding droplets stick together, coalescence process occurs. The probability of the collision is associated with the relative size of the collector to the collected droplets, and the possibility of two colliding droplets that stick together is the coalescence efficiency.

The equations for the evolution of the mass and number densities of the two interacting particle ensembles (particle "a" collects "b" to form larger particles of type "a") can be parameterized by:

$$\frac{\partial L_a}{\partial t}\Big|_{coll,ab} = \frac{\pi}{4}\overline{E}_{ab} N_a L_b \left[\delta_a^0 D_a^2(\overline{x}_a) + \delta_{ab}^1 D_b(\overline{x}_b) D_a(\overline{x}_a) + \delta_b^1 D_b^2(\overline{x}_b)\right] \times \left[\vartheta_a^0 \upsilon_a^2(\overline{x}_a) - \vartheta_{ab}^1 \upsilon_b(\overline{x}_b)\upsilon_a(\overline{x}_a) + \vartheta_b^1 \upsilon_b^2(\overline{x}_b) + \sigma_a + \sigma_b\right]^{1/2} \tag{A17}$$

$$\frac{\partial N_b}{\partial t}\Big|_{coll,ab} = -\frac{\pi}{4}\overline{E}_{ab} N_a N_b \left[\delta_a^0 D_a^2(\overline{x}_a) + \delta_{ab}^1 D_b(\overline{x}_b) D_a(\overline{x}_a) + \delta_b^1 D_b^2(\overline{x}_b)\right] \times \left[\vartheta_a^0 \upsilon_a^2(\overline{x}_a) - \vartheta_{ab}^1 \upsilon_b(\overline{x}_b)\upsilon_a(\overline{x}_a) + \vartheta_b^1 \upsilon_b^2(\overline{x}_b) + \sigma_a + \sigma_b\right]^{1/2} \tag{A18}$$

$$\frac{\partial L_b}{\partial t}\Big|_{coll,ab} = -\frac{\partial L_a}{\partial t}\Big|_{coll,ab} \tag{A19}$$

Where δ and ϑ are dimensionless constants, depending on the chosen size distributions, the velocity, and diameter-mass relations of two particles. The diameter (D)-mass(x)- and the velocity(υ)-mass(x)-relations of various hydrometer particles are described by power laws:

$$D(x) \cong a x^b \tag{A20}$$

$$\upsilon(x) \cong a x^\beta \left(\frac{\rho_0}{\rho}\right)^\gamma \tag{A21}$$

The constant coefficients a, b, α, β, γ could be found in Table 1 in Seifert and Beheng (2006).

σ is the velocity variance. For cloud ice and snow, σ=0.2 m s^{-1}; while σ=0 for cloud droplets, raindrops, and graupel.

$\overline{E}_{ab}$ is the mean collision efficiency, and within Seifert two-moment scheme, the collision efficiency for the collection of cloud droplets by cloud ice, snow, and graupel is:

$$E_{coll,ec}(\overline{D}_e, \overline{D}_c) = \overline{E}_c(\overline{D}_c)\overline{E}_e(\overline{D}_e) \tag{A22}$$

Where $e \in \{i, s, g\}$,

$$\overline{E}_c(\overline{D}_c) = \begin{cases} 0, if\ \overline{D}_c < \overline{D}_{c,0} \\ \dfrac{\overline{D}_c - \overline{D}_{c,0}}{\overline{D}_{c,1} - \overline{D}_{c,0}}, if\ \overline{D}_{c,0} \le \overline{D}_c \le \overline{D}_{c,1} \\ 1, if\ \overline{D}_c > \overline{D}_{c,1} \end{cases} \tag{A23}$$

Here $\overline{D}_{c,0} = 15um, \overline{D}_{c,1} = 40um$.

$$\overline{E}_e(\overline{D}_e) = \begin{cases} 0, if\ \overline{D}_e \le \overline{D}_{e,0} \\ \overline{E}_{e,\max}, if\ \overline{D}_e > \overline{D}_{e,0} \end{cases} \tag{A24}$$

Here $\overline{D}_{i,0} = \overline{D}_{s,0} = \overline{D}_{g,0} = 150um$, $\overline{E}_{i,\max} = \overline{E}_{s,\max} = 0.8, \overline{E}_{g,\max} = 1.0$.

The coalescence efficiencies of the gruapel-ice- and graupel-graupel-collisions are assumed to be 0, while of the snow-snow-, ice-ice-, snow-ice-, and graupel-snow-collisions are temperature dependent:

$$\overline{E}_{coal}(T) = \exp(0.09T). \tag{A25}$$

10.1 Riming process

The collection of supercooled liquid droplets onto the surface of ice crystal is riming (or accretion) process, which is analogous to droplet collision. Ice crystals could serve as collector, and once the supercooled droplets impinge the ice surface, they can freeze and accumulate on the ice (Cotton et al., 2010). This results in rapid growth of ice crystals, and acceleration of their falling speeds. The collection efficiencies among different categories contain two main components: one the hydrodynamic efficiency or the collision probability; and secondly the coalescence efficiency or the sticking probability. Both of these two efficiencies involve large uncertainties (Cotton et al., 1986). The calculation formula is similar to that for collection process.

10.2 Aggregation

Aggregation is the process that two colliding ice particles merge together to form a larger frozen particle. This is another important way of the growth of ice crystals, and can form snowflakes. Aggregation can take place among ice crystals (snow), or between different frozen particles. The aggregation rate is also determined by the collision efficiency and coalescence efficiency. A thin coating of liquid water on the surface of ice particles favors for the aggregation process, which make ice crystals more "adhesive".

10.3 Conversion process

The riming ice crystals could convert to be graupel when the collected water mass fills up the enveloping sphere, and the critical mass $x_{crit,rime}$ for the conversion is:

$$x_{crit,rime} = \alpha_0 \rho_w (\frac{\pi}{6} \overline{D}_i^3 - \frac{\overline{x}_i}{\rho_\varepsilon}) \tag{A26}$$

The densities of water and ice class ρ_w =1000 kg m^{-3}, and ρ_ε =900 kg m^{-3}, and the space filling coefficient α_0 =0.68. $\overline{D}_i$ is the maximum diameter of ice crystals associated with the sphere, and only when $\overline{D}_i$ exceeds 500 microns, can the conversion process occurs.

The corresponding characteristic time τ_{conv} for the conversion process can be calculated based on the riming rate $\frac{\partial L_i}{\partial t}|_{rime}$:

$$\tau_{conv} = \frac{x_{crit,rime}}{\frac{\partial \overline{x}_i}{\partial t}|_{rime}} = \frac{x_{crit,rime}}{\frac{1}{N_i}\frac{\partial L_i}{\partial t}|_{rime}} = \frac{N_i \alpha_0 \rho_w (\frac{\pi}{6} \overline{D}_i^3 - \frac{\overline{x}_i}{\rho_\varepsilon})}{\frac{\partial L_i}{\partial t}|_{rime}} \tag{A27}$$

Therefore the conversion rate from ice crystals to graupel substance resulting from riming process is described as follows:

$$\frac{\partial L_g}{\partial t}\Big|_{conv} = \frac{L_i}{\tau_{conv}} = \frac{1}{\alpha_0 \frac{\rho_w}{\rho_\varepsilon}(\frac{\frac{\pi}{6}\rho_\varepsilon \overline{D_i^3}}{\overline{x_i}} - 1)} \frac{\partial L_i}{\partial t}\Big|_{rime} \tag{A28}$$

$$\frac{\partial N_g}{\partial t}\Big|_{conv} = \frac{1}{\overline{x_i}} \frac{\partial L_g}{\partial t}\Big|_{conv} . \tag{A29}$$

This approach is also applied to the snow-graupel conversion, and the space filling coefficient α_0 =0.01, denoting a rapid conversion.

At given supercooled water content and temperature, graupel particles with diameter D exceeding a certain threshold value D_c, can efficiently grows by accretion of ice particles and convert to hail by wet growth process (Blahak, 2008). The critical diameter for graupel-hail conversion is derived from a lookup table.

10.4 Ice multiplication

Ice multiplication process is based on the work of Hallett and Mossop (1974). The generation rate (R_i, in m^{-3} s^{-1}) of N_i due to ice splinter multiplication of cloud ice is parameterized as follows:

$$R_i = \rho \times 3.5 \times 10^8 f(T_c)(P_{s,sacw} + P_{g,sacw}) \tag{A30}$$

Where $f(T_c)$ is 0 when T<265K and T>270K, while is 1 when T=268K, and increases linearly between these two extremes for 265K $\leq T \leq$ 270K. $P_{s,sacw}$ and $P_{g,sacw}$ are the generation rate of snow/graupel by that portion of collected cloud water by snow which is converted to snow/graupel, which are derived from Ikawa and Saito (1991). The generation rate of ice crystals (P_i, in s^{-1}) from this process is given as:

$$P_i = \frac{R_i \times m_{io}}{\rho} \tag{A31}$$

Where m_{io} is the mass of the smallest particle (1×10^{-12} kg), and ρ is the density of air.

11. Evaporation process

The evaporation rate of raindrops is calculated on the basis of Pruppacher and Klett (1997):

$$\frac{\partial M_r}{\partial t} = 2\pi D_r(\bar{x}_r) N_r S G_{lv}(T,p) \overline{F}_v(\bar{x}_r) . \tag{A32}$$

D_r is the diameter of raindrops (in m), N_r is the number density of raindrops (in m^{-3}), S is supersaturation with respect to water. $G_{lv}(T,p)$ is a thermodynamic function:

$$G_{lv}(T,p) = \left[\frac{R_v T}{p_{lv}(T) D_v} + \frac{L_{lv}}{K_T T}\left(\frac{L_{lv}}{R_v T} - 1 \right) \right]^{-1} \tag{A33}$$

Where L_{lv} is latent heat of evaporation, which is 2.501×10^6 J kg^{-1}, $p_{lv}(T)$ is the saturation vapor pressure over liquid water; R_v is the specific gas constant for water vapor, which is 461.51 J kg^{-1} K^{-1}; K_T is the conductivity of heat (2.5×10^{-2} J m^1 s^{-1} K^{-1}); D_v is the diffusivity of water vapor (3.0×10^{-5} m^2 s^{-1}).

The averaged ventilation factor is calculated by:

$$\overline{F}_v(\bar{x}_r) = \bar{a}_v + \bar{b}_v N_{Sc}^{1/3} N_{\mathrm{Re}}^{1/2}(\bar{x}_r) \tag{A34}$$

Where the constants $\bar{a}_v$ and $\bar{b}_v$ are available in Seifert and Beheng (2006).

The treatment of the evaporation process of frozen particles is parameterized similar to the evaporation of raindrops.

12. Shedding process

The liquid water collected by frozen particles will be shed if temperature is above 0 ℃, instead of being frozen. It is assumed that the shedding rate of the water from frozen particles equals to the rate at which it is collected (Rutledge and Hobbs, 1984). All the liquid water will be shed to rain category.

13. Sedimentation process

The sedimentation of raindrops is the key process that determines the production of surface precipitation. Sedimentation is considered by using the number and mass weighted mean fall velocities:

$$\upsilon_r = \left(\frac{\rho_0}{\rho}\right)^{1/2}\left[a_R - b_R\left(1+\frac{c_R}{\lambda_r}\right)^{-(3k+1)}\right] \tag{A35}$$

Where a_R=9.65 m s^{-1}, b_R=10.3 m s^{-1}, c_R=600 m^{-1}; k=0 for number densities, and k=1 for mass densities. λ_r is the slope in raindrop size distribution. This equation takes account of the increase in the terminal fall velocity with height.

The sedimentation treatment of ice crystals, snow, graupel and hail is similar to raindrops, assuming generalized Γ-distributions.

Appendix B: A list of abbreviations

ATHAM	Active Tracer High Resolution Atmospheric Model
CCN	Cloud Condensation Nuclei
IN	Ice Nuclei
pyroCb	Pyro-cumulonimbus
RH	Relative humidity
RS	Relative sensitivity
FF	Fire forcing
LA	Low aerosol concentration
HA	High aerosol concentration
LU	Low updraft condition
HU	High updraft condition
WBF	Wegener-Bergeron-Findeisen process

Appendix C: Symbols and acronyms for individual microphysical process

Symbol	Process
crg/h	Riming of cloud droplets to form graupel/hail
cri/s	Riming of cloud droplets to form ice crystals/snow
cfi$^{(1)}$	Freezing of cloud water to form ice crystals
hom	Homogeneous ice nucleation
imm	Immersion freezing nucleation
dep	Deposition freezing nucleation
au	Autoconversion of cloud water to form raindrops
ac	Accretion of cloud water by raindrops
cn	Cloud nucleation
in	Deposition-condensation ice nucleation
rsc	Self-collection of raindrops
imc/r	Melting of ice crystals to form cloud water/raindrops
icg	Conversion of ice crystals to form graupel
rri/s/g/h	Riming of raindrops to form ice crystals/snow/graupel/hail
irg	Riming of ice crystals to form graupel
vdc/i/g/s	Depositional growth of cloud droplets/ice crystals/graupel/snow
rfi/g/h	Freezing of raindrops to form ice crystals/graupel/hail
iscs	Self-collection of ice crystals to form snow
iclg/h/s	Collection of ice crystals to form graupel/hail/snow
g/h/s/imr	Melting of graupel/hail/snow/ice to form raindrops

gsr	Shedding of graupel to form raindrops
r/i/s/g/hep	Evaporation of raindrops/ice/snow/graupel/hail
scg	Conversion of snow to form graupel

(1) *cfi* process includes both heterogeneous and homogeneous freezing processes.

Appendix D: List of symbols for ice nucleation

Symbol (units)	Description
J (s^{-1})	Ice nucleation rate per particle and time
$J_{dep,x}$ (s^{-1})	Deposition nucleation rate per particle and time of species x
$J_{imm,x}$ (s^{-1})	Immersion freezing rate per particle and time of species x
$f_{\ell,x}$(%)	The fraction of particles that is activated to liquid droplets of species x
$f_{x,coated}$(%)	The coated fraction of particles of species x
a_w	Water activity
N_{CN} (m^{-3})	Aerosol number concentration
$\Delta N_{i,\,dep}$ (m^{-3})	Change in ice crystal concentration due to deposition nucleation
$\Delta N_{i,\,imm}$ (m^{-3})	Change in ice crystal concentration due to immersion nucleation

List of Figures

List of Tables

References

Ackerman, A. S., Toon, O. B., Stevens, D. E., Heymsfield, A. J., Ramanathan, V., and Welton, E. J.: Reduction of tropical cloudiness by soot, Science, 288, 1042-1047, doi: 10.1126/science.288.5468.1042, 2000.

Ackerman, A. S., Toon, O. B., Stevens, D. E., and Coakley, J. A.: Enhancement of cloud cover and suppression of nocturnal drizzle in stratocumulus polluted by haze, Geophys Res Lett, 30, 1381, doi: 10.1029/2002gl016634, 2003.

Albrecht, B. A.: Aerosols, Cloud Microphysics, and Fractional Cloudiness, Science, 245, 1227-1230, doi: 10.1126/science.245.4923.1227, 1989.

Altaratz, O., Koren, I., Reisin, T., Kostinski, A., Feingold, G., Levin, Z., and Yin, Y.: Aerosols' influence on the interplay between condensation, evaporation and rain in warm cumulus cloud, Atmospheric Chemistry and Physics, 8, 15-24, 2008.

Andreae, M. O.: Biomass burning: its history, use, and distribution and its impact on environmental quality and global climate, in: Global Biomass Burning: Atmospheric, Climatic, and Biospheric Implications edited by: Levine, J. S., MIT Press, Cambridge, MA, 1-21, 1991.

Andreae, M. O., Rosenfeld, D., Artaxo, P., Costa, A. A., Frank, G. P., Longo, K. M., and Silva-Dias, M. A. F.: Smoking Rain Clouds over the Amazon, Science, 303, 1337-1342, 2004.

ASRD: Final documentation report-Chisholm Fire (LWF-063), Forest Protection Division, Alberta Sustainable Resource Development, 2001.

Bigg, E. K.: The Formation of Atmospheric Ice Crystals by the Freezing of Droplets, Q J Roy Meteor Soc, 79, 510-519, doi: 10.1002/qj.49707934207, 1953.

Blahak, U.: Towards a Better Representation of High Density Ice Particles in a State-of-the-Art Two-Moment Bulk Microphysical Scheme, 15th International Conf. on Clouds and Precipitation, Cancun, Mexico, July 7–11, 2008.

Burrows, S. M., Hoose, C., Poschl, U., and Lawrence, M. G.: Ice nuclei in marine air: biogenic particles or dust?, Atmospheric Chemistry and Physics, 13, 245-267, doi: 10.5194/acp-13-245-2013, 2013.

Bytnerowicz, A., Arbaugh, M., Andersen, C., and Riebau, A.: Wildland Fires and Air Pollution, Dev Environm Sci, 8, 1-638, 2009.

Camponogara, G., Dias, M. A. F. S., and Carrio, G. G.: Relationship between Amazon biomass burning aerosols and rainfall over the La Plata Basin, Atmospheric Chemistry and Physics, 14, 4397-4407, doi: 10.5194/acp-14-4397-2014, 2014.

Chang, D., and Song, Y.: Comparison of L3JRC and MODIS global burned area products from 2000 to 2007, J Geophys Res-Atmos, 114, doi: 10.1029/2008jd011361, 2009.

Conant, W. C., VanReken, T. M., Rissman, T. A., Varutbangkul, V., Jonsson, H. H., Nenes, A., Jimenez, J. L., Delia, A. E., Bahreini, R., Roberts, G. C., Flagan, R. C., and Seinfeld, J. H.: Aerosol-cloud drop concentration closure in warm cumulus, J Geophys Res-Atmos, 109, doi: 10.1029/2003jd004324, 2004.

Cotton, R. J., and Field, P. R.: Ice nucleation characteristics of an isolated wave cloud, Q J Roy Meteor Soc, 128, 2417-2437, doi: 10.1256/Qj.01.150, 2002.

Cotton, W. R., Tripoli, G. J., Rauber, R. M., and Mulvihill, E. A.: Numerical-Simulation of the Effects of Varying Ice Crystal Nucleation Rates and Aggregation Processes on Orographic Snowfall, J Clim Appl Meteorol, 25, 1658-1680, Doi: 10.1175/1520-0450(1986)025, 1986.

Cotton, W. R., Bryan, G. H., and van den Heever, S. C.: Storm and Cloud Dynamics, International Geophysics (Book 99), 99, Academic Press, 2010.

DeMott, P. J., Cziczo, D. J., Prenni, A. J., Murphy, D. M., Kreidenweis, S. M., Thomson, D. S., Borys, R., and Rogers, D. C.: Measurements of the concentration and composition of nuclei for cirrus formation, P Natl Acad Sci USA, 100, 14655-14660, doi: 10.1073/pnas.2532677100, 2003a.

DeMott, P. J., Sassen, K., Poellot, M. R., Baumgardner, D., Rogers, D. C., Brooks, S. D., Prenni, A. J., and Kreidenweis, S. M.: African dust aerosols as atmospheric ice nuclei, Geophys Res Lett, 30, doi: 10.1029/2003gl017410, 2003b.

Diehl, K., and Wurzler, S.: Heterogeneous drop freezing in the immersion mode: Model calculations considering soluble and insoluble particles in the drops, J Atmos Sci, 61, 2063-2072, doi: 10.1175/1520-0469(2004)061, 2004.

Eidhammer, T., DeMott, P. J., and Kreidenweis, S. M.: A comparison of heterogeneous ice nucleation parameterizations using a parcel model framework, J Geophys Res-Atmos, 114, doi: 10.1029/2008jd011095, 2009.

Fan, J. W., Yuan, T. L., Comstock, J. M., Ghan, S., Khain, A., Leung, L. R., Li, Z. Q., Martins, V. J., and Ovchinnikov, M.: Dominant role by vertical wind shear in regulating aerosol effects on deep convective clouds, J Geophys Res-Atmos, 114, doi: 10.1029/2009jd012352, 2009.

Fan, J. W., Comstock, J. M., and Ovchinnikov, M.: The cloud condensation nuclei and ice nuclei effects on tropical anvil characteristics and water vapor of the tropical tropopause layer, Environ Res Lett, 5, doi: 10.1088/1748-9326/5/4/044005, 2010.

Fan, J. W., Leung, L. R., Rosenfeld, D., Chen, Q., Li, Z. Q., Zhang, J. Q., and Yan, H. R.: Microphysical effects determine macrophysical response for aerosol impacts on deep convective clouds, P Natl Acad Sci USA, 110, E4581-E4590, doi: 10.1073/pnas.1316830110, 2013.

Feingold, G.: Modeling of the first indirect effect: Analysis of measurement requirements, Geophys Res Lett, 30, doi: 10.1029/2003gl017967, 2003.

Fountoukis, C., Nenes, A., Meskhidze, N., Bahreini, R., Conant, W. C., Jonsson, H., Murphy, S., Sorooshian, A., Varutbangkul, V., Brechtel, F., Flagan, R. C., and Seinfeld, J. H.: Aerosol-cloud drop concentration closure for clouds sampled during the International Consortium for Atmospheric Research on Transport and Transformation 2004 campaign, J Geophys Res-Atmos, 112, doi: 10.1029/2006jd007272, 2007.

Fromm, M., Tupper, A., Rosenfeld, D., Servranckx, R., and McRae, R.: Violent pyro-convective storm devastates Australia's capital and pollutes the stratosphere, Geophys Res Lett, 33, doi: 10.1029/2005gl025161, 2006.

Fromm, M., Shettle, E. P., Fricke, K. H., Ritter, C., Trickl, T., Giehl, H., Gerding, M., Barnes, J. E., O'Neill, M., Massie, S. T., Blum, U., McDermid, I. S., Leblanc, T., and Deshler, T.: Stratospheric impact of the Chisholm pyrocumulonimbus eruption: 2. Vertical profile perspective, J Geophys Res-Atmos, 113, doi: 10.1029/2007jd009147, 2008.

Graf, H. F., Herzog, M., Oberhuber, J. M., and Textor, C.: Effect of environmental conditions on volcanic plume rise, J Geophys Res-Atmos, 104, 24309-24320, 1999.

Graf, H. F.: Atmospheric science - The complex interaction of aerosols and clouds, Science, 303, 1309-1311, DOI 10.1126/science.1094411, 2004.

Grandey, B. S., Stier, P., and Wagner, T. M.: Investigating relationships between aerosol optical depth and cloud fraction using satellite, aerosol reanalysis and general circulation model data, Atmospheric Chemistry and Physics, 13, 3177-3184, doi: 10.5194/acp-13-3177-2013, 2013.

Grandey, B. S., Gururaj, A., Stier, P., and Wagner, T. M.: Rainfall-aerosol relationships explained by wet scavenging and humidity, Geophys. Res. Lett., 41, doi:10.1002/2014GL060958, 2014.

Gunthe, S. S., Rose, D., Su, H., Garland, R. M., Achtert, P., Nowak, A., Wiedensohler, A., Kuwata, M., Takegawa, N., Kondo, Y., Hu, M., Shao, M., Zhu, T., Andreae, M. O., and Poschl, U.: Cloud condensation nuclei (CCN) from fresh and aged air pollution in the megacity region of Beijing, Atmospheric Chemistry and Physics, 11, 11023-11039, doi: 10.5194/acp-11-11023-2011, 2011.

Hallett, J., and Mossop, S. C.: Production of Secondary Ice Particles during Riming Process, Nature, 249, 26-28, doi: 10.1038/249026a0, 1974.

Herzog, M.: Simulation der dynamik eines multikomponentensystems am beispiel vulkanischer eruptionswolken, Ph. D, University of Hamburg, Hamburg, Germany, 153 pp., 1998.

Herzog, M., Graf, H. F., Textor, C., and Oberhuber, J. M.: The effect of phase changes of water on the development of volcanic plumes, J Volcanol Geoth Res, 87, 55-74, 1998.

Herzog, M., Oberhuber, J. M., and Graf, H. F.: A prognostic turbulence scheme for the nonhydrostatic plume model ATHAM, J Atmos Sci, 60, 2783-2796, 2003.

Hobbs, P. V., and Locatelli, J. D.: Ice nuclei from a natural forest fire, J Appl Meteorol, 8, 833-834, 1969.

Hobbs, P. V., and Radke, L. F.: Cloud Condensation Nuclei from a Simulated Forest Fire, Science, 163, 279-280, 1969.

Hoose, C., Kristjansson, J. E., Chen, J. P., and Hazra, A.: A Classical-Theory-Based Parameterization of Heterogeneous Ice Nucleation by Mineral Dust, Soot, and Biological Particles in a Global Climate Model, J Atmos Sci, 67, 2483-2503, doi: 10.1175/2010jas3425.1, 2010.

Hoose, C., and Mohler, O.: Heterogeneous ice nucleation on atmospheric aerosols: a review of results from laboratory experiments, Atmospheric Chemistry and Physics, 12, 9817-9854, doi: 10.5194/acp-12-9817-2012, 2012.

Ikawa, M., and Saito, K.: Description of a nonhydrostatic model developed at the forecast research department of the MRI, 238, 1991.

IPCC: Climate Change 2013: The Physical Science Basis. Working Group I Contribution to the Fifth Assessment Report of the Intergovernmental Panel on Climate Change, edited by: Stocker, T. F., Qin, D., Plattner, G.-K., Tignor, M., Allen, S. K., Boschung, J., Nauels, A., Xia, Y., Bex, V., and Midgley, P. M., Cambridge University Press, Cambridge, United Kingdom and New York, USA, 1535 pp., 2013.

Jayaweer, K., and Ryan, B. F.: Terminal Velocities of Ice Crystals, Q J Roy Meteor Soc, 98, 193-&, DOI 10.1002/qj.49709841516, 1972.

Jeffery, C. A., and Austin, P. H.: Homogeneous nucleation of supercooled water: Results from a new equation of state, J Geophys Res-Atmos, 102, 25269-25279, doi: 10.1029/97jd02243, 1997.

Joos, H., Spichtinger, P., Reutter, P., and Fusina, F.: Influence of heterogeneous freezing on the microphysical and radiative properties of orographic cirrus clouds, Atmospheric Chemistry and Physics, 14, 6835-6852, doi: 10.5194/acp-14-6835-2014, 2014.

Karydis, V. A., Capps, S. L., Russell, A. G., and Nenes, A.: Adjoint sensitivity of global cloud droplet number to aerosol and dynamical parameters, Atmospheric Chemistry and Physics, 12, 9041-9055, doi: 10.5194/acp-12-9041-2012, 2012.

Kaufman, Y. J., and Fraser, R. S.: The effect of smoke particles on clouds and climate forcing, Science, 277, 1636-1639, 1997.

Kaufman, Y. J., Tanre, D., and Boucher, O.: A satellite view of aerosols in the climate system, Nature, 419, 215-223, doi: 10.1038/Nature01091, 2002.

Kaufman, Y. J., and Koren, I.: Smoke and pollution aerosol effect on cloud cover, Science, 313, 655-658, doi: 10.1126/science.1126232, 2006.

Kay, J. E., and Wood, R.: Timescale analysis of aerosol sensitivity during homogeneous freezing and implications for upper tropospheric water vapor budgets, Geophys Res Lett, 35, L10809, doi: 10.1029/2007gl032628, 2008.

Khain, A., Rosenfeld, D., and Pokrovsky, A.: Aerosol impact on the dynamics and microphysics of deep convective clouds, Q J Roy Meteor Soc, 131, 2639-2663, doi: 10.1256/Qj.04.62, 2005.

Khain, A. P., BenMoshe, N., and Pokrovsky, A.: Factors determining the impact of aerosols on surface precipitation from clouds: An attempt at classification, J Atmos Sci, 65, 1721-1748, doi: 10.1175/2007jas2515.1, 2008.

Khain, A. P.: Notes on state-of-the-art investigations of aerosol effects on precipitation: a critical review, Environ Res Lett, 4, doi: 10.1088/1748-9326/4/1/015004, 2009.

Khain, A. P., Leung, L. R., Lynn, B., and Ghan, S.: Effects of aerosols on the dynamics and microphysics of squall lines simulated by spectral bin and bulk parameterization schemes, J Geophys Res-Atmos, 114, doi: 10.1029/2009jd011902, 2009.

Khvorostyanov, V. I., and Curry, J. A.: A new theory of heterogeneous ice nucleation for application in cloud and climate models, Geophys Res Lett, 27, 4081-4084, doi: 10.1029/1999gl011211, 2000.

Kohler, H.: The nucleus in and the growth of hygroscopic droplets., Transactions of the Faraday Society, 32, 1152-1161, doi: 10.1039/Tf9363201152, 1936.

Koren, I., Kaufman, Y. J., Remer, L. A., and Martins, J. V.: Measurement of the effect of Amazon smoke on inhibition of cloud formation, Science, 303, 1342-1345, doi: 10.1126/science.1089424, 2004.

Koren, I., Martins, J. V., Remer, L. A., and Afargan, H.: Smoke invigoration versus inhibition of clouds over the Amazon, Science, 321, 946-949, doi: 10.1126/science.1159185, 2008.

Korolev, A., and Isaac, G. A.: Relative humidity in liquid, mixed-phase, and ice clouds, J Atmos Sci, 63, 2865-2880, Doi 10.1175/Jas3784.1, 2006.

Kulmala, M., Laaksonen, A., Charlson, R. J., and Korhonen, P.: Clouds without supersaturation, Nature, 388, 336-337, doi: 10.1038/41000, 1997.

Laaksonen, A., Korhonen, P., Kulmala, M., and Charlson, R. J.: Modification of the Kohler equation to include soluble trace gases and slightly soluble substances, J Atmos Sci, 55, 853-862, 1998.

Lee, S. S., Donner, L. J., Phillips, V. T. J., and Ming, Y.: The dependence of aerosol effects on clouds and precipitation on cloud-system organization, shear and stability, J Geophys Res-Atmos, 113, doi: 10.1029/2007jd009224, 2008.

Lee, S. S., and Penner, J. E.: Aerosol effects on ice clouds: can the traditional concept of aerosol indirect effects be applied to aerosol-cloud interactions in cirrus clouds?, Atmospheric Chemistry and Physics, 10, 10345-10358, doi: 10.5194/acp-10-10345-2010, 2010.

Lee, S. S., and Feingold, G.: Aerosol effects on the cloud-field properties of tropical convective clouds, Atmospheric Chemistry and Physics, 13, 6713-6726, doi:10.5194/acp-13-6713-2013, 2013.

Levin, Z., and Cotton, W.: Aerosol Pollution Impact on Precipitation: A Scientific Review, World Meteorol. Organ, Geneva, Switzerland, 2007.

Li, G. H., Wang, Y., and Zhang, R. Y.: Implementation of a two-moment bulk microphysics scheme to the WRF model to investigate aerosol-cloud interaction, J Geophys Res-Atmos, 113, doi: 10.1029/2007jd009361, 2008.

Lin, Y. L., Farley, R. D., and Orville, H. D.: Bulk Parameterization of the Snow Field in a Cloud Model, J Clim Appl Meteorol, 22, 1065-1092, doi: 10.1175/1520-0450(1983)022, 1983.

Liu, X. H., Zhang, Y., Xing, J., Zhang, Q. A., Wang, K., Streets, D. G., Jang, C., Wang, W. X., and Hao, J. M.: Understanding of regional air pollution over China using CMAQ, part II. Process analysis and sensitivity of ozone and particulate matter to precursor emissions, Atmos Environ, 44, 3719-3727, doi: 10.1016/j.atmosenv.2010.03.036, 2010.

Liu, X. H., Wang, Y., and Hoose, C.: Implement a Classical-Theory-Based Parameterization of Heterogeneous Ice Nucleation in CAM5, Aip Conf Proc, 1527, 763-765, doi: 10.1063/1.4803383, 2013.

Luderer, G., Trentmann, J., Winterrath, T., Textor, C., Herzog, M., Graf, H. F., and Andreae, M. O.: Modeling of biomass smoke injection into the lower stratosphere by a large forest fire (Part II): sensitivity studies, Atmospheric Chemistry and Physics, 6, 5261-5277, 2006.

Luderer, G. G.: Modeling of Deep-Convective Vertical Transport of Foreset Fire Smoke into the Upper Troposphere and Lower Stratosphere, Ph.D, Physics Department, Johannes Gutenberg University Mainz, Mainz, 2007.

McComiskey, A., and Feingold, G.: The scale problem in quantifying aerosol indirect effects, Atmospheric Chemistry and Physics, 12, 1031-1049, DOI 10.5194/acp-12-1031-2012, 2012.

McFiggans, G., Artaxo, P., Baltensperger, U., Coe, H., Facchini, M. C., Feingold, G., Fuzzi, S., Gysel, M., Laaksonen, A., Lohmann, U., Mentel, T. F., Murphy, D. M., O'Dowd, C. D., Snider, J. R., and Weingartner, E.: The effect of physical and chemical aerosol properties on warm cloud droplet activation, Atmospheric Chemistry and Physics, 6, 2593-2649, 2006.

Meyers, M. P., Demott, P. J., and Cotton, W. R.: New Primary Ice-Nucleation Parameterizations in an Explicit Cloud Model, J Appl Meteorol, 31, 708-721, doi: 10.1175/1520-0450(1992)031, 1992.

Mitchell, D. L., and Heymsfield, A. J.: Refinements in the treatment of ice particle terminal velocities, highlighting aggregates, J Atmos Sci, 62, 1637-1644, Doi 10.1175/Jas3413.1, 2005.

Morris, G. A., Hersey, S., Thompson, A. M., Pawson, S., Nielsen, J. E., Colarco, P. R., McMillan, W. W., Stohl, A., Turquety, S., Warner, J., Johnson, B. J., Kucsera, T. L., Larko, D. E., Oltmans, S. J., and Witte, J. C.: Alaskan and Canadian forest fires exacerbate ozone pollution over Houston, Texas, on 19 and 20 July 2004, J Geophys Res-Atmos, 111, doi: 10.1029/2006jd007090, 2006.

Morrison, H.: On the robustness of aerosol effects on an idealized supercell storm simulated with a cloud system-resolving model, Atmospheric Chemistry and Physics, 12, 7689-7705, doi: 10.5194/acp-12-7689-2012, 2012.

Muhlbauer, A., Hashino, T., Xue, L., Teller, A., Lohmann, U., Rasmussen, R. M., Geresdi, I., and Pan, Z.: Intercomparison of aerosol-cloud-precipitation interactions in stratiform orographic mixed-phase clouds, Atmospheric Chemistry and Physics, 10, 8173-8196, doi: 10.5194/acp-10-8173-2010, 2010.

Norris, J. R.: Has northern Indian Ocean cloud cover changed due to increasing anthropogenic aerosol?, Geophys Res Lett, 28, 3271-3274, doi: 10.1029/2001gl013547, 2001.

Oberhuber, J. M., Herzog, M., Graf, H. F., and Schwanke, K.: Volcanic plume simulation on large scales, J Volcanol Geoth Res, 87, 29-53, 1998.

Petters, M. D., and Kreidenweis, S. M.: A single parameter representation of hygroscopic growth and cloud condensation nucleus activity, Atmospheric Chemistry and Physics, 7, 1961-1971, 2007.

Phillips, V. T. J., DeMott, P. J., and Andronache, C.: An empirical parameterization of heterogeneous ice nucleation for multiple chemical species of aerosol, J Atmos Sci, 65, 2757-2783, doi: 10.1175/2007jas2546.1, 2008.

Pinsky, M., Khain, A., and Shapiro, M.: Collision efficiency of drops in a wide range of Reynolds numbers: Effects of pressure on spectrum evolution, J Atmos Sci, 58, 742-764, Doi: 10.1175/1520-0469(2001)058, 2001.

Prenni, A. J., Harrington, J. Y., Tjernstrom, M., DeMott, P. J., Avramov, A., Long, C. N., Kreidenweis, S. M., Olsson, P. Q., and Verlinde, J.: Can ice-nucleating aerosols affect arctic seasonal climate?, B Am Meteorol Soc, 88, 541-550, doi: 10.1175/Bams-88-4-541, 2007.

Pruppacher, H. R., and Klett, J. D.: Microphysics of Clouds and Precipitation, Second Revised and Enlarged Edition with an Introduction to Cloud Chemistry and Cloud Electricity, Kluwer Academic Publishers, Reidel, Dordrecht, 954 pp., 1997.

Ramanathan, V., Crutzen, P. J., Kiehl, J. T., and Rosenfeld, D.: Atmosphere - Aerosols, climate, and the hydrological cycle, Science, 294, 2119-2124, doi: 10.1126/science.1064034, 2001.

Reid, J. S., Koppmann, R., Eck, T. F., and Eleuterio, D. P.: A review of biomass burning emissions part II: intensive physical properties of biomass burning particles, Atmospheric Chemistry and Physics, 5, 799-825, 2005.

Reisner, J., Rasmussen, R. M., and Bruintjes, R. T.: Explicit forecasting of supercooled liquid water in winter storms using the MM5 mesoscale model, Q J Roy Meteor Soc, 124, 1071-1107, doi: 10.1002/qj.49712454804, 1998.

Reutter, P., Su, H., Trentmann, J., Simmel, M., Rose, D., Gunthe, S. S., Wernli, H., Andreae, M. O., and Poschl, U.: Aerosol- and updraft-limited regimes of cloud droplet formation: influence of particle number, size and hygroscopicity on the activation of cloud condensation nuclei (CCN), ATMOSPHERIC CHEMISTRY AND PHYSICS, 9, 7067-7080, 10.5194/acp-9-7067-2009, 2009.

Reutter, P., Trentmann, J., Seifert, A., Neis, P., Su, H., Chang, D., Herzog, M., Wernli, H., Andreae, M. O., and Poschl, U.: 3-D model simulations of dynamical and microphysical interactions in pyro-convective clouds under idealized conditions, Atmospheric Chemistry and Physics, 14, 7573-7583, doi:10.5194/acp-14-7573-2014, 2014.

Richardson, M. S., DeMott, P. J., Kreidenweis, S. M., Cziczo, D. J., Dunlea, E. J., Jimenez, J. L., Thomson, D. S., Ashbaugh, L. L., Borys, R. D., Westphal, D. L., Casuccio, G. S., and Lersch, T. L.: Measurements of heterogeneous ice nuclei in the western United States in springtime and their relation to aerosol characteristics, J Geophys Res-Atmos, 112, doi: 10.1029/2006jd007500, 2007.

Roberts, P., and Hallett, J.: A Laboratory Study of Ice Nucleating Properties of Some Mineral Particulates, Q J Roy Meteor Soc, 94, 25-&, doi: 10.1002/qj.49709439904, 1968.

Rosenfeld, D.: TRMM observed first direct evidence of smoke from forest fires inhibiting rainfall, Geophys Res Lett, 26, 3105-3108, 1999.

Rosenfeld, D.: Suppression of rain and snow by urban and industrial air pollution, Science, 287, 1793-1796, 2000.

Rosenfeld, D., Fromm, M., Trentmann, J., Luderer, G., Andreae, M. O., and Servranckx, R.: The Chisholm firestorm: observed microstructure, precipitation and lightning activity of a pyro-cumulonimbus, Atmos Chem Phys, 7, 645-659, 2007.

Rosenfeld, D., Lohmann, U., Raga, G. B., O'Dowd, C. D., Kulmala, M., Fuzzi, S., Reissell, A., and Andreae, M. O.: Flood or drought: How do aerosols affect precipitation?, Science, 321, 1309-1313, doi: 10.1126/science.1160606, 2008.

Rutledge, S. A., and Hobbs, P. V.: The Mesoscale and Microscale Structure and Organization of Clouds and Precipitation in Midlatitude Cyclones .12. A Diagnostic Modeling Study of Precipitation Development in Narrow Cold-Frontal Rainbands, J Atmos Sci, 41, 2949-2972, doi: 10.1175/1520-0469(1984)041, 1984.

Saleeby, S. M., and Cotton, W. R.: A large-droplet mode and prognostic number concentration of cloud droplets in the Colorado State University Regional Atmospheric Modeling System (RAMS). Part I: Module descriptions and supercell test simulations, J Appl Meteorol, 43, 182-195, doi: 10.1175/1520-0450(2004)043, 2004.

Saleeby, S. M., Cotton, W. R., Lowenthal, D., Borys, R. D., and Wetzel, M. A.: Influence of Cloud Condensation Nuclei on Orographic Snowfall, J Appl Meteorol Clim, 48, 903-922, doi: 10.1175/2008jamc1989.1, 2009.

Sassen, K., and Khvorostyanov, V. I.: Cloud effects from boreal forest fire smoke: evidence for ice nucleation from polarization lidar data and cloud model simulations, Environ Res Lett, 3, 12, doi: 10.1088/1748-9326/3/2/025006, 2008.

Seifert, A., and Beheng, K. D.: A double-moment parameterization for simulating autoconversion, accretion and selfcollection, Atmos Res, 59, 265-281, Doi: 10.1016/S0169-8095(01)00126-0, 2001.

Seifert, A., and Beheng, K. D.: A two-moment cloud microphysics parameterization for mixed-phase clouds. Part 1: Model description, Meteorol Atmos Phys, 92, 45-66, doi: 10.1007/s00703-005-0112-4, 2006.

Seifert, A., Khain, A., Pokrovsky, A., and Beheng, K. D.: A comparison of spectral bin and two-moment bulk mixed-phase cloud microphysics, Atmos Res, 80, 46-66, DOI 10.1016/j.atmosres.2005.06.009, 2006.

Seifert, A., Kohler, C., and Beheng, K. D.: Aerosol-cloud-precipitation effects over Germany as simulated by a convective-scale numerical weather prediction model, Atmospheric Chemistry and Physics, 12, 709-725, doi: 10.5194/acp-12-709-2012, 2012.

Shulman, M. L., Jacobson, M. C., Charlson, R. J., Synovec, R. E., and Young, T. E.: Dissolution behavior and surface tension effects of organic compounds in nucleating cloud droplets, Geophys Res Lett, 23, 603-603, doi: 10.1029/96gl00594, 1996.

Sorooshian, A., Feingold, G., Lebsock, M. D., Jiang, H. L., and Stephens, G. L.: On the precipitation susceptibility of clouds to aerosol perturbations, Geophys Res Lett, 36, L13803, doi: 10.1029/2009gl038993, 2009.

Spichtinger, P., and Cziczo, D. J.: Impact of heterogeneous ice nuclei on homogeneous freezing events in cirrus clouds, J Geophys Res-Atmos, 115, doi: 10.1029/2009jd012168, 2010.

Stevens, B., and Seifert, A.: Understanding macrophysical outcomes of microphysical choices in simulations of shallow cumulus convection, J Meteorol Soc Jpn, 86, 143-162, 2008.

Stevens, B., and Feingold, G.: Untangling aerosol effects on clouds and precipitation in a buffered system, Nature, 461, 607-613, doi: 10.1038/Nature08281, 2009.

Su, H., Rose, D., Cheng, Y. F., Gunthe, S. S., Massling, A., Stock, M., Wiedensohler, A., Andreae, M. O., and Poschl, U.: Hygroscopicity distribution concept for measurement data analysis and modeling of aerosol particle mixing state with regard to hygroscopic growth and CCN activation, Atmospheric Chemistry and Physics, 10, 7489-7503, doi: 10.5194/acp-10-7489-2010, 2010.

Tao, W. K., Li, X. W., Khain, A., Matsui, T., Lang, S., and Simpson, J.: Role of atmospheric aerosol concentration on deep convective precipitation: Cloud-resolving model simulations, J Geophys Res-Atmos, 112, D24S18, doi: 10.1029/2007jd008728, 2007.

Tao, W. K., Chen, J. P., Li, Z. Q., Wang, C., and Zhang, C. D.: Impact of Aerosols on Convective Clouds and Precipitation, Rev Geophys, 50, doi: 10.1029/2011rg000369, 2012.

Teller, A., and Levin, Z.: Factorial method as a tool for estimating the relative contribution to precipitation of cloud microphysical processes and environmental conditions: Method and application, J Geophys Res-Atmos, 113, doi: 10.1029/2007jd008960, 2008.

Tessendorf, S. A., Weeks, C. E., Axisa, D., and Bruintjes, R. T.: Aerosol characteristics observed in southeast Queensland and implications for cloud microphysics, J Geophys Res-Atmos, 118, 2858-2871, doi: 10.1002/Jgrd.50274, 2013.

Tonse, S. R., Brown, N. J., Harley, R. A., and Jinc, L.: A process-analysis based study of the ozone weekend effect, Atmos Environ, 42, 7728-7736, doi: 10.1016/j.atmosenv.2008.05.061, 2008.

Trentmann, J., Luderer, G., Winterrath, T., Fromm, M. D., Servranckx, R., Textor, C., Herzog, M., Graf, H. F., and Andreae, M. O.: Modeling of biomass smoke injection into the lower stratosphere by a large forest fire (Part I): reference simulation, Atmospheric Chemistry and Physics, 6, 5247-5260, 2006.

van den Heever, S. C., Carrio, G. G., Cotton, W. R., DeMott, P. J., and Prenni, A. J.: Impacts of nucleating aerosol on Florida storms. Part I: Mesoscale simulations, J Atmos Sci, 63, 1752-1775, doi: 10.1175/Jas3713.1, 2006.

Van Den Heever, S. C., and Cotton, W. R.: Urban aerosol impacts on downwind convective storms, J Appl Meteorol Clim, 46, 828-850, doi: 10.1175/Jam2492.1, 2007.

van Lier-Walqui, M., Vukicevic, T., and Posselt, D. J.: Quantification of Cloud Microphysical Parameterization Uncertainty Using Radar Reflectivity, Mon Weather Rev, 140, 3442-3466, doi: 10.1175/Mwr-D-11-00216.1, 2012.

Wang, Y., Wan, Q., Meng, W., Liao, F., Tan, H., and Zhang, R.: Long-term impacts of aerosols on precipitation and lightning over the Pearl River Delta megacity area in China, Atmospheric Chemistry and Physics, 11, 12421-12436, 10.5194/acp-11-12421-2011, 2011.

Wang, Y., Fan, J. W., Zhang, R. Y., Leung, L. R., and Franklin, C.: Improving bulk microphysics parameterizations in simulations of aerosol effects, J Geophys Res-Atmos, 118, 5361-5379, doi: 10.1002/Jgrd.50432, 2013.

Wang, Y., Liu, X., Hoose, C., and Wang, B.: Impact of heterogeneous ice nucleation by natural dust and soot based on a probability density function of contact angle model with the Community Atmospheric Model version 5, Atmos. Chem. Phys. Discuss., 14, 7141-7186, doi:10.5194/acpd-14-7141-2014, 2014a.

Wang, Y., Zhang, R. Y., and Saravanan, R.: Asian pollution climatically modulates mid-latitude cyclones following hierarchical modelling and observational analysis, Nat Commun, 5, doi: 10.1038/Ncomms4098, 2014b.

Wood, R.: Drizzle in stratiform boundary layer clouds. Part II: Microphysical aspects, J Atmos Sci, 62, 3034-3050, doi: 10.1175/Jas3530.1, 2005.

Xue, H. W., and Feingold, G.: Large-eddy simulations of trade wind cumuli: Investigation of aerosol indirect effects, J Atmos Sci, 63, 1605-1622, 2006.

Yin, Y., Carslaw, K. S., and Feingold, G.: Vertical transport and processing of aerosols in a mixed-phase convective cloud and the feedback on cloud development, Q J Roy Meteor Soc, 131, 221-245, doi: 10.1256/qj.03.186, 2005.

Yu, S. C., Mathur, R., Kang, D. W., Schere, K., and Tong, D.: A study of the ozone formation by ensemble back trajectory-process analysis using the Eta-CMAQ forecast

model over the northeastern US during the 2004 ICARTT period, Atmos Environ, 43, 355-363, doi: 10.1016/j.atmosenv.2008.09.079, 2009.

Yun, Y. X., and Penner, J. E.: Global model comparison of heterogeneous ice nucleation parameterizations in mixed phase clouds, J Geophys Res-Atmos, 117, doi: 10.1029/2011jd016506, 2012.

Zhang, L. M., Michelangeli, D. V., and Taylor, P. A.: Influence of aerosol concentration on precipitation formation in low-level, warm stratiform clouds, J Aerosol Sci, 37, 203-217, doi: 10.1016/j.jaerosci.2005.04.002, 2006.

Zuberi, B., Bertram, A. K., Cassa, C. A., Molina, L. T., and Molina, M. J.: Heterogeneous nucleation of ice in (NH4)(2)SO4-H2O particles with mineral dust immersions, Geophys Res Lett, 29, doi: 10.1029/2001gl014289, 2002.